RESEARCH REPORT No. 96203–1

THE MICROWAVE POWER TRANSISTOR AS A COMMUNICATIONS AMPLIFIER

R.G. Harrison

FINAL REPORT
AUGUST 1972

Prepared for
Director General
COMMUNICATIONS RESEARCH CENTRE
Shirley Bay
Ottawa, Ontario K1N 8T5
Canada
under
Contract No. OPF1–0063

RCA Research Laboratories

RCA Limited | Ste-Anne-de-Bellevue 810, Qué. | Canada

RCA Research Laboratories

THE MICROWAVE POWER TRANSISTOR AS A COMMUNICATIONS AMPLIFIER

R.G. Harrison

FINAL REPORT

Prepared for
Director General
COMMUNICATIONS RESEARCH CENTRE
Shirley Bay, Ottawa, Ontario K1N 8T5
Canada
under
Contract No. OPF1-0063

RCA Report No. : 96203-1
Lab Report No. :
RCA Project No.: 64.2.45
Shop Order No. : 96203

Approved By: R.J. McIntyre
DR. R.J. MCINTYRE, DIRECTOR
SEMICONDUCTOR ELECTRONICS LABORATORY

Dated: AUGUST 1972

THE MICROWAVE POWER TRANSISTOR AS A COMMUNICATIONS AMPLIFIER

R.G. Harrison

Final Report

August 1972

Prepared for

Communications Research Centre
Ottawa, Canada

SUMMARY

This report contains the results of a study of the tradeoffs between the power capability and the communications potential of a microwave power transistor. After the introduction, which gives the rationale for this study, the relevant previously published work is surveyed. This is followed by the substance of the present report: the results of a detailed series of measurements of the power versus communications capability of a 2 GHz microwave power transistor amplifier. The emphasis is on the relative merits of the class A and class C modes of operation. The present results indicate that the behaviour of the microwave power transistor amplifier is in many respects unlike that of the TWT power amplifiers conventionally used in satellite systems.

The device type selected for investigation has earlier been the subject of a theoretical and experimental study[1,2] of its performance as a single-carrier class C microwave amplifier, a mode of operation previously resistant to mathematical simulation. Numerical

time-domain methods were developed which permitted the steady-state ac class C performance of a device model to be computed for a reasonable expenditure of machine time. However, it is shown that such techniques become impractical when as few as two carriers are present and are virtually unusable in a typical multicarrier communications environment.

An investigation of several other approaches revealed that no satisfactory method appears to exist at present which can predict the multicarrier performance of a microwave power transistor in terms of its device model. This is because the device is essentially nonlinear, even under class A conditions. Nevertheless, a more empirical approach, which is based on the measurement of the single carrier nonlinear gain and phase characteristics and was originally developed for TWT applications, predicts the third, fifth and seventh-order intermodulation products with reasonable accuracy, as well as the gain.

In spite of the large amount of experimental data obtained in the course of this work, further effort is required to gain an overall view of the potentialities of the microwave power transistor in a multicarrier environment in which each carrier can be independently FM modulated (the present results have been obtained for a maximum of 3 carriers). In addition, further development of existing software and computational methods is needed to permit:

(a) Prediction of the dc-to-rf conversion efficiency under multicarrier conditions, and

(b) Optimization of network parameters to realize the best communications-performance with respect to thermal and IM noise while being constrained by minimum gain and efficiency specifications.

It would then be a valuable exercise to compare the optimized communications-performance of several different device types.

TABLE OF CONTENTS

TABLE OF CONTENTS (continued)

FIGURES

FIGURES (continued)

FIGURES (continued)

TABLES

1. INTRODUCTION

This report describes the results of a program of investigations undertaken for the Communications Research Centre (CRC), Ottawa, Canada. The aim of the program was to determine the potential of a typical microwave power transistor as an amplifier for modern communications applications.

The original objectives of this project were:

(1) To characterize the power-communications capability trade-off of microwave amplifiers assuming application in L-band (0.39 to 1.55 GHz) systems employing narrow-band frequency modulation of voice information.

(2) To investigate active device and/or package design modifications which hold promise of improving the communications capability of amplifiers studies in (1).

(3) To investigate the effect upon the communications-capability of practical power-combining techniques, leading to an increase in amplifier power output.

Subsequently, the frequency-band designated in (1) was changed by mutual agreement between RCA and CRC to S-band (1.55 - 5.2 GHz); reflecting a shift of interest on the part of CRC and simultaneously entering a region of the microwave spectrum wherein previous experimental and theoretical studies had been conducted by RCA[1],[2].

In order to maximize the relevance of this work to real-life problems, the program of measurements was oriented specifically toward satellite communications applications rather than being restricted to cases of academic interest only.

For the same reason, it was decided to concentrate on a compre-

hensive series of measurements in order to gain insight into the real-life problems incurred in the design of such systems. It is evidently useless to develop an elaborate theoretical explanation of phenomena of only marginal engineering interest.

Items (2) and (3) have not been emphasized because it was considered that:

(a) The effects of active device and/or package design modifications

and

(b) The relative merits of various power-combining schemes

could not be properly evaluated until the trade-offs between power performance and communications-capability, as referred to in (1), had been understood.

The present report begins by reviewing the previous experimental and theoretical work relating to distortion in frequency multiplexed communications systems. This review covers both mathematically and experimentally-oriented papers, and refers to a particular approach[42] which was subsequently found by RCA Limited to be particularly effective in the case of microwave power transistors.

The report goes on to describe in detail a series of communications-oriented measurements on a microwave power transistor. These include two- and three-carrier measurements of both intermodulation distortion and cross-talk as well as a group of single-carrier tests which serve as a reference for comparison with the multi-carrier cases. It is found that the microwave power transistor is in several respects unlike the TWT conventionally used in satellite communications systems.

Next, the report discusses the various methods of nonlinear circuit analysis and investigates their relevance to studies of intermodulation distortion.

The report concludes with a description of the application of one of these methods to the prediction of intermodulation distortion in an microwave power transistor.

The author wishes to express his thanks to G. Kadar and M. Gauvin for their invaluable contributions to the communications aspects of the experimental work and to H.J. Moody and N. Epstein for much assistance with computational procedures.

2. SURVEY OF PREVIOUS WORK ON DISTORTION IN FREQUENCY MULTIPLEXED COMMUNICATIONS SYSTEMS

2.1 Cahn, 1960

Intermodulation distortion (IMD) and cross-talk noise due to amplitude nonlinearity have been discussed by Cahn[3]. His approach is empirical and involves the classic device of representing the nonlinearity as a (fictitious) zero-memory antisymmetric instantaneous amplitude characteristic as shown in Fig. 2-1. This kind of characteristic is known as a "hard limiter". Cahn showed that for an input consisting of two equal carriers

$$v_{in}(t) = V_{in}(\sin\omega_1 t + \sin\omega_2 t) \tag{2.1}$$

the level of the third-order IMD products with respect to the carrier level could be expressed as

$$10 \lg_{10} \left\{ \frac{4}{9} \frac{(1 - X^2)^3}{(\sqrt{1 - X^2} + \frac{1}{X} \arcsin X)^2} \right\} \text{dB} \tag{2.2}$$

and the input power level with respect to the threshold clipping level as

$$10\lg_{10}(X^2/4)\text{dB} \tag{2.3}$$

where $X = V_c/(2\, v_{in})$.

His investigation of cross-talk represents the signals in a plurality of channels by random noise with Gaussian amplitude distribution and again considers the characteristic of Fig. 2-1. Only the case of a large number of carriers is treated. Cross-talk is calculated for a single sinusoidal signal in a narrow slot in the centre of the spectrum. His results for the output signal-to-cross-talk ratio agree

---

* E.g. $f(x) = -f(-x)$.

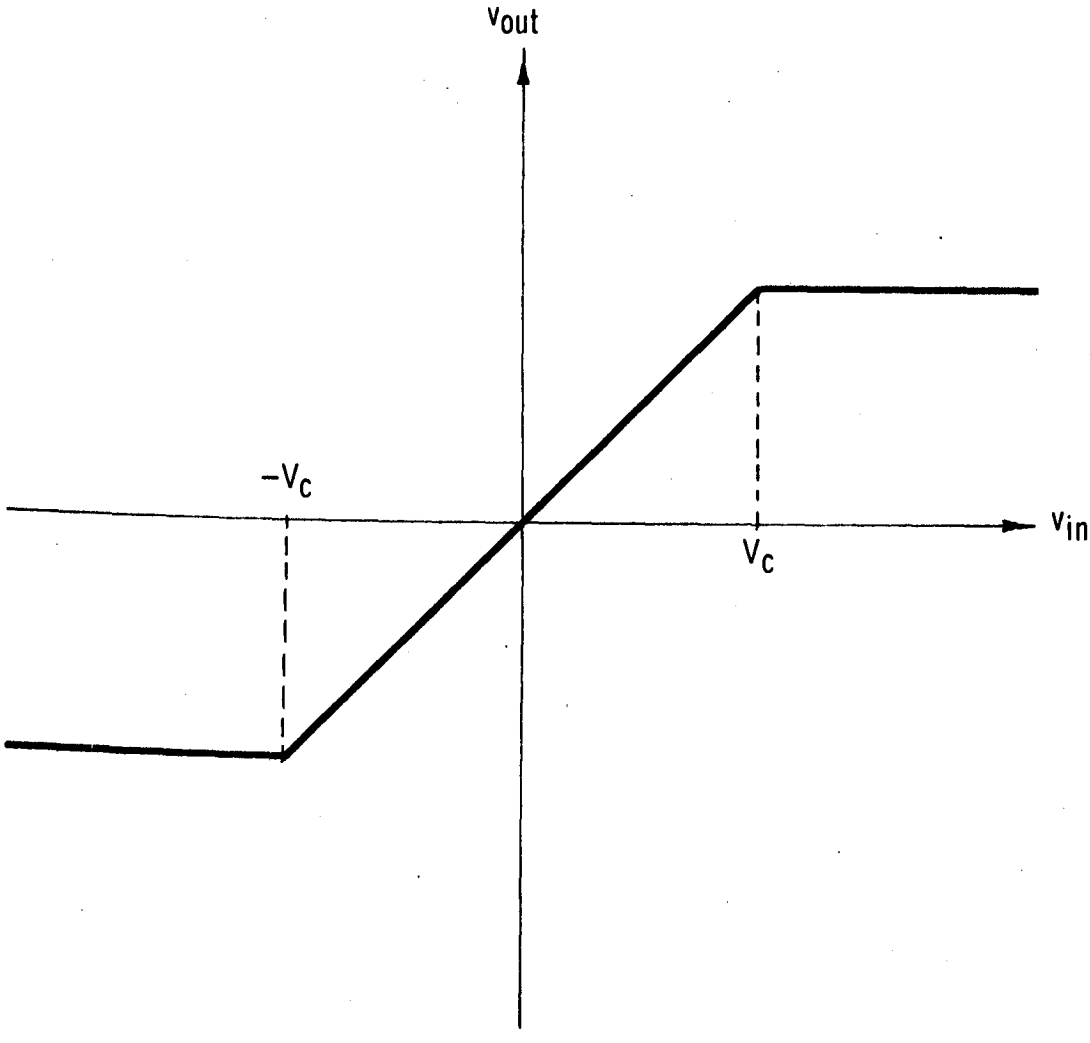

Figure 2-1 Simplified "hard limiter" antisymmetric instantaneous amplitude characteristic.

fairly well with 8 experimental points for an unspecified device, presumably a TWT. The best agreement (within about 0.5 dB) is seen when the rms input is near the clipping level. For lower inputs the disagreement is as much as 12 dB. (Theory predicts lower IMD levels).

2.2 Sunde, 1965

The same type of "hard limiter" characteristic was employed by Sunde[4] in his study of intermodulation distortion in multicarrier FM systems employing TWTs. He considers both 3rd-order IMD due to two carriers and the total IMD in a narrow band at the output for a multicarrier input simulated by noise. His discussion is restricted to cases of equal carrier spacing and power. His two-carrier result is similar to Ca n's, but as a better approximation to the actual situation in multicarrier FM transmission his multicarrier calculation assumes a flat spectrum rather than the Gaussian spectrum assumed by Cahn. However, the results obtained in the two cases for the total IMD power as a function of the total input power agree within about 1 dB [see Fig. 4 of reference 4]. Sunde then goes on to consider the IMD due to phase nonlinearity, i.e. caused by AM-to-PM conversion, for the same two extreme cases. For two input carriers he derives the following approximate expression for the third-order IMD power relative to one of the fundamentals:[4, eq. (32)]

$$-10 \lg_{10} \left\{ 1 + \frac{J_0^2 (2k_0)}{J_1^2 (2k_0)} \right\} \text{ dB} \qquad (2.4)$$

where $2k_o(P_{in})$ is the coefficient of the difference frequency $(\omega_2 - \omega_1)$ component of the Taylor series expansion of the nonlinear phase function,

i.e. an approximation to the relation

$$\psi(t) = \mathfrak{F}\left[2P_{in}\left(1 + \cos\left(\frac{\omega_2 - \omega_1}{2}\right)t\right)\right] \qquad (2.5)$$

between the phase modulation $\psi(t)$ and the argument of $\mathfrak{F}[.]$, the square of the envelope function. The result (2.4) is more accurate for low input powers than for powers near the saturation point. By suitably combining the nonlinear-amplitude and nonlinear-phase contributions to the 3rd-order IMD he achieved a 1-dB agreement with measured results over an input power range of -16 to +4 dBm [Fig. 8, reference 4]. These results show that for a TWT, at low power levels, the third-order IMD is primarily due to AM-to-PM conversion but that amplitude-nonlinearity dominates at higher levels. The results obtained for an infinite number of carriers agree less well with measurements using a random noise input.

2.3 Berman and Podraczky, 1967

Berman and Podraczky[5] addressed the problem of determining the IMD produced in a wideband communications repeater in a different way. Their method is applicable to a large number of input signals randomly distributed in both amplitude and frequency. Their experimental measurements, however, were restricted to 8 equal carriers with uniform frequency spacing. In this approach no attempt is made to define an ampirical TWT amplitude characteristic such as the "hard limiter" model of Fig. 2.1. Instead, a four-term Fourier series approximation is made of the input-output transfer characteristic:

$$v_{out}(t) = c_1 \sin[\alpha v_{in}(t)] + c_2 \sin[2\alpha\, v_{in}(t)] + c_3 \sin[3\alpha\, v_{in}(t)] + c_5 \sin[5\alpha v_{in}(t)] \qquad (2.6)$$

This gave a good fit from zero input to saturation and a reasonable fit for instantaneous inputs up to 12 dB beyond the saturation level. The coefficients of this series were determined graphically from the corresponding single-carrier characteristic.

In the multicarrier case the input is

$$v_{in}(t) = \sum_{i=1}^{N} V_i \sin(\omega_i t + \int \psi_i dt) \tag{2.7}$$

where: V_i is the amplitude of the i^{th} carrier

ω_i is the centre-frequency of the i^{th} carrier

ψ_i is the RMS frequency deviation.

Thus the output becomes

$$v_{out}(t) = \sum_{m=1,2,3,5} \left(c_m \sin \left[m\alpha \sum_{i=1}^{N} \left\{ V_i \sin(\omega_i t + \int \psi_i dt) \right\} \right] \right) \tag{2.8}$$

and finally the spectrum of the output is

$$V_{out}(t) = \sum_{m=1,2,3,5} \left\{ c_m \sum_{x=-\infty}^{\infty} \cdots \sum_{b=-\infty}^{\infty} \sum_{a=-\infty}^{\infty} J_a(m\alpha V_1) \cdot J_b(m\alpha V_2) \cdots J_x(m\alpha V_N) \cos \left[(a\omega_1 + b\omega_2 + \cdots + x\omega_N)t + \int \psi_r dt \right] \right\} \tag{2.9}$$

where a,b,..., x take all ± integral values, the $J_n(\cdot)$ are Bessel functions of integral order n and

$$\psi_r = \sqrt{(a\psi_1)^2 + (b\psi_2)^2 + \cdots (x\psi_N)^2} \tag{2.10}$$

if the spectrum of each carrier is Gaussian. Although each term of (2.9) contains an infinite number of spectral components, in practice only the interesting classes of products need be computed. Because it was concluded from measurements on a TWT that the IMD was due primarily

to the amplitude nonlinearity, this theory does not account for IMD due to phase-nonlinearity. Over a 20 dB range of input power levels, the computed third-order products were within 3 dB of the measured values, while the fifth-order products were within 6 dB.

2.4 Narayanan, 1967

Yet another approach to the analysis of IMD was introduced by Narayanan[6]. This is a fundamentally different approach from those discussed above in that it treats a mathematical model of the amplifying device itself rather than working in terms of "black box" input/output characteristics. This paper appears to be the first to deal with IMD in transistors.

The transistor model considered includes four types of nonlinearity: the exponential i-v junction characteristics, avalanche multiplication, the current-dependence of h_{FE} and the voltage-dependence of the collector depletion capacitance. These nonlinearities are approximated by truncated Volterra-series representations, and the method of analysis depends strongly on the work of Ku and Wolfe[40].

The Volterra series approach may be outlined as follows. Consider a function

$$y(t) = \mathcal{F}[x(t)]. \tag{2.11}$$

If $\mathcal{F}[.]$ is a zero-memory nonlinear (ZMNL) function it can be represented by a power series:

$$\mathcal{F}[x(t)] = \sum_{i=1}^{\infty} c_i x^i(t) \tag{2.12}$$

However, if $\mathcal{F}[.]$ is nonlinear with memory (NLWM) then the linear term

$c_1 x(t)$ can be replaced by the convolution $\int_o^t c_1(t-\tau)x(\tau)d\tau$ while the higher order terms can be replaced by expressions of the form

$$y_n(t) = \int_o^t \cdots \int_o^t c_n(t-\tau_1, \ldots, t-\tau_n)x(\tau_1)\ldots x(\tau_n)\, d\tau_1 \ldots d\tau_n \qquad (2.13)$$

where the n^{th}-degree Volterra kernels $c_n(t_1, \ldots t_n)$ may be viewed as the impulse-responses of equivalent component nonlinear systems. A method for evaluating the Volterra kernels is given in [40], and involves the n-dimensional Laplace transform of $y_n(t)$:

$$Y_n(s_1, \ldots, s_n) = \int_o^\infty \cdots \int_o^\infty \left[\int_o^\infty \cdots \int_o^\infty c_n(t_1-\tau_1, \ldots, t_n-\tau_n)x(\tau_1)\ldots x(\tau_n)d\tau_1 \ldots d\tau_n \right] dt_1 \ldots dt_n$$

$$= c_n(s_1, \ldots, s_n)X(s_1)\ldots X(s_n) \qquad (2.14)$$

Such transforms are used by Narayanan because the response to sinusoidal inputs is desired.

The Volterra series approach is applied to the computation of the level of the $f_2 - f_1$ IMD term for two carriers and the $f_2+f_3 - f_1$ IMD term for three carriers. The results are compared with experimental values obtained for

$$f_1 = 14.5 \text{ MHz}$$

$$f_2 = 15.2 \text{ MHz}$$

$$f_3 = 16.6 \text{ MHz} \ .$$

The agreement is in the range 1 to 9 dB for the $f_2 - f_1$ term and in the range 0 to 9 dB for the $f_2 + f_3 - f_1$ term as the collector bias is varied from 5 to 25 volts. Experimental results for the IMD term $f_1 + f_2$ and the single-carrier harmonic distortion terms 2f and 3f are also given

but not compared with theory. Other important terms, such as the third-order IMD terms $2f_1 - f_2$ and $2f_2 - f_1$ are not considered at all.

This method is restricted to quasi-linear cases where the nonlinearities are extremely small; these nonlinearities can, however, be either frequency dependent (NLWM) or not (ZMNL). Gross nonlinearities cannot be treated because of the rapidly increasing difficulty of handling terms of high degree and it is concluded that the approach is not potentially useful for the treatment of highly nonlinear modes of operation such as class C, or even for more linear modes (class A) when accuracy is required.

2.5 Hilling and Salmon, 1968

These authors[7] employ a conventional power series i(v) relation as a vehicle for discussion of the origins of various types of harmonic and IM distortion in transistors:

$$i(t) = c_o + c_1 v(t) + c_2 v^2(t) + \ldots \qquad (2.15)$$

Although their theoretical results have little quantitative value, they do indicate the possibility of certain terms cancelling in such a way as to reduce particular distortions. Experiments with two input carriers in the 100 to 200 MHz range confirmed the existance of such cancellations for second-order ($f_1 \pm f_2$) and third-order ($2f_1 - f_2$) and ($2f_2 - f_1$) IMD products for particular values of emitter current I_E. In both cases, the distortion minima correlated with the peak of the $h_{FE}(I_E)$ characteristic. A flat $h_{FE}(I_E)$ characteristic gave a broad distortion minimum.

Other experiments at 50 to 500 MHz with varying source resistance indicated that the exponential i(v) characteristic of the base-emitter junction was largely responsible for the $(f_1 \pm f_2)$ IMD products.

Their conclusion that the distortion-cancellation phenomenon cannot be used to improve the performance of practical amplifiers is at variance with the conclusion of Thomas[41] (1967). He shows that for a simple ZMNL quasi-linear transistor model incorporating:

(i) the emitter-base junction i(v) nonlinearity

(ii) the $h_{FE}(I_E)$ characteristic

(iii) avalanche multiplication,

cancellation can always be obtained by suitably adjusting the magnitudes of voltages and currents. If both absolute and relative levels are correct, he states that simultaneous cancellation of both second and third order products can occur, and recommends external reactive compensation to achieve broadband compensation.

2.6 Neill, 1969

This[8] is still another approach involving physical-mathematical nonlinear device models. It is based on the formulation of the nonlinear differential equations of the network as Volterra integral equations. The fast Fourier transform is used to find the frequency-domain solution. The method, which is discussed further in Section 4.3 of this report, was used to perform both harmonic and IM distortion calculations on the transistor model given by Narayanan. Levels of the second to tenth harmonics inclusive were computed for a 10 MHz input carrier at 21 different

levels in 11 minutes and 160 different IM products were computed for 10 and 11 MHz input carriers at a fixed level in 13 minutes, both using an Elliot 503 computer. Comparison with experiment was not given.

2.7 Cahn, 1969

This paper[9] presents a Monte Carlo computational scheme for determining IM products due to an arbitrary number of carriers assessing a ZMNL channel, the phydical nature of which is unspecified. The channel may be either hard limiting (e.g. Figure 2.1) or soft limiting. The scheme depends on the series expansion of the output autocorrelation function. Multiple input carriers are viewed in the time-domain as forming a single resultant with both amplitude modulation and phase modulation. The ZMNL channel has no effect on the PM, only the AM, and the resultant output is completely specified. For the special case of a hard-limiting channel accessed by three carriers equally-spaced in frequency but with arbitrary phase-angles, the IM falling on the centre channel can be computed exactly. The results show that the quadrature IM component has greater power than the inphase component.

The statistical Monte Carlo scheme is applied to cases with from 3 to 15 carriers (inclusive). The three-carrier results are in close agreement with the exact computation; the others show that the power imbalance between the phase and quadrature IM components decreases when there is a large number of carriers.

Since this paper considers only ZMNL channels, its validity for transistor amplifiers is questionable.

2.8 Shimbo, 1971

In this important paper[10] the IM due to a TWT is analyzed when the input consists of a combination of arbitrarily modulated carriers and Gaussian noise. The TWT is considered to be a NLWM device, i.e. both amplitude $P_{out}(P_{in})$ and phase $\phi_{out}(P_{in})$ nonlinearities are included. The multicarrier input is represented (in the absence of thermal noise) as

$$v_{in}(t) = \sum_{i=1}^{N} V_i \cos[\omega_o t + \omega_i t + \phi_i(t) + \lambda_i] \tag{2.16}$$

where for the i^{th} carrier:

(i) V_i is the amplitude

(ii) $\omega_o + \omega_i$ is the carrier frequency (ω_o is the midband frequency)

(iii) $\phi_i(t)$ is the phase modulation signal

(iv) λ_i is the phase angle.

Again, these signals are viewed as a single time-domain resultant:

$$v_{in}(t) = \rho(t)\cos\left\{\omega_o t + \mu(t)\right\} \tag{2.17}$$

where

$$x(t) = \sum_{i=1}^{N} V_i \cos[\omega_i t + \phi_i(t) + \lambda_i] \tag{2.18}$$

$$y(t) = \sum_{i=1}^{N} V_i \sin[\omega_i t + \phi_i(t) + \lambda_i] \tag{2.19}$$

and

$$\begin{cases} \rho^2(t) & = x^2(t) + y^2(t). \\ \tan[\mu(t)] & = y(t)/x(t) \end{cases} \tag{2.20}$$

The central idea is that the TWT output can be written

$$v_{out}(t) = g(\rho)\cos\left\{\omega_o t + \mu(t) + f(\rho)\right\} \tag{2.21}$$

where $g(\rho)$ is due to the amplitude nonlinearity and $f(\rho)$ is due to the phase nonlinearity. It is shown that the magnitude of the IM product whose angular frequency is

$$k_1\omega_1 + k_2\omega_2 + \ldots + k_N\omega_N + \omega_o$$

is given by the absolute value of the complex quantity

$$M_{k_1,k_2,\ldots k_N} = \int_o^\infty r\, J_{k_1}(V_1 r)\cdot J_{k_2}(V_2 r)\ldots J_{kN}(V_n r)dr \cdot \int_o^\infty \rho\, g(\rho)e^{jf(\rho)}\, J_1(r\rho)d\rho \tag{2.22}$$

where the k_i can take any $\pm$ integral value or zero but are constrained by the condition

$$k_1 + k_2 + \ldots + k_N = 1 \ . \tag{2.23}$$

Thus the representation of the TWT boils down to the representation of its gain and phase nonlinearities in terms of the function

$$g(\rho)\exp[\,jf(\rho)\,] \tag{2.24}$$

The magnitude of the pure component $\omega_o + \omega_1$, i.e. one of the carriers, is $M_{k_1} M^*_{k_1}$ where k_1 is 1 and all the others are zero.

In [10] Shimbo considers the case where the complex nonlinear characteristic is given by a power series

$$g(\rho)\exp[\,jf(\rho)\,] = c_1\rho + c_3\rho^3 + c_5\rho^5 + \ldots \tag{2.25}$$

wherein the c_i are in general complex; he also considers the Fourier-series case

$$g(\rho)\exp[jf(\rho)] = c_1 \sin(\alpha\rho) + c_2 \sin(2\alpha\rho) + c_3 \sin(3\alpha\rho) + \ldots \qquad (2.26)$$

where the c_i are again complex. Using the power-series representation, predicted values of IM for a TWT with two input carriers lie within 1 dB of measured values over a 20 dB range of carrier levels.

More recently[42] Shimbo has recommended the use of the Bessel series representation

$$g(\rho)\exp[jf(\rho)] = c_1 J_1(\alpha\rho) + c_2 J_1(2\alpha\rho) + c_3 J_1(3\alpha\rho) + \ldots \qquad (2.27)$$

again with complex coefficients c_i.

Recent investigations at RCA Limited have shown that the Bessel series representation gives very good results for a microwave power transistor. Since most of this work has been done after the expiration of the contract period, it is described only briefly in Section 6; more detail will be found in Reference [39].

2.9 Boag and Newby, 1971

The earliest experimental measurements of IMD due to a microwave class C transistor were made at RCA Limited by Boag and Newby[11]. Their results were obtained using a 2N5470 coaxial transistor arranged as a class C power amplifier at 1.8 GHz with an output power of approximately 1 watt. In all cases two carriers were employed with a spacing of ~ 1 MHz. Three conditions were investigated:

(1) Class C (no applied emitter bias) over a range of input levels, the output matching not being optimized.

(2) Class C with the output matched for maximum P_{out}.

(3) Class "AB", in which a small emitter bias current was applied.

They concluded that for 0.1 watt $\leq P_{out} \leq$ 0.8 watt, the device generated third-order IMD in the range -10 to -14 dB relative to one of the carriers, and that class A operation did not improve these levels. They did, however, record that certain tuning conditions led to a reduction of sideband magnitudes, a phenomenon further investigated in References [39] and [43].

2.10 Meyer, Shensa and Eschenbach, 1972

These authors investigate[13] cross-modulation and intermodulation in amplifiers at high frequencies. At low frequencies, they use the conventional power-series representation of the output amplitude as a function of the input amplitude to obtain expressions for cross-modulation and IMD terms for two carriers. At higher frequencies they introduce the Volterra series (following Narayanan[6]) to extend the analysis to amplifier nonlinearities with memory. Their application of the Volterra series shows that distinction should be made between amplitude cross-modulation, phase cross-modulation and frequency-domain cross-modulation.

The results are limited to cases of small distortion. Under those conditions, however, it is shown that the ratio of frequency-domain cross-modulation to third-order IMD is 4:1 if the carriers are closely-spaced in frequency.

The effects of feedback are also considered, and it is found that the relationship between amplitude and phase cross-modulation can be controlled via the phase-angle of the feedback loop gain at a

particular frequency. However, it is considered unlikely that feedback could be used at microwave frequencies because of device-gain limitations.

The experimental work relates to a low-power ($P_{out} \sim 0$ dBm) two-transistor feedback amplifier designed for 50 ohm source and load impedances. Over a frequency range 60 to 180 MHz, the calculated and measured values of third-order IMD and phase-cross modulation agree within about 1 dB while the frequency-domain cross-modulation values agree within about 2 dB. In the case of amplitude cross-modulation, however, differences of as much as 12 dB are seen. These are ascribed to inaccurate measurement of loop phase-shift at the higher frequencies.

3. COMMUNICATIONS-ORIENTED MEASUREMENTS ON A MICROWAVE POWER TRANSISTOR

The type of device selected for these measurements is the same as the one previously characterized[1],[2] for large-signal single-carrier class C operation. It is the RCA 2N5470, a coaxial overlay transistor capable of providing 1 watt of output power at 2.0 GHz.

In accordance with the objective of relating this work to practical applications, a program of measurements has been planned to provide useful information to communications system designers.

Although class C operation is inherently a nonlinear mode and is therefore not normally associated with communications amplifiers, in satellite transponders in which power is at a premium, efficiency is highly important. Therefore measurements are made here under conditions of zero applied emitter-base bias (clas C) and also with a fixed forward emitter-base bias (class A). In the former case we expect to see enhanced efficiency at the expense of linearity; in the latter we expect linearity at the expense of efficiency. An additional advantage of class C is that the collector current, and consequently the consumption of dc power, is negligible in the absence of RF input. This can lead to a useful increase in effective overall efficiency when the amplifier is lightly loaded, (i.e. not driven all the time). Comparisons will be made between class A and class C performance.

The measurements will be further subdivided into single-carrier, two-carrier and three-carrier tests.

3.1 Single-Carrier Tests

In order to establish the basic single-carrier performance of the microwave power transistor selected for detailed investigation, the set-up depicted in Figure 3-1 is employed. For flexibility of both circuit arrangement and device tuning range, coaxial components are used throughout. This is consistent with the coaxial geometry of the 2N5470 package itself. Slightly improved power performance could have been expected from the device had specially-designed (electrically short) matching transformers been designed. However, such networks are typically valid only over a restricted range of frequencies. Double-slug tuners are used to match both input and output ports of the transistor beoause of their ability to synthesize impedancesover the entire Smith chart. Their disadvantage is they are not electrically short. This means that a high VSWR can exist in the section of line between the device and the region wherein the impedance transformation takes place. Such high VSWRS are accompanied by local regions of high surface current density in which significant loss can occur.

As indicated in Figure 3-1, the device is used in the grounded-base configuration. This is primarily because the coaxial package of the 2N5470 device is specifically designed for this mode of operation. The coaxial jig in which the device is mounted is forced air cooled.

Since the double-slug tuners conduct dc, biassing is accomplished via dc feed units placed at the ends of the tuners remote from the device. This configuration helps to minimize the lengths of the

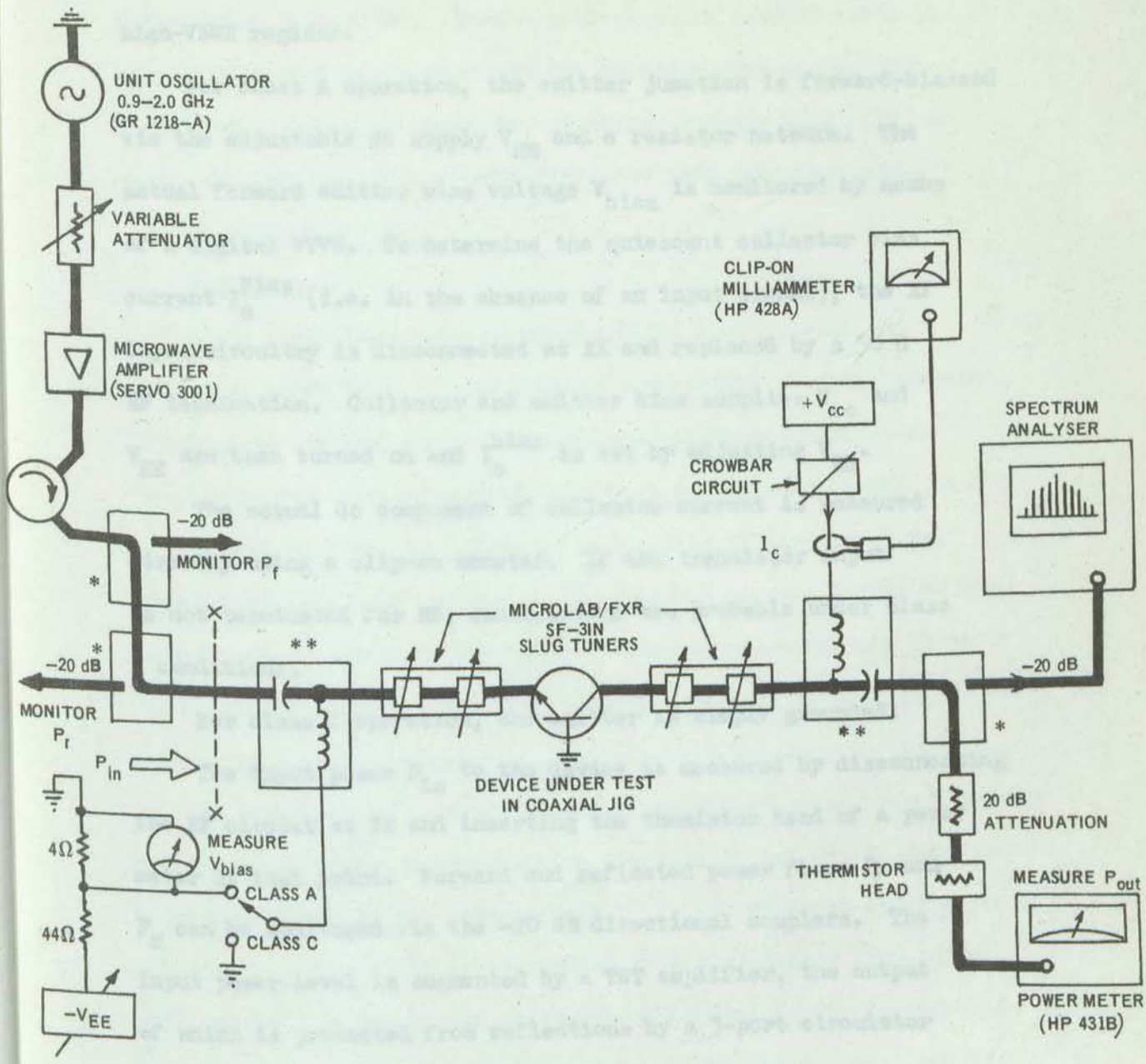

* Wideband directional coupler
HP 779–D, 1.7–12.4 GHz

** DC feed unit, Rohde & Schwarz
BN35616

Figure 3–1 Basic set-up for single-carrier tests

high-VSWR regions.

For class A operation, the emitter junction is forward-biassed via the adjustable dc supply V_{EE} and a resistor network. The actual forward emitter bias voltage V_{bias} is monitored by means of a digital VTVM. To determine the quiescent collector bias current I_c^{bias} (i.e. in the absence of an input signal), the RF input circuitry is disconnected at XX and replaced by a 50 Ω RF termination. Collector and emitter bias supplies V_{cc} and V_{EE} are then turned on and I_c^{bias} is set by adjusting V_{EE}.

The actual dc component of collector current is measured directly using a clip-on ammeter. If the transistor input is not terminated for RF, oscillations are probable under class A conditions.

For class C operation, the emitter is simply grounded.

The input power P_{in} to the device is measured by disconnecting the RF circuit at XX and inserting the themistor head of a power meter at that point. Forward and reflected power flows P_f and P_r can be monitored via the -20 dB directional couplers. The input power level is augmented by a TWT amplifier, the output of which is protected from reflections by a 3-port circulator terminated at the third port.

Other equipment included in this set-up includes a power meter to measure the power output, a high quality spectrum analyser (HP 8551B + 851B) and a fast adjustable "crowbar" circuit to protect the transistor under test from potentially destructive

high-current conditions. When a predetermined current level is exceeded, an SCR is triggered to the low-impedance state, thus effectively short-circuiting the collector voltage supply V_{cc} to ground and diverting the current flow away from the transistor.

3.1.1 Effect of bias

Procedure

Using a single-carrier fixed-frequency input signal, of sufficient power level P_{in} to produce saturation, the bias current is increased step by step and the tuning/matching circuits are re-optimized at each bias level to obtain the maximum output power P_{out}. Both P_{out} and the collector conversion efficiency η_c are measured at each level. This is repeated for various values of bias current, this traversing the range of possibilities between class C (no bias) and class A (where the amplifier becomes insensitive to further increases in bias).

In practice, it is found that the collector conversion efficiency η_c is a considerably more sensitive function of the tuning and matching adjustments than is the power output P_{out}. In order to simultaneously maximize P_{out} and η_c it is convenient to derive analog signals proportional to P_{out} and to the dc collector current I_c (in the presence of RF). These signals are used to drive respectively the X and Y axes of a CRT. The tuning is done in such a way as to drive the spot into the lower right hand corner of the screen thus optimizing gain and efficiency simultaneously. This is more effective than attempting to monitor two meters simultaneously.

Results

The results of this test for a 2.0 GHz input signal at a level of +23 dBm are illustrated in Figure 3-2 and listed in Table 3(1). In the class C case (no bias applied) the greatest P_{out} is obtained when the emitter is short-circuited for dc, whereas the best efficiency is found when the emitter is connected to the resistive biasing network (albeit with no applied bias voltage).

It can be seen from Figures 3-2(a) and 3-2(b) that the amplifier performance under class A conditions is virtually independent of bias ourrent, provided that the current is greater than 20 mA. The olass A measurements described elsewhere in this report are therefore made for $I_c^{bias} = 30$ mA.

Figures 3-2(o) and 3-2(d) show gain G and collector conversion efficiency η_o are funotions of the measured do voltage V_{BE}^{bias} across the emitter-base terminals. The highest observed bias ($V_{BE}^{bias} = 800$ mV) corresponds with the greatest efficiency (nearly 40%).

3.1.2 Maximum output power

Procedure

In order to compare the maximum output powers attainable under class A and class C conditions, the following test is performed. For each value of input power P_{in}, the amplifier is optimized for maximum power output $\hat{P}_{out}$; the oorresponding values of oollector conversion efficiency are also recorded.

Results

The results of tests performed at 2.0 GHz are summarized in Figures 3-3, 3-4 and 3-5. Figure 3-3 shows the relationship between

f = 2.0 GHz P_{in} = + 23 dBm V_{cc} = + 28 V	Device = 2N5470 No. 10	(41652-63)

I_c^{bias} mA	V_{EE}^{bias} mV	P_{out} dBm	I_c mA	η_c %	Comments
0	-	29.3	87.0	34.9	Emitter of transistor grounded (class C only).
0	3.1	28.4	63.5	38.9	Emitter connected to resistive biasing network (class A and C)
0	3.1	28.35	64	38.2	"
0+	200.7	29.0	80	35	"
2.5	784	30.1	92	39.8	"
5	729	30.3	100	38.25	"
10	729	30.3	103	37.1	"
20	731	30.35	107	36.2	"
30	722	30.35	106	36.5	"
40	713.4	30.35	107	36.2	"
50	699	30.35	107	36.2	"

Table 3(1) Effect of dc bias on single-carrier amplifier performance. See Figure 3-2 for graphs.

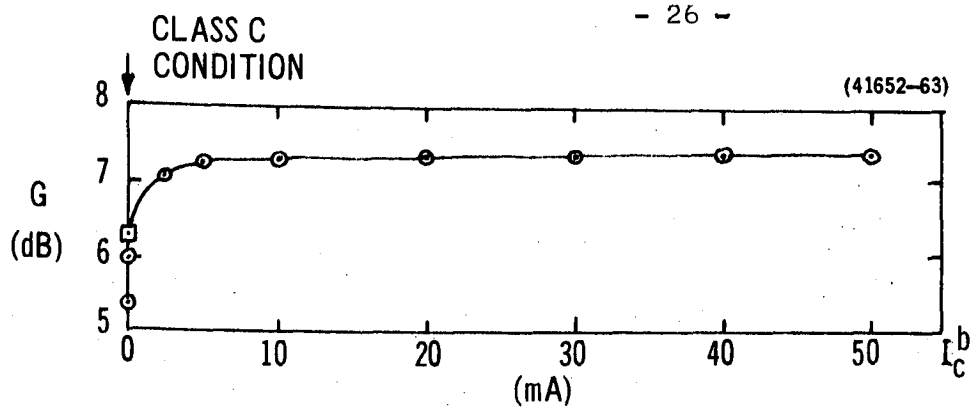

Figure 3-2(a)
Gain as a function of collector bias current

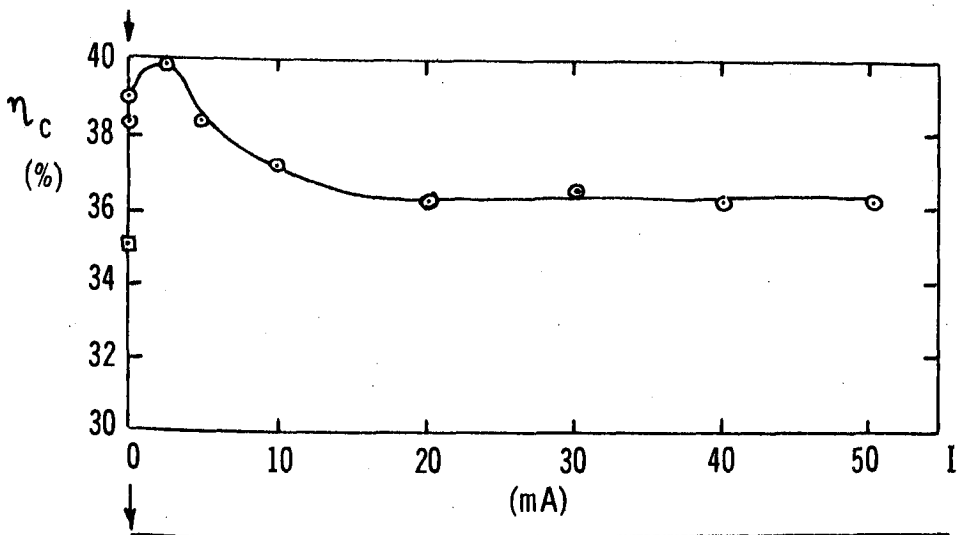

Figure 3-2(b)
Collector conversion efficiency as a function of bias current

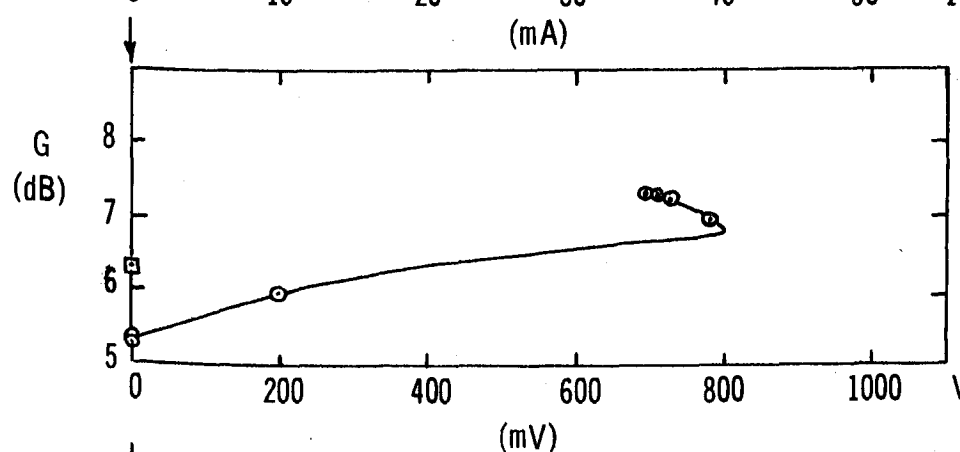

Figure 3-2(c)
Gain as a function of base-emitter forward bias voltage

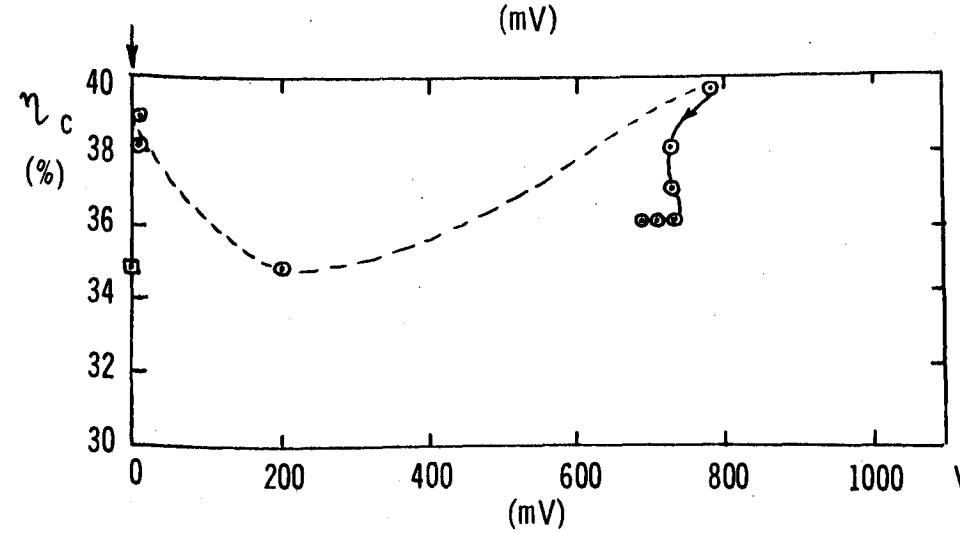

Figure 3-2(d)
Collector efficiency as a function of base-emitter bias voltage

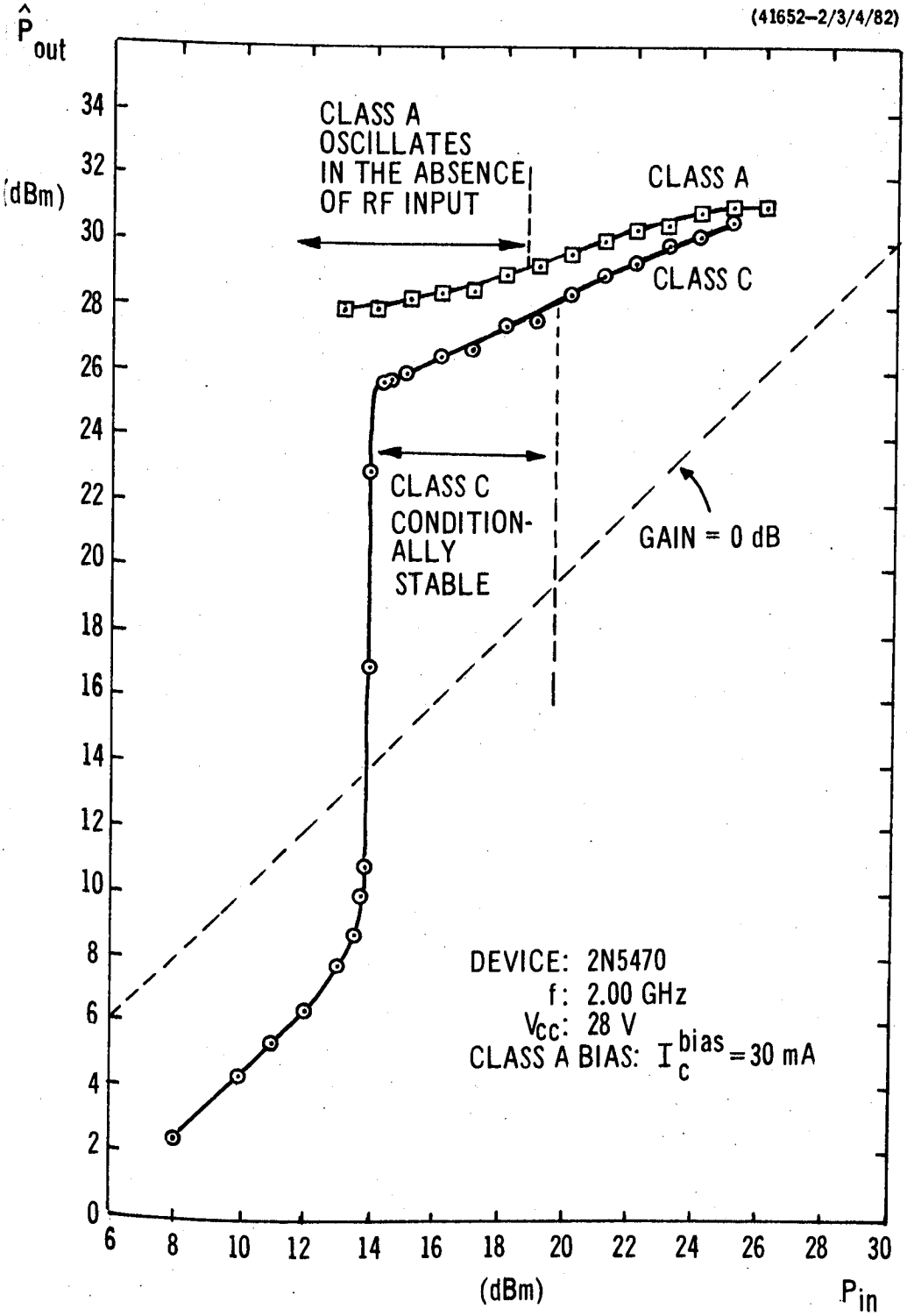

Figure 3-3 The maximum attainable output power $\hat{P}_{out}$ as a function of the incident power P_{in}; Class A and Class C cases compared.

the maximum attainable output power $\hat{P}_{out}$ and the input power P_{in}. In general, the class A condition provides a $\hat{P}_{out}$ 1 to 2 dB greater than does class C. In both cases, however, stable operation is observed only for the higher levels of P_{in}. In the class A mode, values of P_{in} less than 19 dBm result in tuning conditions which lead to oscillation in the absence of RF input (e.g. when the source of RF is replaced by a termination). In the class C case a different problem is encountered. For values of P_{in} between approximately 14 and 20 dBm, the amplifier is only conditionally stable. This means that in this range, if either P_{in} or the collector bias voltage V_{cc} is removed and then re-applied, the output power falls to a low value. The only way to re-establish $\hat{P}_{out}$ is to increase P_{in}, tune up and then slowly reduce P_{in} to the required value, re-tuning all the way. An interpretation of this effect is as follows. Class C amplifiers are self-biasing: the emitter-base junction of the transistor rectifies part of the incident power. The resulting dc component of current turns the device on, if the incident power is high enough. However at lower levels, the incident power is insufficient to make the biasing mechanism "self-starting". This leads to the conditionally-stable condition.

It is interesting to note that stability is lost in classes A and C for values of P_{in} which are only 1 dB apart. The significance of this apparent correlation is not known at present.

Figure 3-4 presents the same information in another way: the maximum attainable gain $\hat{G}$ as a function of P_{in}.

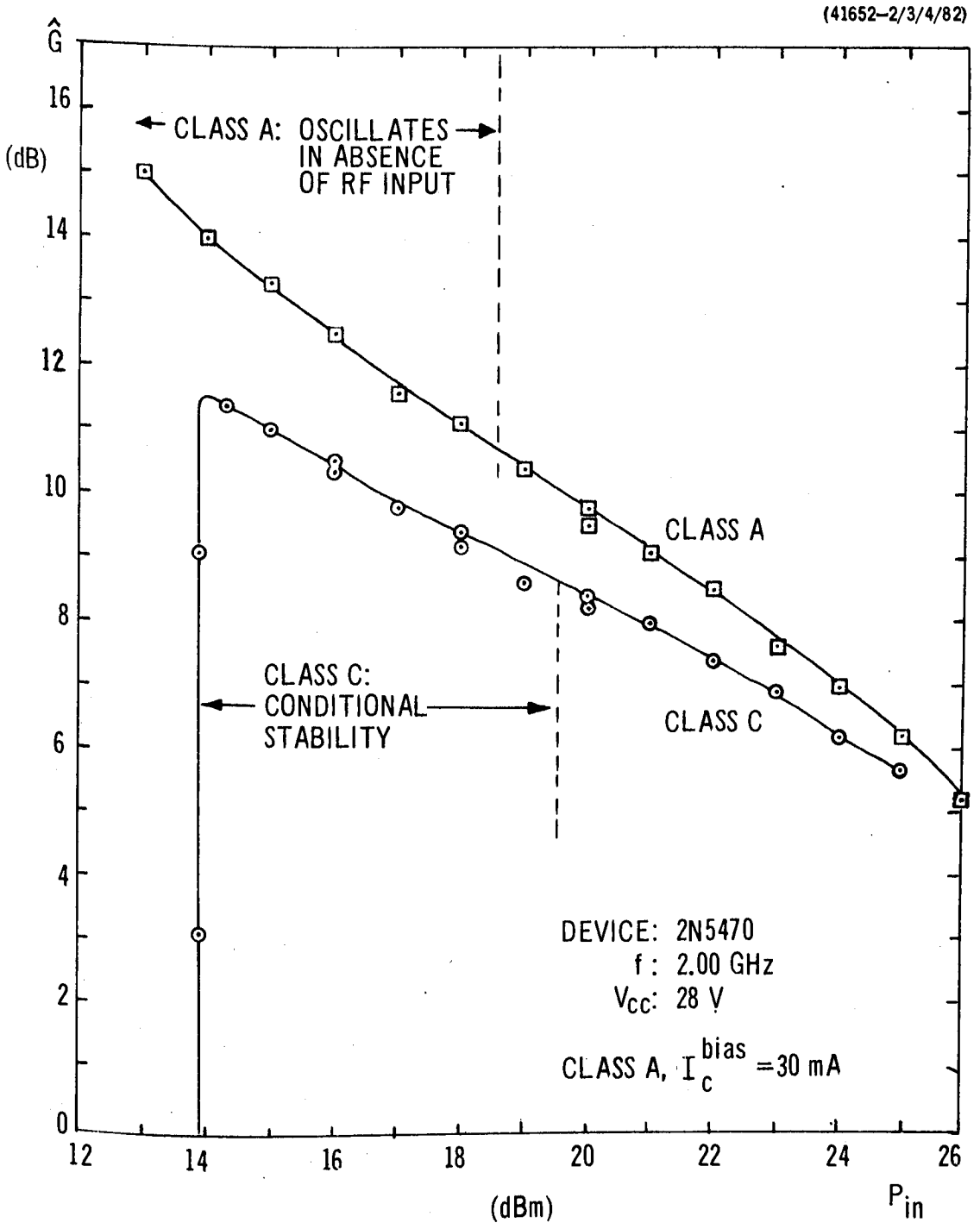

Figure 3–4 The maximum attainable gain $\hat{G}$ as a function of the incident power P_{in} ; Class A and Class C cases compared.

Finally, Figure 3-5 shows the maximum collector conversion efficiency $\hat{\eta}_c$ as a function of P_{in} when the amplifier is tuned for $\hat{G}$. For values of P_{in} less than approximately +23 dBm, class A operation offers higher efficiency than class C. However, for higher values of P_{in} the class C mode is the more efficient, the difference being nearly 20% when P_{in} reaches +26 dBm. The drop in the class A efficiency for P_{in} > +24 dBm may be a consequence of reduced device performance due to internal heating at the higher power levels. The relatively small difference between the class A and class C efficiencies may be ascribed to the fact that at 2.00 GHz the device is operating near its maximum useful frequency (~ 2.3 GHz). A greater difference would be expected at lower frequencies.

3.1.3 Effect of varying the power level

Procedure

Again using a single-carrier fixed-frequency input, the amplifier is optimized for maximum output power P_{out} by adjusting the incident power P_{in} and the tuning/matching elements.

A determination of the amplifier bandwidth is made under this condition. This information will be required subsequently in the tests involving more than one carrier.

Then, without altering any of the adjustments, P_{in} is reduced step-by-step and the relationship between P_{in} and P_{out} is established. This P_{in},P_{out} - characteristic shows how the amplifier would behave were it subjected to a dynamic range of input signals. In addition,

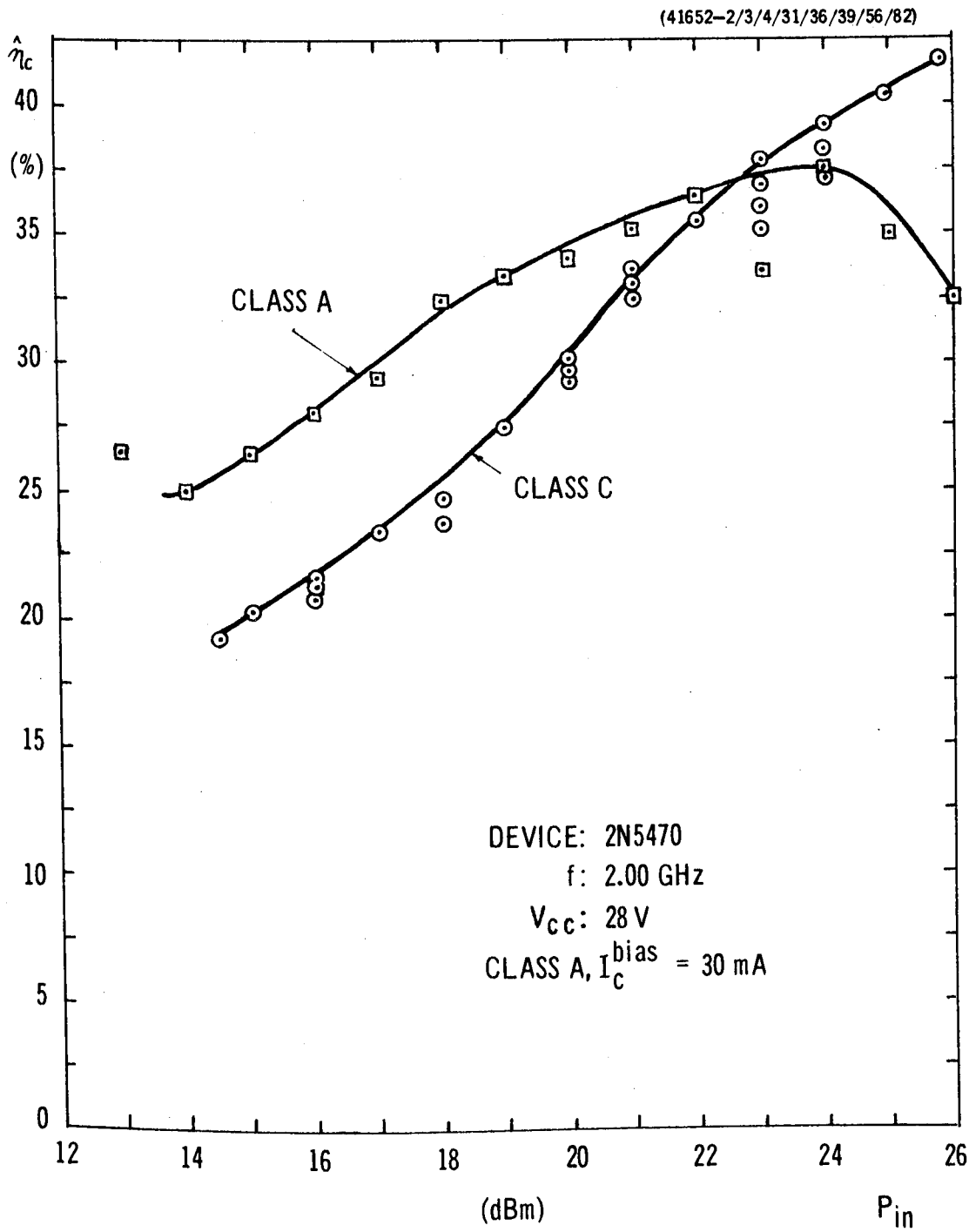

Figure 3–5 Maximum collector conversion efficiency $\hat{\eta}_c$ as a function of Pin, the amplifier always being tuned for maximum gain $\hat{G}$. Class A and Class C cases compared.

the dc-to-rf collector conversion efficiency η_c is measured for each value of P_{in}.

The complete test is performed under both class A and class C conditions.

Results

Figure 3-6 compares the bandwidths measured for the optimized class A and class C amplifiers, the incident power being the same in each case. For the chosen centre-frequency of 2.000 GHz, in addition to providing an extra dB of gain, the class A amplifier has a 1-dB bandwidth of 50 MHz, compared with a 1-dB bandwidth of 30 MHz for the class C amplifier.

Thus, under this condition at least, the only advantage likely to be offered by the class C mode will be in the area of efficiency. Figure 3-7 shows the "efficiency-response" the f, η_c-characteristic for the two modes. At the centre-frequency the efficiencies are nearly equal. As the frequency increases, however, the class C efficiency increases to a maximum of 44% at 2.017 GHz whereas the class A efficiency decreases steadily.

It should be pointed out that the coaxial amplifier circuit used for these tests is not intrinsically a broad-band circuit. Wider bandwidths could be obtained by using specially-designed matching networks, but then the ability to tune over large ranges of frequency and to match a wide variety of impedances would be lost.

Table 3(2) contains the frequency-response data used to generate Figures 3-6 and 3-7.

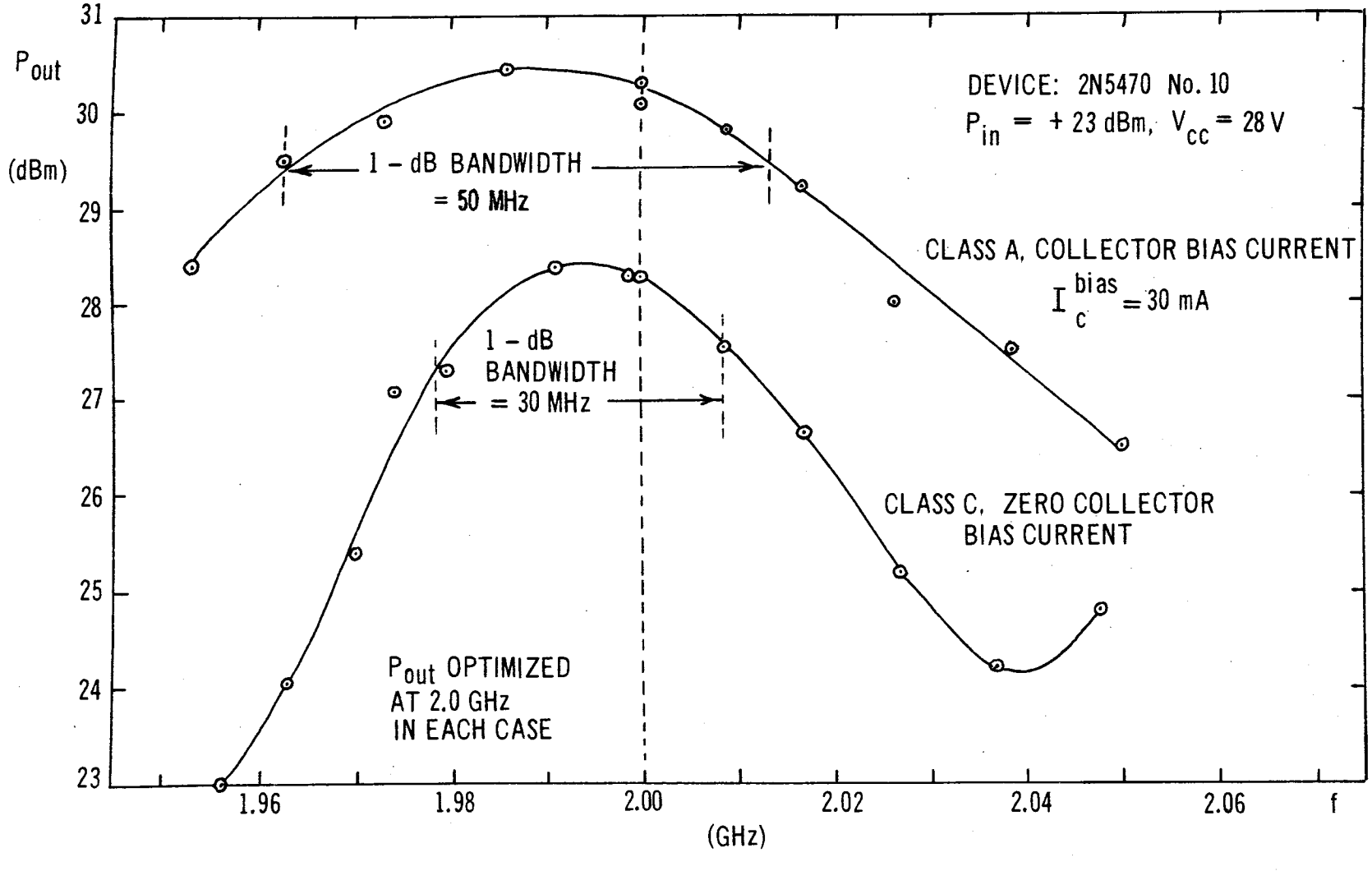

Figure 3–6 Bandwidth of coaxial slug-tuned amplifier: Class A and Class C compared

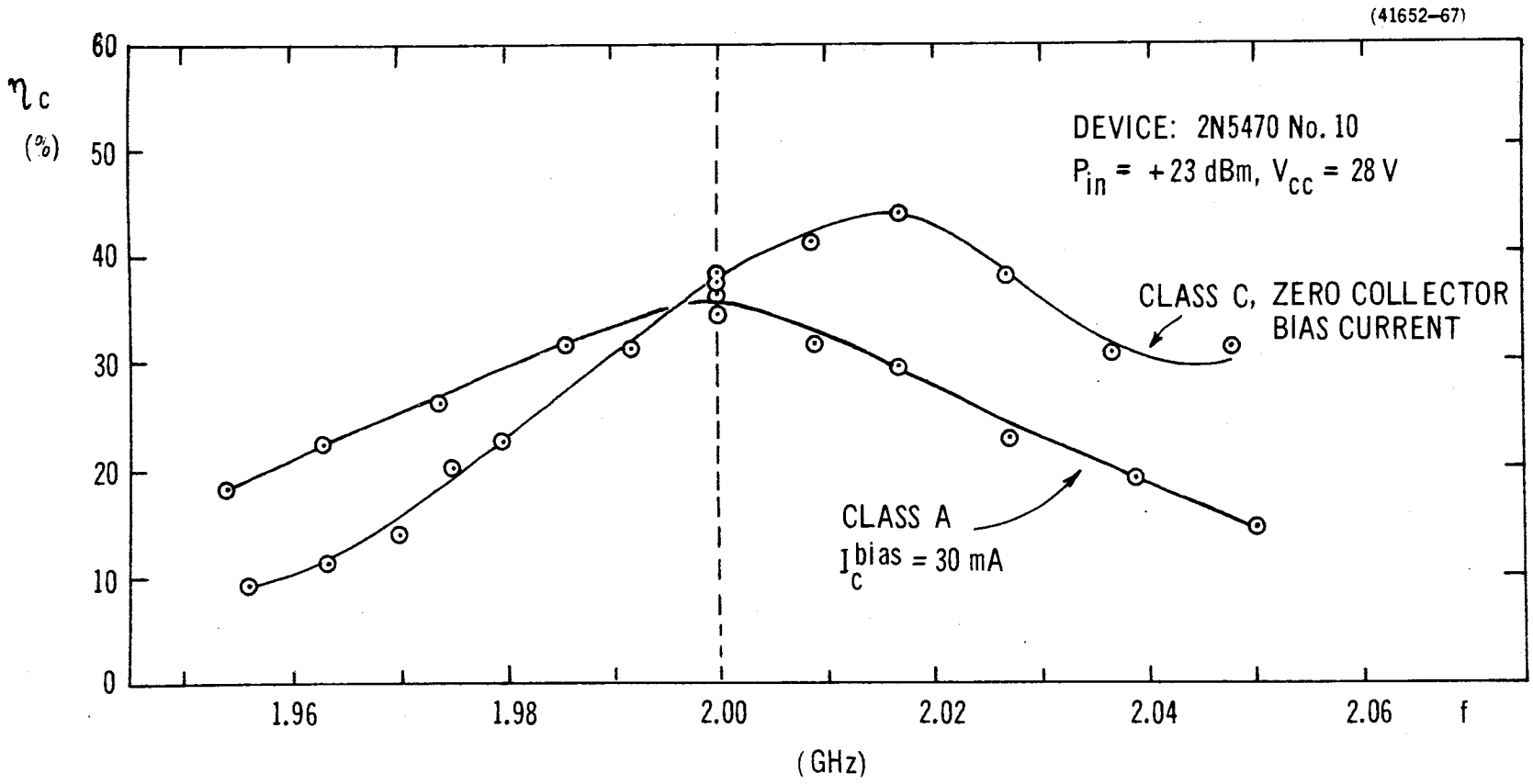

Figure 3–7 "Efficiency-response" of coaxial slug-tuned amplifier: Class A and Class C compared.

TABLE 3(2) FREQUENCY-RESPONSE MEASUREMENTS

Class A (P_{in} = + 23 dBm, I_c^{bias} = 30 mA)

f	P_{out}	I_c	Gain	η_c
GHz	dBm	mA	dB	%
1.954	28.4	136	5.4	18.2
1.963	29.5	140	6.5	22.7
1.974	29.9	132	6.9	26.4
1.986	30.45	125	7.45	31.7
2.000	30.1	106	7.1	34.5
Optimized → 2.000	30.3	113	7.3	36.5
2.009	29.8	107	6.8	31.8
2.017	29.2	100	6.2	29.7
2.027	28.0	98	5.0	23.0
2.039	27.5	105	4.5	19.1
2.050	26.5	109	3.5	14.7

Amplifier optimized at 2.000 GHz in each case.

Class C (P_{in} = + 23 dBm, zero I_c^{bias})

f	P_{out}	I_c	Gain	η_c
GHz	dBm	mA	dB	%
1.956	23.0	76	0	9.4
1.963	24.1	81.5	1.1	11.3
1.970	25.4	88.0	2.4	14.1
1.975	27.1	90.0	4.1	20.4
1.980	27.3	93.0	4.3	20.6
1.992	28.5	81.0	5.5	31.3
1.999	28.3	65.0	5.3	37.2
Optimized → 2.000	28.3	63.0	5.3	38.4
2.009	27.55	49.5	4.55	41.1
2.017	26.65	37.5	3.65	44.0
2.027	25.20	31.0	2.20	38.1
2.037	24.2	30.5	1.2	30.8
2.048	24.8	34.4	1.8	31.4

The "dynamic" class A and class C P_{in},P_{out} - characteristics (for which the amplifier is not re-optimized at each power level) are compared in Figure 3-8. In each case the amplifier is optimized for P_{in} = +23 dBm. At this value of P_{in}, the output power is approximately 1 dB more for class A than for class C. As P_{in} is decreased, however, the class C output power starts to fall off drastically when P_{in} reaches about +20 dBm, whereas the class A output power is such that the gain G is still increasing at P_{in} = +13 dBm. By comparison, the class C gain has fallen to OdB at $P_{in} \approx$ +19 dBm.

Figure 3-9 depicts the "dynamic" gain for the two modes of operation. The strong dependence of the class C gain on P_{in} is apparent.

3.1.4 Measurement of amplitude - modulation-to-phase-modulation (AM-to-FM) conversion factor.

Procedure

Using the same conditions as before, and again without altering the tuning/matching adjustments, the characteristic relating the output phase-angle ϕ_{out} to P_{in} is measured at the centre of the band. A static test such as this is permissible for a microwave transistor with its relatively very small thermal inertia. A TWT, on the other hand, has a rather large thermal inertia and requires dynamic modulation for a meaningful test.

Having obtained the P_{in},ϕ_{out} phase-nonlinearity characteristic, the objective here is to determine the P_{in},$(\partial\phi_{out}/\partial P_{in})$ - curve and see whether it correlates with the P_{in},$(\partial P_{out}/\partial P_{in})$ - curve, where

(41652-58/74/76/78)

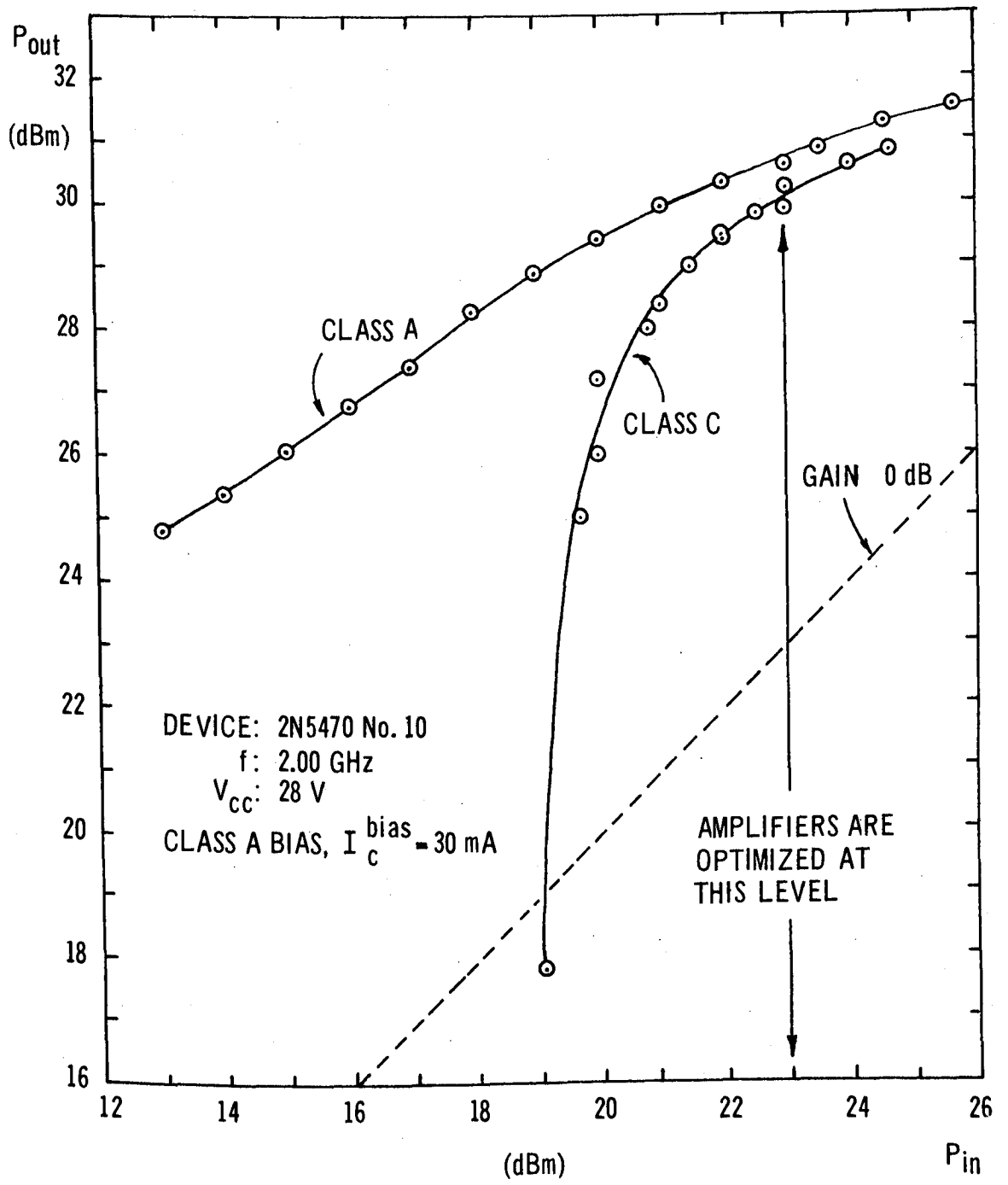

Figure 3-8 Class A and Class C P_{in}, P_{out} – characteristics compared. In each case the amplifier is optimized at P_{in} = 23 dBm. It is not thereafter retuned for other values of P_{in}.

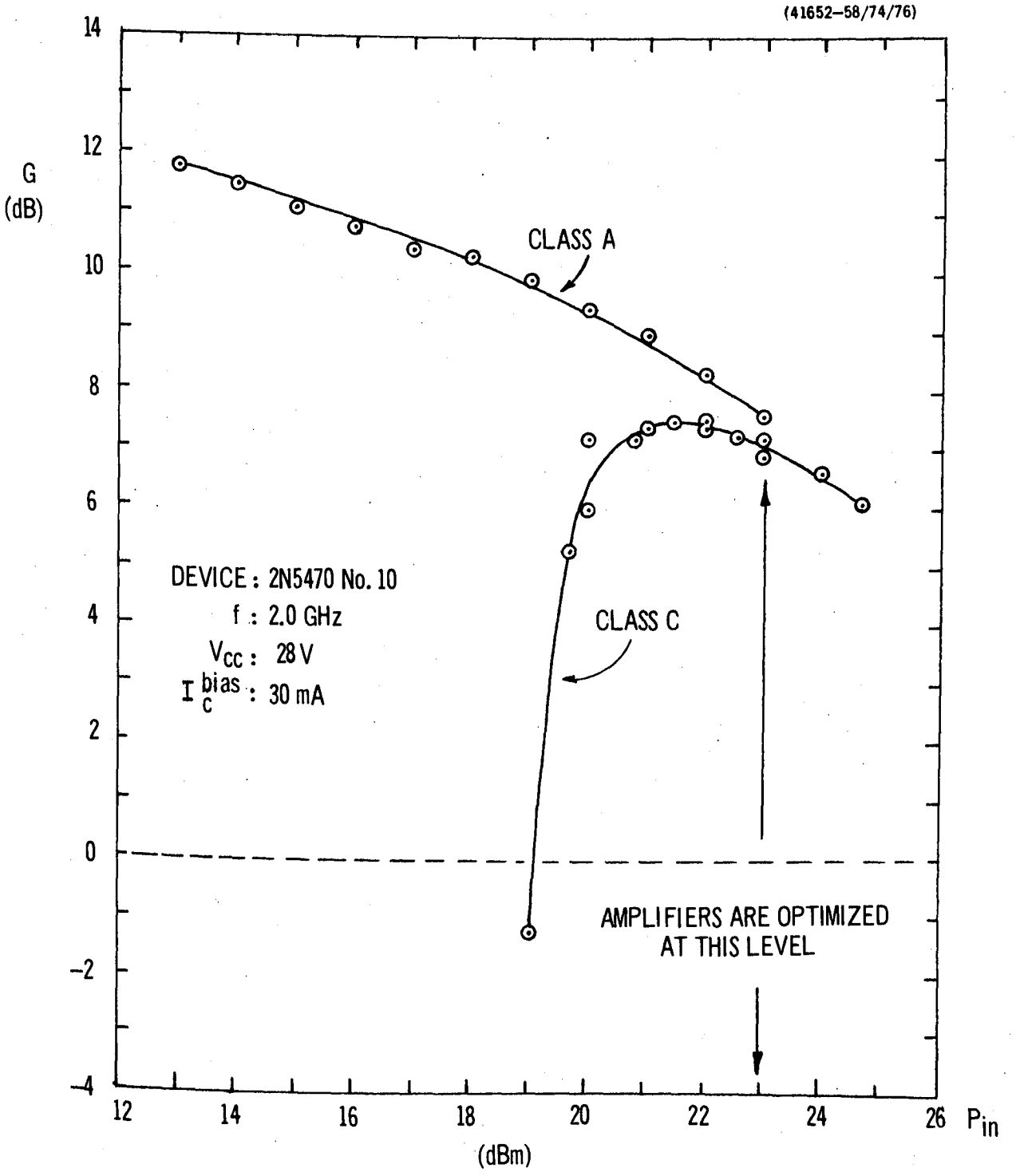

Figure 3-9 Class A and Class C gain G as functions of input power P_{in}. The amplifiers are optimized at P_{in} = +23 dBm

where $(\partial P_{out}/\partial P_{in})$ is the incremental, rather than the absolute, gain.

The set-up used to determine the phase-nonlinearity characteristic is depicted in Figure 3-10. A 2.0 GHz input signal is split into two branches by means of the HP 8740A transmission test unit. One branch is amplified before entering the transistor amplifier via a circulator. A directional coupler is included to permit the incident power to be monitored. The other branch provides the reference signal for the phase-angle measurement and is fed via an adjustable attenuator to the "reference" input of the HP 8411A harmonic frequency converter. The output of the amplifier goes to the "test" input of the harmonic frequency converter via a second directional coupler (allowing P_{out} to be monitored) and attenuator. The analog output of the frequency converter is fed to the network analyser for measurement of the relative phase-angle between the signals in the "reference" and "test" channels.

Results

Figure 3-11(a) shows the relative phase shift of the amplifier output compared with the input. In both class A and class C cases, the phase reference is set to zero at the maximum value of P_{in}, which in this case is +23 dBm.

In the class A mode, the phase shift increases with decreasing P_{in} at an initial rate of approximately 3°/dB, falling to 0°/dB at P_{in}=14.5 dBm. This AM-to-FM conversion characteristic is given explicitly in Figure 3-11(b), and is similar to Sunde's result for a TWT[4,p.142].

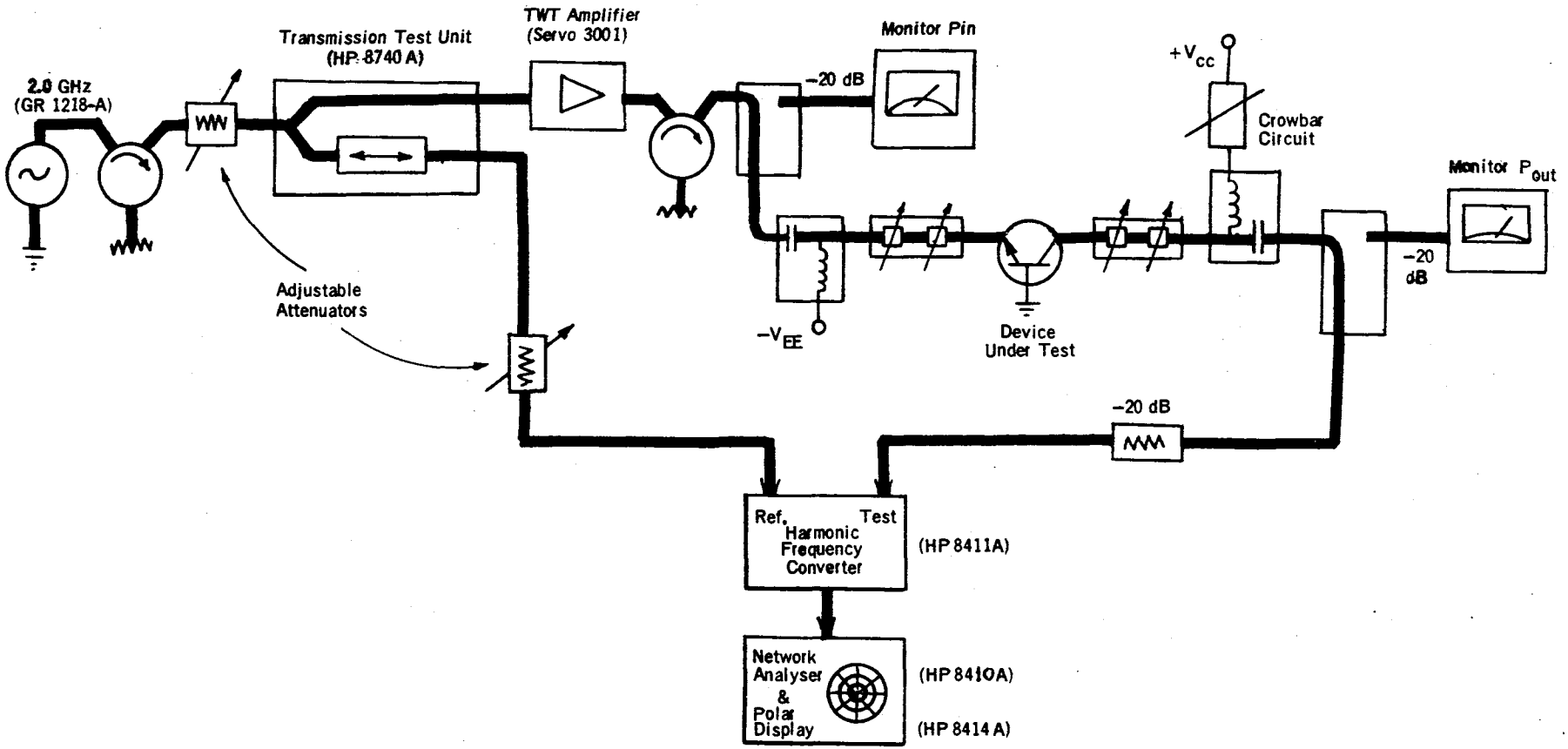

Figure 3-10 Set-up for AM-to-PM conversion measurements

(41652-74/76)

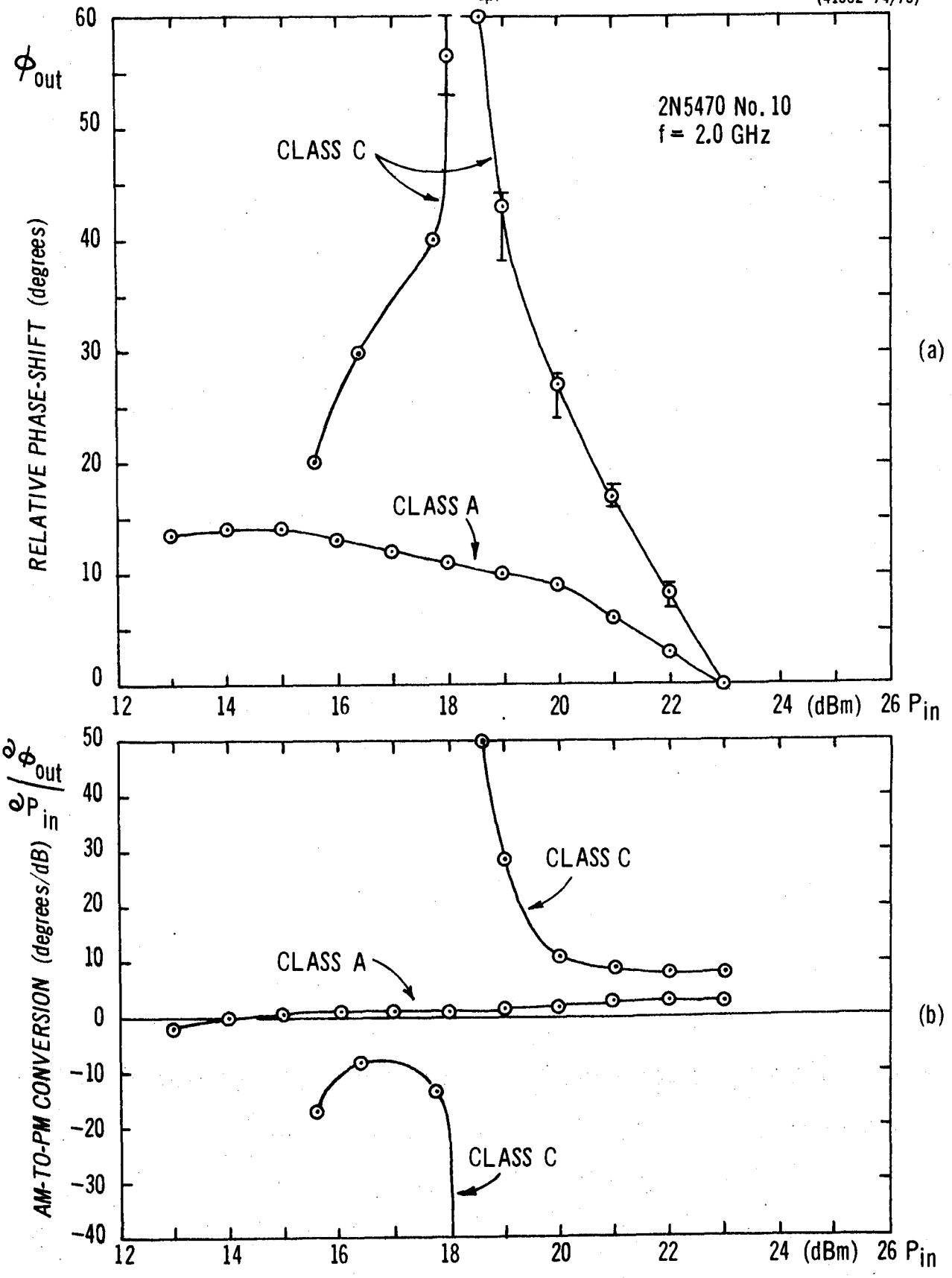

Figure 3-11(a) – Relative phase-shift as a function of P_{in}, Class A and Class C compared. Phase reference zero is for P_{in} = 23 dBm.

Figure 3-11 (b) – Corresponding AM-to-PM conversion $(\partial \phi_{out})/(\partial P_{in})$ as a function of P_{in}

In the class C mode, the AM-to-PM conversion is approximately 8.4°/dB at the 23 dBm maximum input level, but rapidly increases to as much as 50°/dB at P_{in} = 18.6 dBm. This drastic behaviour correlates with the class C P_{in},P_{out} - characteristic depicted in Figure 3-8. This it can be seen that large values of AM-to-FM conversion are associated with correspondingly large values of $\partial P_{out}/\partial P_{in}$. That portion of the class C AM-to-PM conversion characteristic lying in the range +15 to +18 dBm corresponds to an amplifier gain of less than zero dB and is therefore not of any practical significance.

3.2 Two-Carrier Tests

The tests described in this section are again performed under both class A and class C conditions.

For these measurements two carriers, usually of equal level, are injected into the amplifier, the frequency separation lying well within the amplifier bandwidth and the total power being sufficient to achieve amplifier saturation. Then the amplifier is tuned for maximum total output power $\hat{P}_o$. Having checked whether the two carriers appear with equal amplitudes at the amplifier output, the following characteristics are measured from saturation down to zero gain, the tuning and matching adjustments being left undisturbed:

(1) The power output as a function of the power input; i.e. the P_{in},P_{out} - characteristic.

(2) The gain as a function of the input; i.e. the P_{in}, G-characteristic.

(3) Collector conversion efficiency η_c as a function of the input; i.e. the P_{in},η_c - characteristic.

(4) The levels of the intermodulation products as functions of P_{in}.

Procedure

Two-carrier tests are carried out using a set-up similar to the one shown in Figure 3-10, with the difference that the circuitry to the left of the plane XX is as shown in Figure 3-12.

Signals from two separate oscillators at frequencies 2.000 GHz + Δf and 2.000 GHz - Δf (where Δf is a few MHz) are combined in the -10 dB directional coupler. The 10 dB loss in the side-arm of the coupler is compensated by the TWT amplifier. Provision for simultaneously varying the amplitudes of the two signals is made by including a variable attenuator.

Each source is isolated from the other by a circulator terminated at the third port. This is necessary to ensure that the input circuit itself does not generate intermodulation products of appreciable magnitude.

Figure 3-13 shows photographs of typical intermodulation distortion spectra obtained with two carriers. The upper spectrum is for class A with a dc bias of 30 mA applied to the transistor, while the lower spectrum is for class C with zero applied bias. The total incident power is the same under both bias conditions. The only noteworthy difference apparent between the two spectra at the maximum level is that the olass C intermodulation spectrum is somewhat more symmetrioal about the two oarriers. Interesting differenoes begin to appear when the input level is reduced, as discussed in Section 3.2.4.

3.2.1 The two-carrier P_{in},P_{out} - characteristics

When two carriers are used, the general shape of the P_{in},P_{out} -

(41652-94)

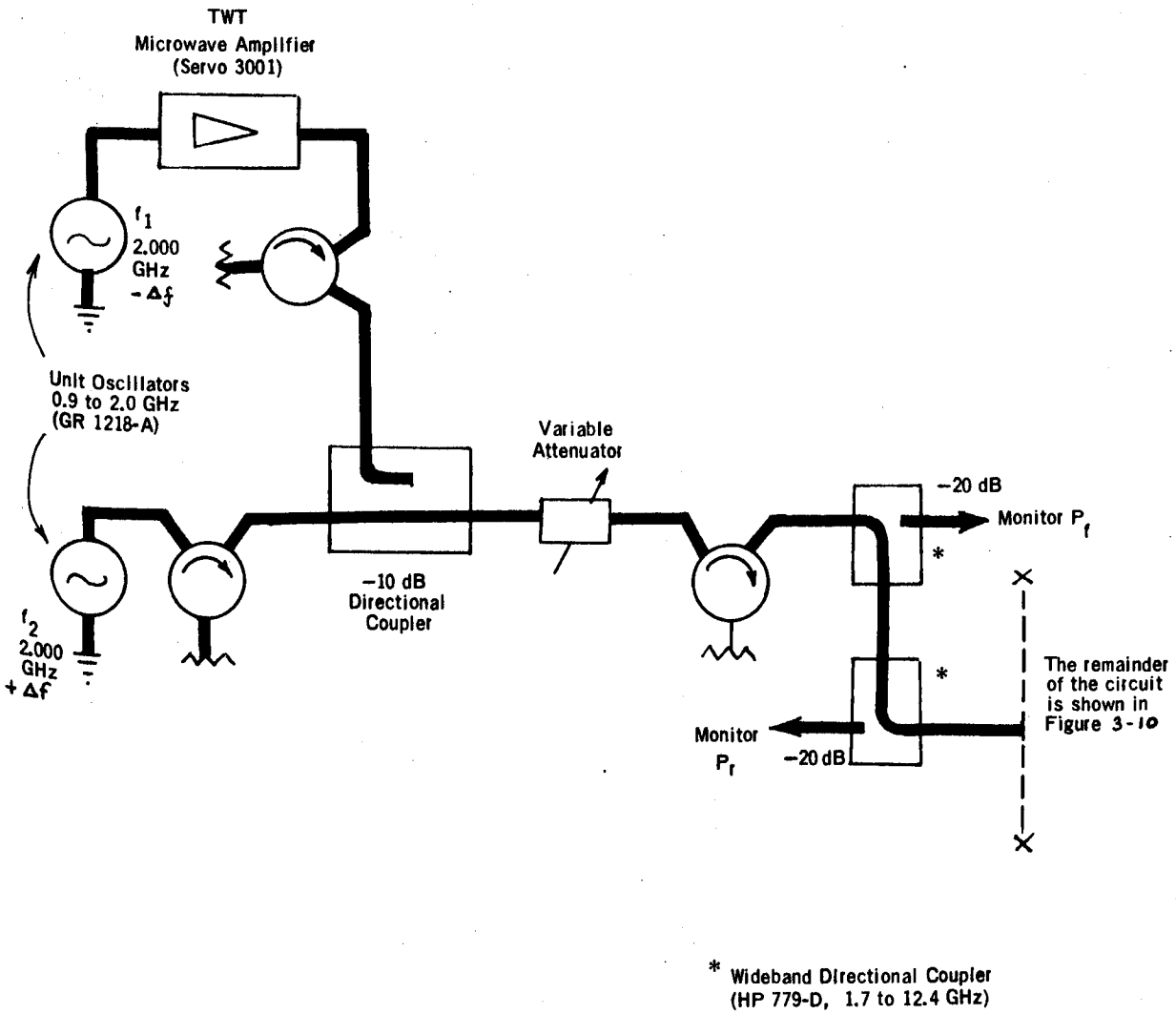

Figure 3–12 Modifications to the input circuitry required for the two-carrier tests.

(41652-71)

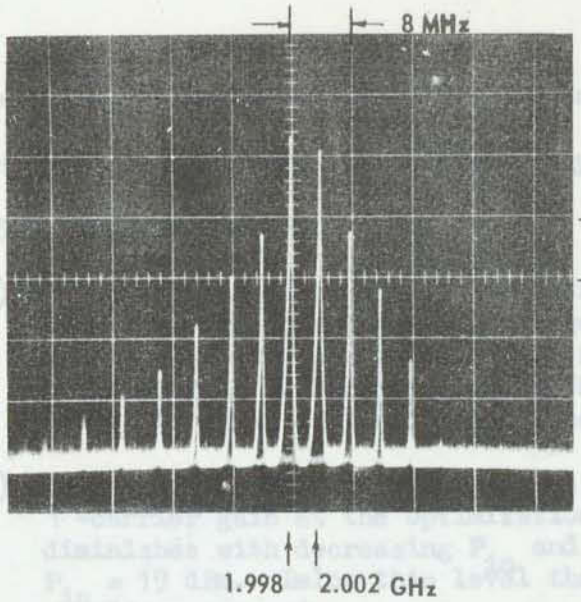

(41652-71)

(a) Class A

(41562-69)

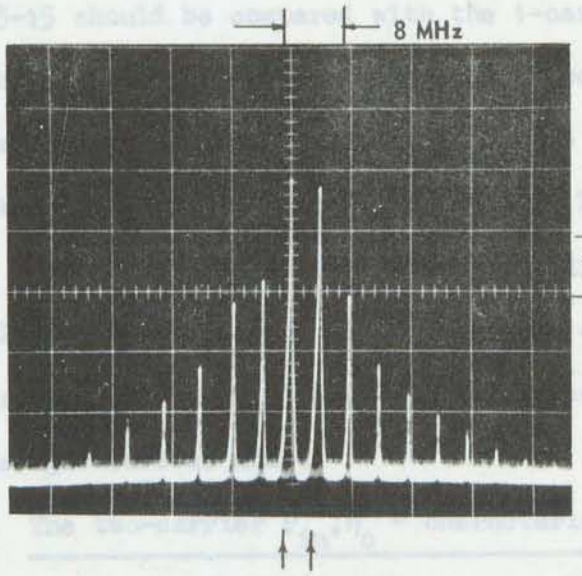

(41562-69)

(b) Class C

Figure 3-13 Intermodulation distortion spectra due to two equal carriers:

(a) Class A; collector bias $I_c^{bias} = 30$ mA

(b) Class C; zero bias

Device: 2N5470 No. 10, $P_{in} = 23$ dBm, $f_1 = 1.998$ GHz,

$f_2 = 2.002$ GHz ($\Delta f = 4$ MHz).

characteristic is similar to the curve obtained in the single-carrier case. However, the following differences may be seen by comparing Figure 3-14 with Figure 3-8:

(a) The 2-carrier class A gain is consistently 1 dB less than the corresponding 1-carrier gain, all other conditions being unchanged. This result is similar to the 1.2 dB difference reported by Sunde [4, page 131] for a TWT under comparable conditions.

(b) The 2-carrier class C gain is some 2.5 dB less than the 1 -carrier gain at the optimization level; this difference diminishes with decreasing P_{in} and becomes zero for P_{in} = 19 dBm. Below this level the two-carrier case provides more gain.

3.2.2 The two-carrier P_{in}, G-characteristic

The two-carrier gain versus input power curves shown in Figure 3-15 should be compared with the 1-carrier curves of Figure 3-9. The class A two-carrier gain is also consistently 1 dB less than the one-carrier gain, increasing from G = 6.5 dB at the optimizing level to 10 dB at P_{in} = 14 dBm. The class C two-carrier gain is as much as 3 dB below the corresponding single-carrier gain. It reaches a peak of 4.4 dB at P_{in} = +21 dBm. Thereafter, it falls steadily as P_{in} decreases, though not as drastically as in the single-carrier mode.

3.2.3 The two-carrier P_{in}, η_c - characteristic

Of particular importance in satellite applications is the collector conversion efficiency η_c. Figure 3-16 shows that in the two-carrier case, class C provides a greater efficiency than does class A provided P_{in} > 20 dBm. At the optimization level, the maximum class C efficiency is 38.2% compared with the 28.9% obtained for class A.

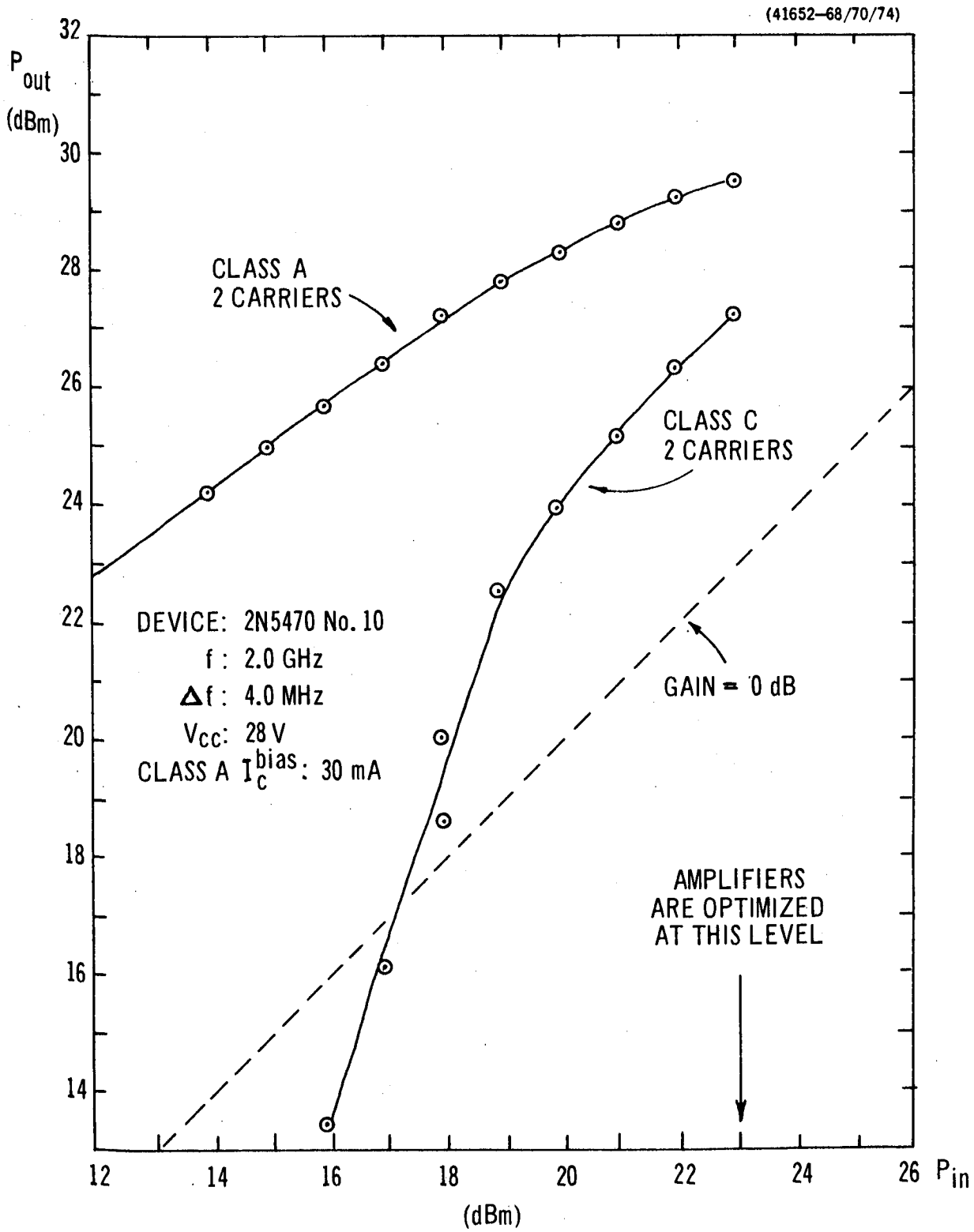

Figure 3-14 Two-carrier Class A and Class C P_{In}, P_{out} -characteristics compared. P_{In} is the TOTAL incident power. In each case the amplifier is optimized for P_{In} = +23 dBm.

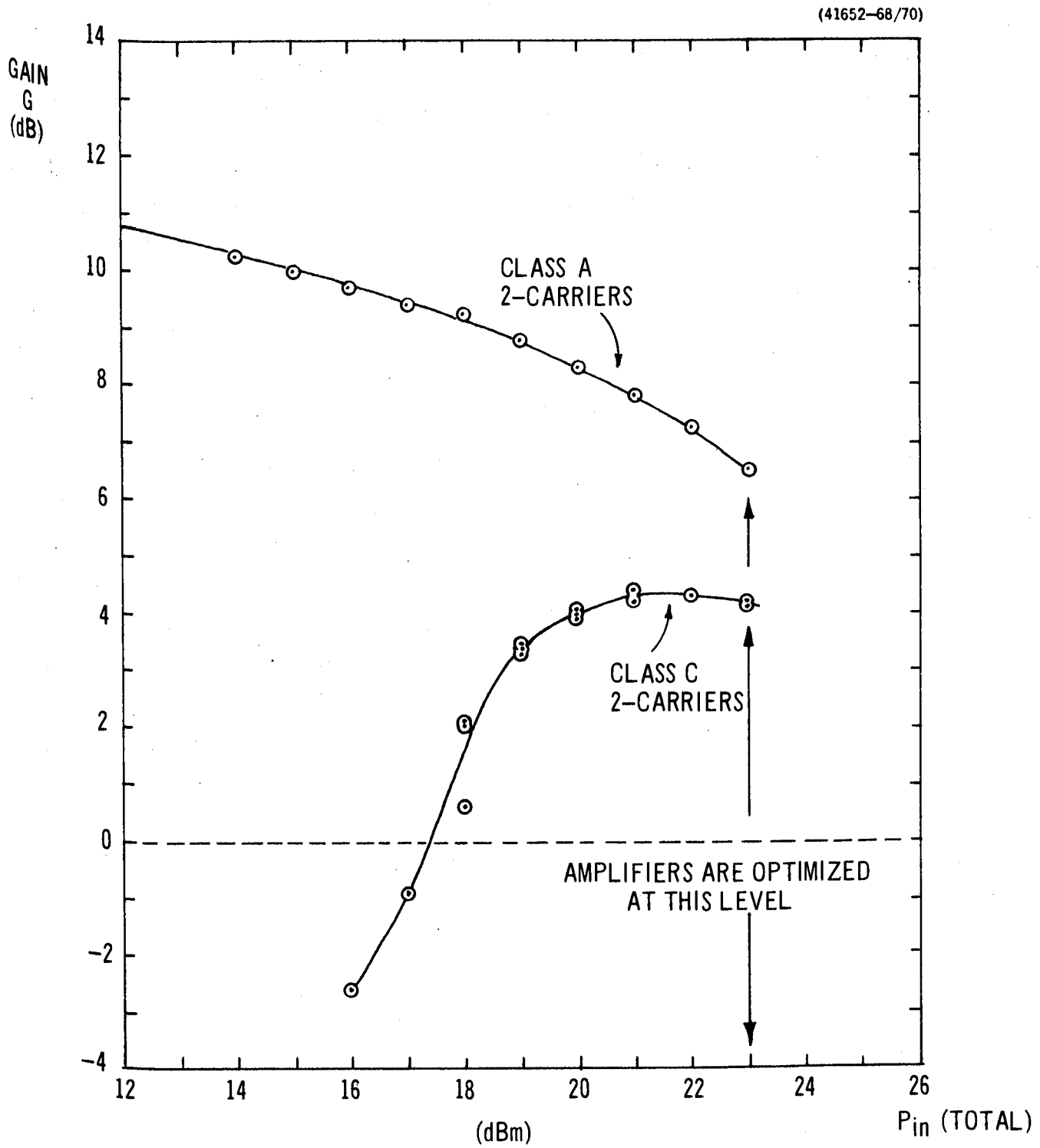

Figure 3-15 Two-carrier P_{in}, G -characteristics for the Class A and Class C modes. The amplifier is optimized at P_{in} = 23 dBm in each case.

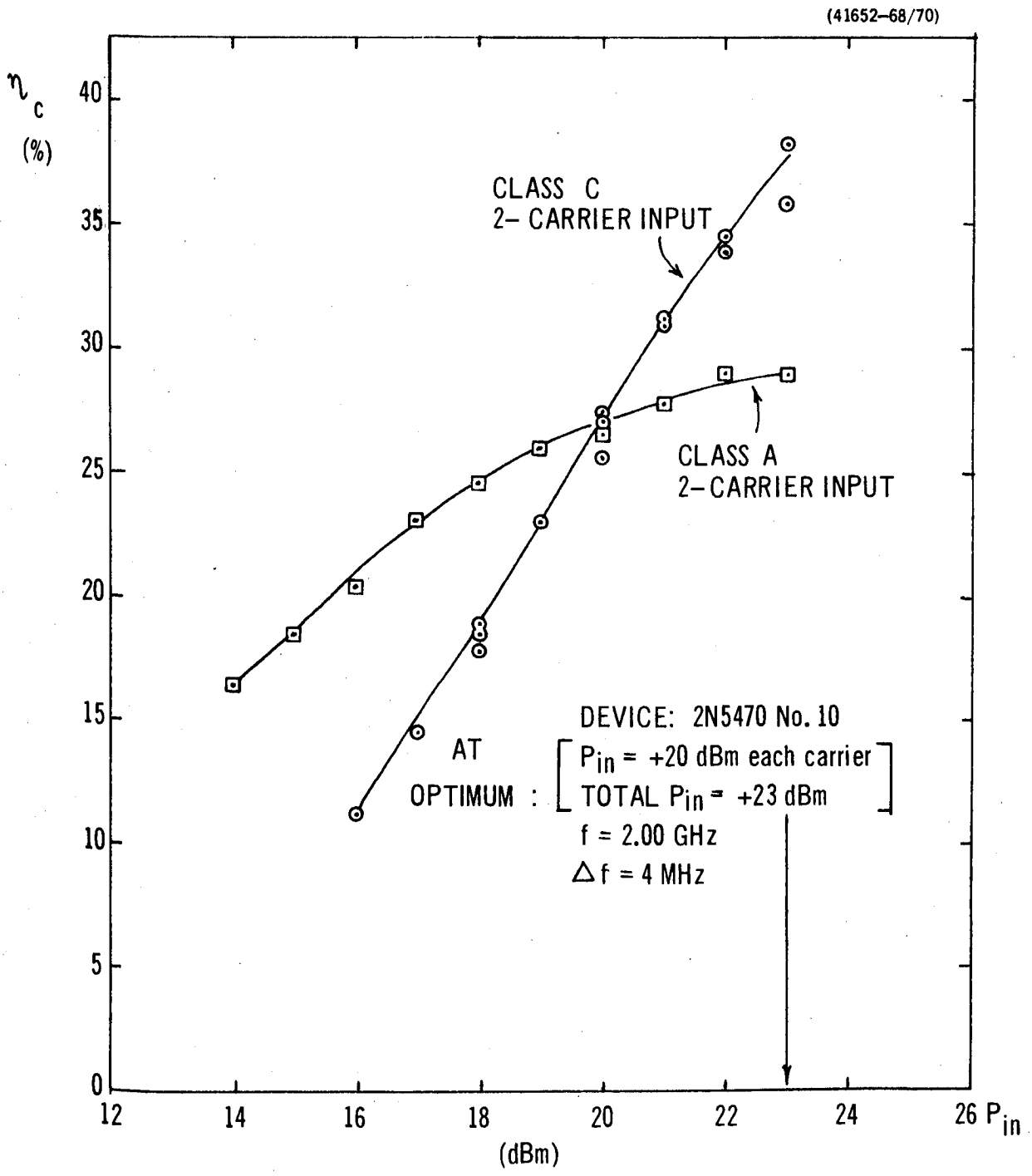

Figure 3-16 Collector conversion efficiency η_c versus P_{in} for two-carrier input. Class A and Class C modes compared.

3.2.4 Levels of intermodulation products as functions of P_{in}

Figure 3-17 summarizes the results of measurements of the dependence of the levels of intermodulation products on P_{in} for the class A mode. The dc bias used is 30 mA. For these measurements the amplifier is gain-optimized for P_{in} = +23 dBm and the tuning and biasing adjustments are not changed thereafter.

Figure 3-17(a) depicts the lower-frequency carrier f_1 and the four adjacent intermodulation products:

$2f_1 - f_2$

$3f_1 - 2f_2$

$4f_1 - 3f_2$

$5f_1 - 4f_2$,

while Figure 3.17(b) shows the higher-frequency carrier f_2 and the other four adjacent intermodulation products:

$2f_2 - f_1$

$3f_2 - 2f_1$

$4f_2 - 3f_1$

$5f_2 - 4f_1$

In both cases the power reference level is that of the greatest carrier, which in this case is the carrier f_1. As might be expected from Figure 8 of reference [4] (which actually relates to TWT operation), over the useful input power range, the levels of the intermodulation products relative to that of the greatest carrier (f_1), tend to decrease with diminishing input power P_{in}. However, for the important third-order products $2f_1-f_2$ and $2f_2-f_1$ (particularly the former) the levels are only slightly dependent on P_{in}.

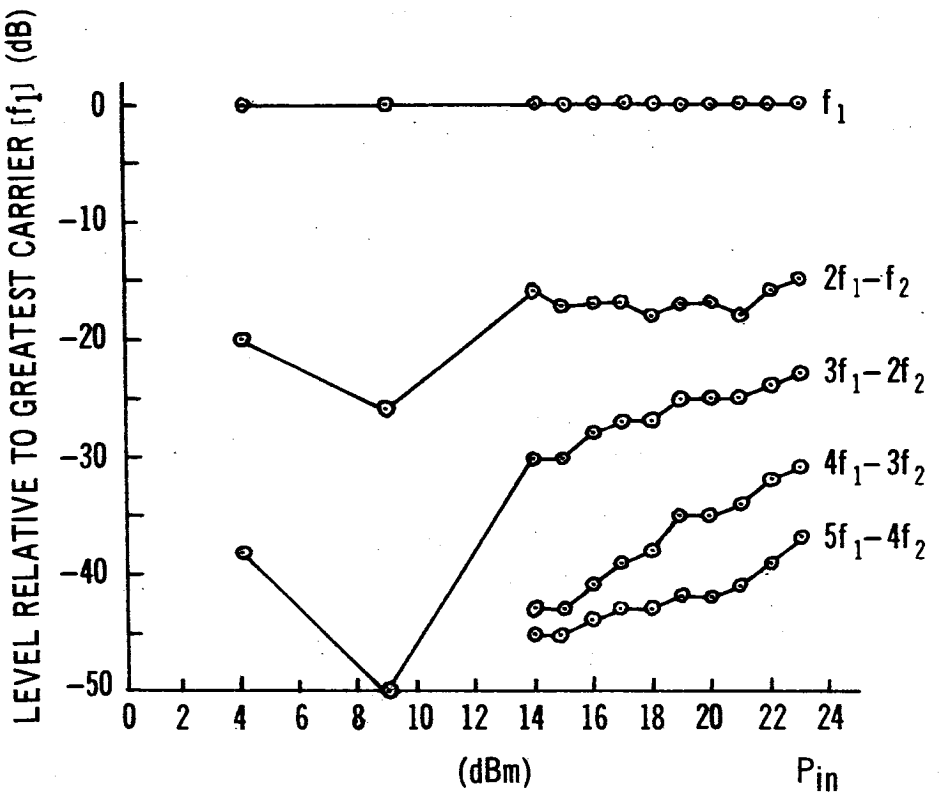

Figure 3–17(a) Class A relative levels of lower carrier (f_1) and intermodulation products as functions of incident power.
[f = 2.0 GHZ, f_2-f_1 = 4.0 MHz, 2N5470, V_{cc} = 28 V]

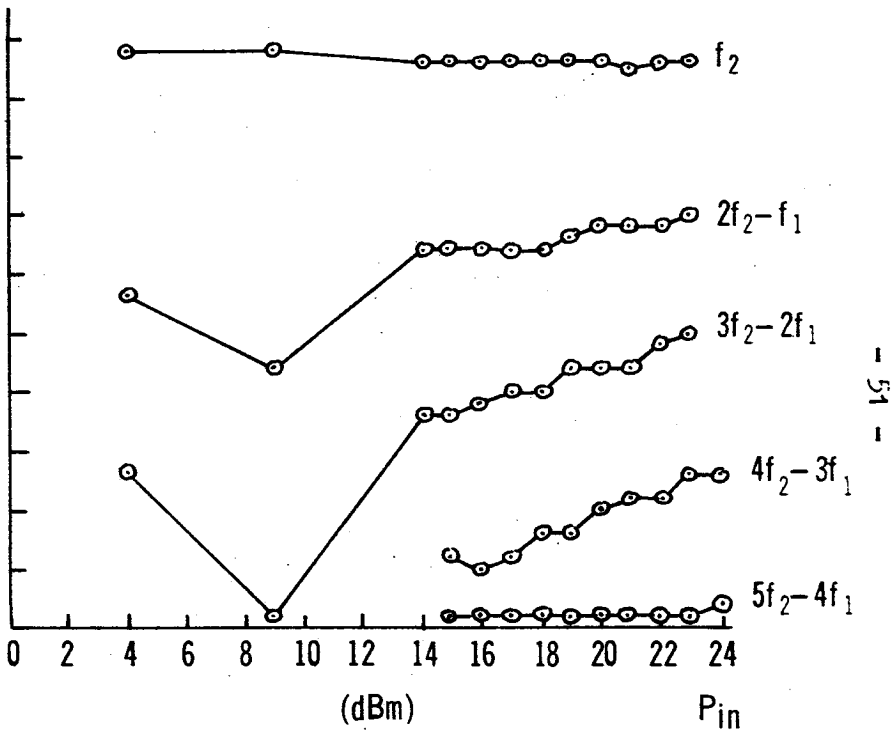

Figure 3–17(b) Class A relative levels of upper carrier (f_2) and intermodulation products as functions of incident power.

Detailed measurements are given for the range 14 dBm $\leq P_{in} \leq$ 24 dBm; additional results are included for P_{in} = 4 and 9 dBm.

Figure 3-18 shows the corresponding results obtained in the class C case, plotted to the same scale as in Figure 3-17 to facilitate comparison between the two modes. Results are not given for P_{in} < 16 dBm, because of the drastic fall-off of gain at that level. The behaviour of the intermodulation products as P_{in} decreases is completely different from the class A case. For all the products, the functional dependancy is much more "wild": indeed the third-order products both tend to increase in relative level as P_{in} is reduced. Other products show increases, decreases or oscillating behaviour. In general it appears that the power-level "backing-off" procedure conventionally used to reduce intermodulation noise in TWTs would not be advantageous in a transistor operating in the class C mode.

3.2.5 Summary of two-carrier measurements

The measured class A numerical data for the two-carrier tests described in section 3.2 are given in Table 3(3); the corresponding class C numerical data is contained in Table 3(4). In addition to the observed values of individual intermodulation products over a range of input power levels, these tables also give information on the input power P_{in}, the gain G and the dc-to-rf collector conversion efficiency η_c.

3.2.6 Possible further two-carrier measurements

Measurements which might be included in a wider study could include the following:

(41652–69)

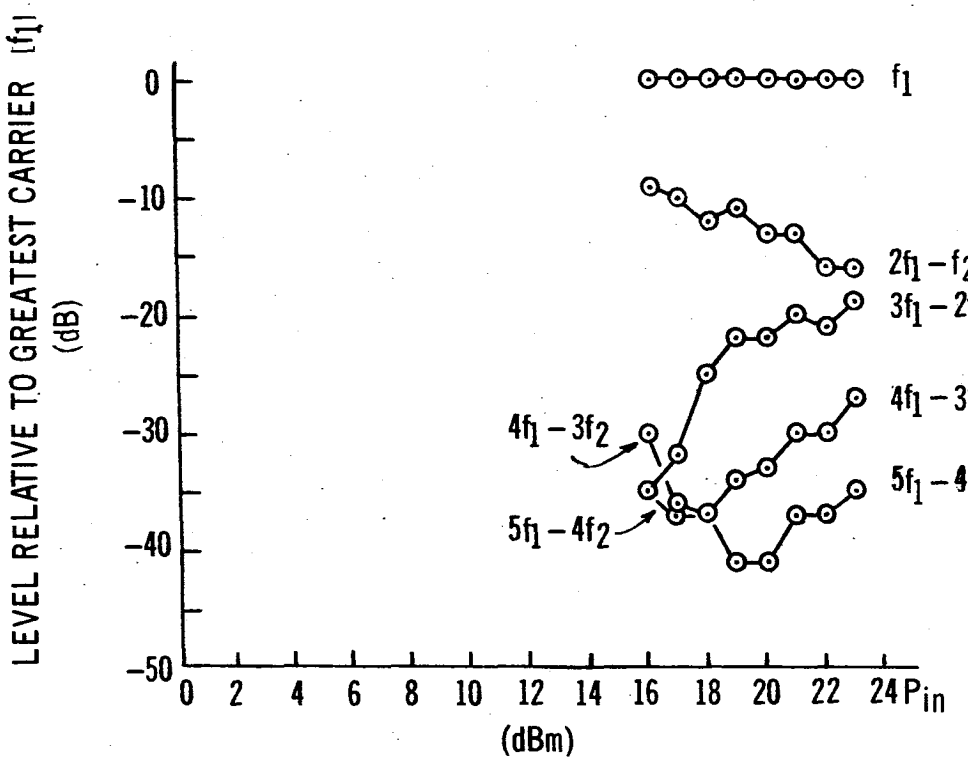

Figure 3–18(a) Class C relative levels of lower carrier (f_1) and intermodulation products as functions of incident power. Scales same as for Class A case to facilitate comparison.

[f = 2.0 GHz, $f_2 - f_1$ = 4 MHz, 2N5470, V_{cc} = 28 V]

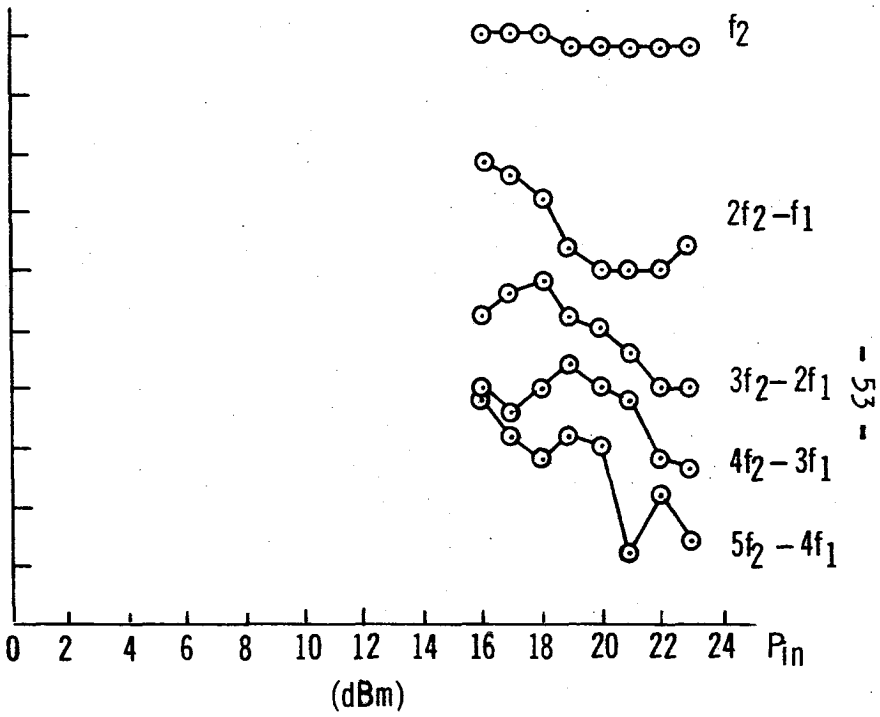

Figure 3–18(b) Class C relative levels of upper carrier (f_2) intermodulation products as functions of incident power.

TABLE 3(3) - CLASS A PERFORMANCE WITH TWO CARRIERS

$f \cong 2.0$ GHz, $\Delta f = 4$ MHz (41652-70)

Device = 2N5470 No. 10

$V_{cc} = 28$ volts, $I_c^{bias} = 30$ mA dc.

Tuned for maximum P_{out} when $P_{in} = +23$ dBm total.

P_{in}	G	P_{out}	I_c	η_c	Intermodulation products in dB relative to greatest carrier									
					Lower Sidebands				Carriers		Upper Sidebands			
(dBm)	(dB)	(dBm)	(mA)	(%)	$5f_1-4f_2$	$4f_1-3f_2$	$3f_1-2f_2$	$2f_1-f_2$	f_1	f_2	$2f_2-f_1$	$3f_2-2f_1$	$4f_2-3f_1$	$5f_2-4f_1$
+23	6.5	29.5	110	28.9	-37	-31	-23	-15	0	-2	-15	-25	-37	-48
22	7.25	29.25	104	28.9	-39	-32	-24	-16	0	-2	-16	-26	-37	-49
21	7.8	28.8	98	27.65	-41	-34	-25	-18	0	-2.5	-16	-28	-39	-49
20	8.3	28.3	91	26.5	-42	-35	-25	-17	0	-2	-16	-28	-39	-49
19	8.8	27.8	83	25.9	-42	-35	-25	-17	0	-2	-17	-28	-40	-49
18	9.25	27.25	77	24.6	-43	-38	-27	-18	0	-2	-18	-30	-42	-49
17	9.4	26.4	72	21.6	-43	-39	-27	-17	0	-2	-18	-30	-42	-49
16	9.7	25.7	65	20.4	-44	-41	-28	-17	0	-2	-18	-31	-44	-49
15	10.0	25.0	61	18.5	-45	-43	-30	-17	0	-2	-18	-32	-45	-49
14	10.25	24.25	58	16.4	-45	-43	-30	-16	0	-2	-18	-32	-44	-49
9	11.3	20.3	40	9.6	-	-	-	-26	0	-1	-28	-	-	-
4	12.6	16.6	27	6.0	-	-	-38	-20	0	-1	-22	-37	-	-

TABLE 3(4) - CLASS C PERFORMANCE WITH TWO CARRIERS

$f \cong 2.0$ GHz, $\Delta f = 4$ MHz (41652 -68)

Device = 2N5470 No. 10

V_{CC} = 28 volts

Tuned for maximum P_{out} when P_{in} = + 23 dBm total

P_{in}	G	P_{out}	I_C	η_C	Intermodulation products in dB relative to greatest carrier									
					Lower Sideband				Carriers		Upper Sidebands			
(dBm)	(dB)	(dBm)	(mA)	%	$5f_1-4f_2$	$4f_1-3f_2$	$3f_1-2f_2$	$2f_1-f_2$	f_1	f_2	$2f_2-f_1$	$3f_2-2f_1$	$4f_2-3f_1$	$5f_2-4f_1$
+23	4.1	27.1	51	35.9	-35	-27	-19	-16	0	-1	-18	-30	-37	-43
22	4.3	26.3	45	33.8	-37	-30	-21	-16	0	-1	-20	-30	-36	-39
21	4.4	25.4	40	31.0	-37	-30	-20	-13	0	-1	-20	-27	-31	-44
20	4.1	24.1	34	27.0	-41	-33	-22	-13	0	-1	-20	-25	-30	-35
19	3.4	22.4	27	23.0	-41	-34	-22	-11	0	-1	-18	-24	-28	-34
18	2.1	20.1	19.8	18.5	-37	-37	-25	-12	0	0	-14	-21	-30	-36
17	-.9	16.1	10	14.5	-37	-36	-32	-10	0	0	-12	-22	-32	-34
16	-2.6	13.4	6.3	12.4	-35	-30	-35	-9	0	0	-11	-24	-30	-31

3.2.6.1 Amplifier optimization for minimum IM distortion

For this test, two equal-level carriers would be injected into the amplifier. First, the amplifier would be tuned and matched to produce the maximum gain for a fixed P_{in}. Then the tuning and matching networks would be optimized for minimum intermodulation distortion while retaining a useful gain. Having obtained this optimum, its sensitivity would be determined by reducing P_{in} step-by-step and observing $\partial G/\partial P_{in}$ and $\partial(IM)/\partial P_{in}$ for each carrier.

3.2.6.2 Effect of bias on IMD minimization

The test envisaged here is similar to 3.2.6.1, but in this case, after maximizing G, the IMD would be minimized by varying the dc biassing only.

3.2.6.3 Minimization of IMD by varying tuning and biassing simultaneously

In this test, after maximizing G, the objective would be to minimize the IMD by varying the tuning and bias simultaneously.

3.3 Intelligible Cross-Talk Measurements

This section is divided into two parts: sections 3.3.1 and 3.3.2 deal respectively with two-carrier and with three-carrier cross-talk measurements.

3.3.1 Two-carrier cross-talk measurements

The purpose of these measurements is to introduce into the transistor amplifier under investigation a composite signal consisting of two carriers, both lying well within the passband of the amplifier. One carrier (f_2) is FM modulated, the other (f_1) is not. The measurement set-up corresponds to a complete microwave communications system. The objective is to determine to what extent the modulation on the f_2 carrier has been transferred to the originally unmodulated f_1 carrier by the time the signal reaches the receiver at the output end of the system.

3.3.1.1 Description of the complete system for two-carrier cross-talk measurements

In the description given below, the paragraph numbers correspond to the circled numbers in Figure 3-19. The somewhat curious frequencies chosen for the system are due to the many constraints imposed by the available equipment.

(1) A Hewlett-Packard 606A signal generator provides a baseband signal at a frequency f_b = 1, 2, 3, 4, 5 or 6 MHz.

(2) The baseband signal is fed to a 70 MHz FM modulator. The level of the signal is set (in this case to -32.8 dBm) to produce an RMS deviation of 200 KHz about the 70 MHz centre-frequency.

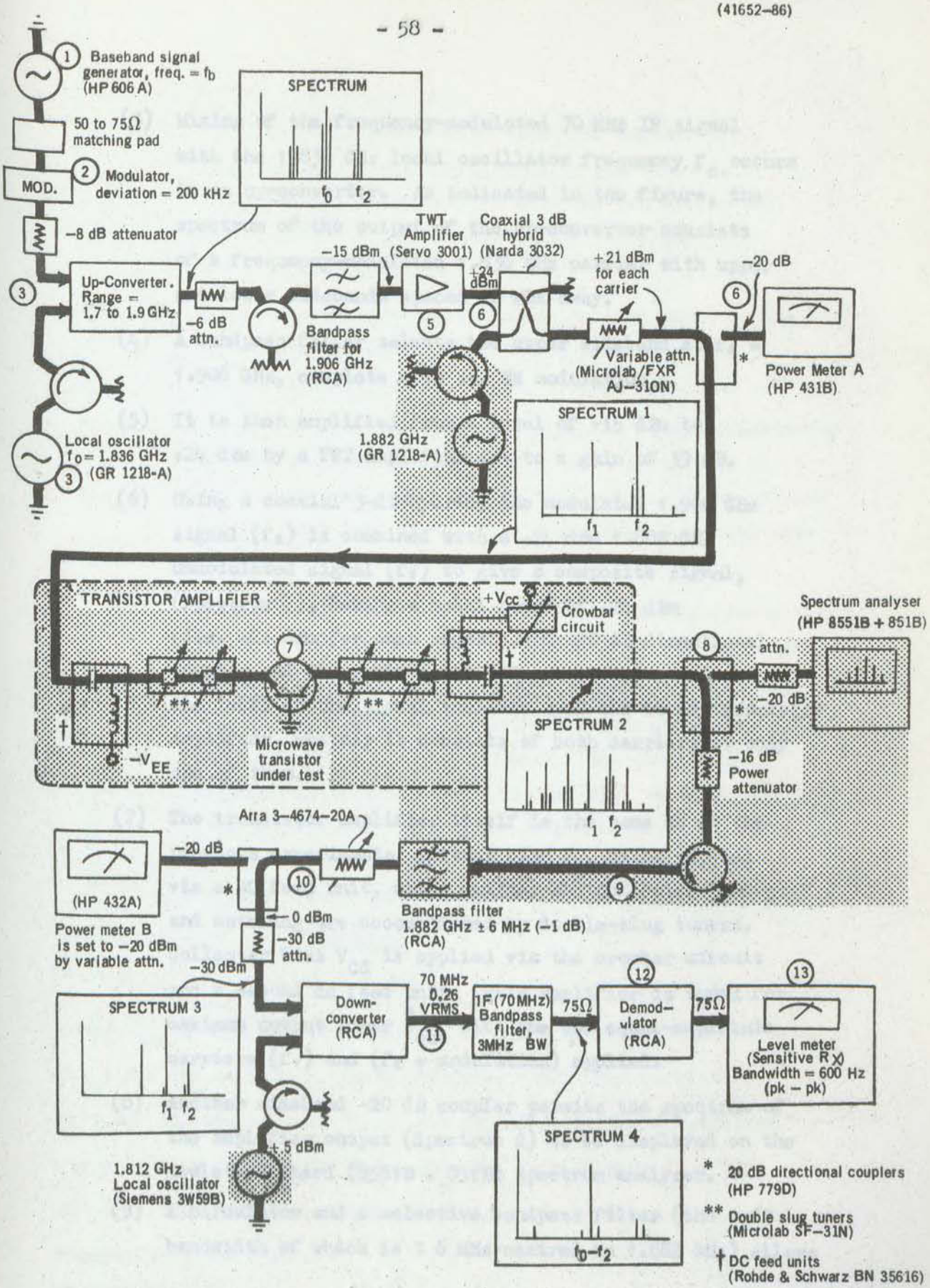

Figure 3–19 Set up for cross-talk measurements

(3) Mixing of the frequency-modulated 70 MHz IF signal with the 1.836 GHz local oscillator frequency f_o occurs in an up-converter. As indicated in the figure, the spectrum of the output of the up-converter consists of a frequency-modulated 1.836 GHz carrier with upper and lower sidebands spaced 70 MHz away.

(4) A bandpass filter selects the upper sideband at f_2 = 1.906 GHz, complete with its FM modulation.

(5) It is then amplified from a level of -15 dBm to +24 dBm by a TWT amplifier set to a gain of 39 dB.

(6) Using a coaxial 3-dB hybrid, the modulated 1.906 GHz signal (f_2) is combined with a +24 dBm 1.882 GHz unmodulated signal (f_1) to give a composite signal, (spectrum 1), having a total power of +24 dBm (i.e. +21 dBm for each signal). A -20 dB directional coupler and the power meter "A" are used to monitor the level of the signal incident upon the tuned transistor amplifier, whether it consists of both carriers or only one of them.

(7) The transistor amplifier itself is the same as in the previous experiments, emitter bias V_{EE} being applied via a DC feed unit, while emitter and collector tuning and matching are accomplished by double-slug tuners. Collector bias V_{CC} is applied via the crowbar circuit and a second dc feed unit. This amplifier is tuned for maximum output power $\hat{P}_{out}$ with the two equal-amplitude carriers (f_1) and (f_2 + modulation) applied.

(8) Another wideband -20 dB coupler permits the spectrum of the amplifier output (Spectrum 2) to be displayed on the Hewlett-Packard (8551B + 851B) spectrum analyser.

(9) A circulator and a selective bandpass filter (the 1-dB bandwidth of which is ± 6 MHz centred on 1.882 GHz) allows

the previously unmodulated 1.882 GHz carrier (f_1), plus the cross-talk transferred to it, to pass. Other signals are reflected back and are dissipated in the termination attached to the third port of the circulator.

(10) A variable attenuator is used to set the input to the down-converter to the appropriate level (-30 dBm in the present case).

(11) The output from the down-converter now consists basically of a 70 MHz carrier modulated by such cross-talk as it has acquired en route through the system. Other extraneous signals are removed by a 3 MHz bandwidth band-pass filter.

(12) Penultimately the 70 MHz signal enters the FM demodulator (a ratio detector). The output is an AM baseband signal.

(13) Finally the level of this baseband signal is measured using a level meter* (a sensitive receiver) set to a bandwidth of 600 Hz peak-to-peak. The cross-talk measured by this receiver (in dBm) will be substracted from the separately-measured reference level of the system itself to yield the final cross-talk values for the transistor amplifier.

3.3.1.2 Initial adjustments

First, the transistor amplifier is tuned for maximum total output power $\hat{P}_{out}$ with an input consisting of two equal-amplitude carriers. The 1.906 GHz carrier f_2 is FM modulated; the other carrier f_1, at 1.882 GHz GHz is not. Since the amplifier is to be optimized for a maximum input power $\hat{P}_{in}$ = +24 dBm, each carrier is set to +21 dBm. The composite input signal is designated Spectrum 1 in Figures 3-19 and 3-20(a).

---

* Wandel and Goltermann type TFPM - 43/BN 8619

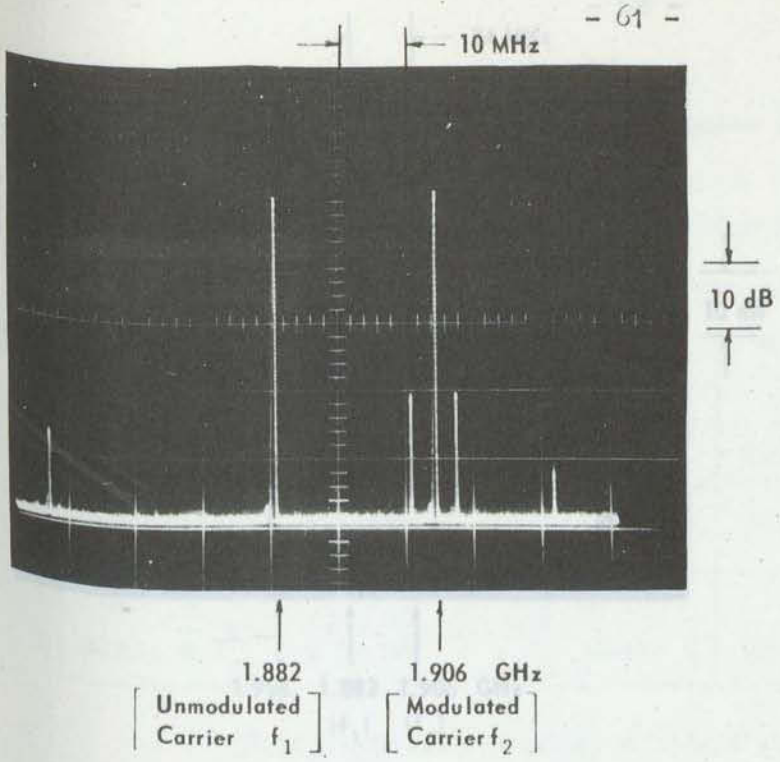

Figure 3–20 (a)
Spectrum of amplifier input signal for cross-modulation test.
[Spectrum 1, Figure 3–19]

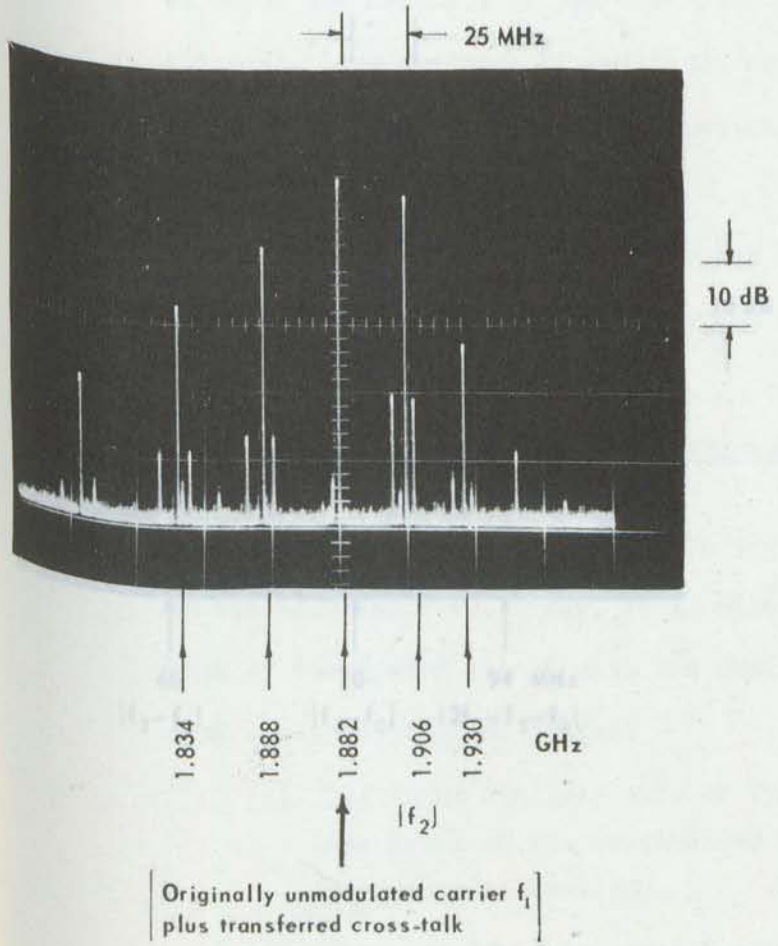

Figure 3–20 (b)
Spectrum of amplifier output signal for cross-modulation test.
[Spectrum 2, Figure 3–19]

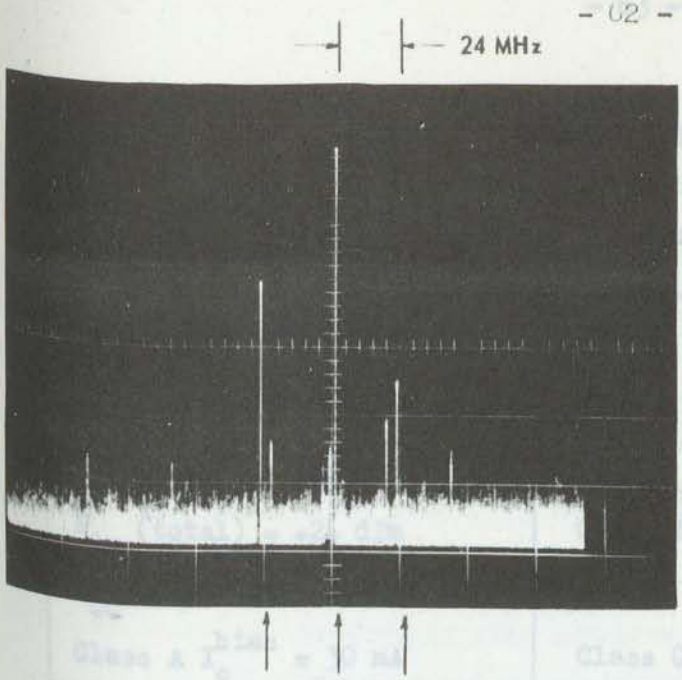

Figure 3–20(c)
Spectrum at input to down-converter.
[Spectrum 3, Figure 3–19]

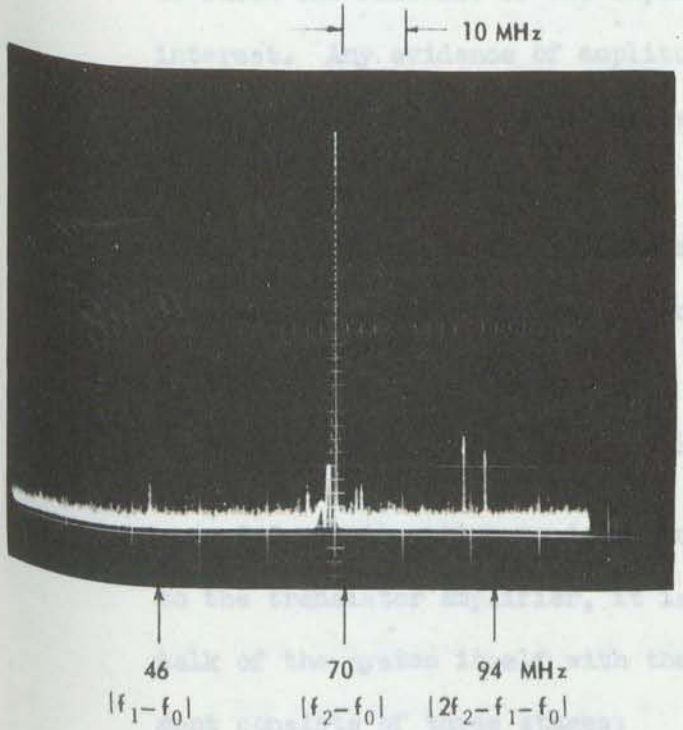

Figure 3–20(d)
Spectrum at input to demodulator.
[Spectrum 4, Figure 3–19]

The optimized performance figures are summarized in Table 3(5).

Table 3(5) - Optimized performance for 2-carrier cross-talk tests

f_1 = 1.882 GHz, unmodulated f_2 = 1.906 GHz, FM modulated $\hat{P}_{in}$ (total) = +24 dBm V_{CC} = 28 volts Class A I_o^{bias} = 30 mA	Mode	P_{out} (dBm)	Gain G (dB)	I_C^{DC} (mA)	Efficiency η_c (%)
	Class A	30.2	6.2	128	29.2
	Class C	29.45	5.45	100	31.4

Next, without retuning, a single unmodulated carrier is used to check the flatness of the amplifier over the frequency range of interest. Any evidence of amplitude/frequency slope over this range would cause additional cross-talk and possibly give rise to erroneous measurements.

When the transistor amplifier has been satisfactorily adjusted, the tuner positions are locked for the remainder of the measurement process.

3.3.1.3 Measurement of the cross-talk level of the reference system

Before attempting to determine the level of cross-talk due to the transistor amplifier, it is necessary to measure the cross-talk of the system itself with the amplifier removed. This measurement consists of three stages:

(1) The input consists only of the FM-modulated carrier f_2. The level of the demodulated signal at the baseband frequency is measured.

(2) Next, an input is applied which consists of both the

modulated carrier f_2 and the unmodulated carrier f_1. The demodulator local oscillator frequency is now set so that the baseband level measured corresponds to modulation transferred to the originally unmodulated carrier f_1.

(3) The difference (in dB) between the measured baseband levels gives the cross-talk of the reference system.

For measurement step (1), the following changes are made to the shaded sections of Figure 3-19:

(a) The transistor amplifier, together with associated tuners, DC feed units and power supplies, is removed.

(b) The (1.882 GHz ± 6 MHz) bandpass filter carrier f_1 is removed, as well as the associated circulator. This permits the modulated carrier f_2 (1.906 GHz) to pass directly to the down-converter.

(c) Since f_1 is not required for this step, the generator for the unmodulated 1.882 GHz carrier is disconnected from the coaxial 3-dB hybrid. It is replaced by a 50-ohm termination.

(d) The frequency of the local oscillator which supplies the down-converter is temporarily changed from $f_1 - (f_2-f_o) = 1.812$ GHz to $f_2 + (f_2-f_o) = 1.976$ GHz. Note that the other possibility, $f_2 - (f_2-f_o) = 1.836$ GHz, is inadmissable because this is precisely the frequency f_o of the local oscillator which supplies the up-converter.

The input now consists only of the modulated carrier f_2.

For measurement step (2), both carriers f_1 and f_2 (set to equal amplitudes) are used. The input P_{in} is now 3 dB greater than before. For this measurement, the down-converter local oscillator is re-set to its original frequency of $f_1 - (f_2-f_o) = 1.812$ GHz.

Results

Tests done over a range of values of P_{in} (for one carrier) indicated that the reference system cross-talk was independent of level. Final measurements for a P_{in} of +24 dBm (the maximum value of interest) are shown in Table 3(6).

3.3.1.4 Measurement of intelligible cross-talk due to the transistor amplifier

Procedure

The transistor amplifier is replaced in the reference set-up, and the sequence followed in determining the system reference cross-talk is repeated. By the time the two-carrier measurements are made, all the shaded items of Figures 3-19 have been replaced in the measurement system.

Results

Table 3(7) gives the actual measurements for the class A mode, Table 3(8) gives the measurements for the class C case. These results are illustrated in Figures 3-21 and 3-22. In the class A mode, for modulating frequencies 2.0 MHz $\leq f_b \leq$ 6.0 MHz, the lowest cross-talk level P_c is obtained at the highest input power level P_{in}. At f_b = 1.0 MHz, however, P_c decreases slightly at the lower levels of P_{in}. Results obtained in the class C mode are quite different, with the exception of the f_b = 1.0 MHz curve for $P_{in} \leq$ 21 dBm. The tendency here is for P_c to increase rapidly as P_{in} decreases. This level-sensitivity is in keeping with the general behaviour of class C amplifiers. The difference between the cross-talk measurements is emphasized in Figure 3-23, in which the results

Table 3(6) - System reference cross-talk measurements. Drive to modulator = -33 dBm for a deviation of 600 Hz.

(41652-93)

Modulation frequency f_b (MHz)	Reading of baseband level meter at 600 Hz bandwidth (dBm)		Hence cross-talk level $P_c = P_{B1} - P_{B2}$ (dBm)
	P_{B1}	P_{B2}	
	Observe the modulation on the previously unmodulated 1.882 GHz carrier f_1	Observe the modulated 1.906 GHz carrier f_2	
	two-carrier power level: P_{in} = +24 dBm	Single-carrier power level: P_{in} = +21 dBm	
1.0	< -101	-24.8	< -76.2
2.0	< -101	-24.9	< -76.1
3.0	< -101	-25.2	< -75.8
4.0	-90.5	-25.3	-65.2
5.0	-88	-25.5	-62.5
6.0	-94.5	-25.7	-68.8

(41652-93)

Table 3(7) -- Measurement of intelligible cross-talk, class A mode. Amplifier optimized for two-equal-carrier input with total P_{in} = +24 dBm. I_{c}^{bias} = 30 mA, V_{CC} = 28 V. Baseband level-meter bandwidth = 600 Hz.

Baseband power level P_{B1} due to modulation transferred to channel f_1. (dBm)

Modulation frequency f_b (MHz) →	2-carrier power level → +4 dBm	+14 dBm	+19 dBm	+20 dBm	+21 dBm	+22 dBm	+23 dBm	+24 dBm
1.0	-68.8	-67.0	-70.7	-71.0	-70.2	-70.5	-68.7	-69.7
2.0	-62.0	-59.0	-63.5	-65.0	-65.8	-66.8	-68.2	-72.8
3.0	-58.2	-55.1	-58.8	-59.6	-60.5	-62.0	-65.0	-68.5
4.0	-57.0	-53.0	-56.9	-56.8	-57.4	-58.8	-60.2	-64.3
5.0	-55.0	-51.0	-55.0	-55.7	-56.0	-58.3	-58.5	-61.0
6.0	-54.5	-50.0	-54.0	-54.3	-54.8	-56.9	-57.3	-59.0

Baseband power level P_{B2} due to modulation on channel f_2. (dBm)

Modulation frequency f_b (MHz) →	1-carrier power level → +1 dBm	+11 dBm	+16 dBm	+17 dBm	+18 dBm	+19 dBm	+20 dBm	+21 dBm
1.0	-25.0	-25.0	-24.8	-24.7	-24.7	-24.7	-24.8	-24.8
2.0	-25.0	-25.0	-25.0	-25.0	-25.0	-25.0	-25.0	-25.0
3.0	-25.0	-25.0	-25.4	-25.3	-25.3	-25.3	-25.3	-25.3
4.0	-25.0	-25.1	-26.0	-25.9	-25.8	-25.8	-25.7	-25.9
5.0	-25.0	-25.1	-26.6	-26.3	-26.2	-26.0	-26.0	-26.2
6.0	-25.0	-25.1	-27.9	-27.7	-27.3	-27.0	-26.8	-26.6

Hence cross-talk power level $P_C = P_{B1} - P_{B2}$ due to class A transistor amplifier. (dBm)

Modulation frequency fb (MHz) →	Level referred to max. (+ 24 dBm) → -20 dB	-10 dB	-5 dB	-4 dB	-3 dB	-2 dB	-1 dB	0 dB
1.0	-43.8	-42.0	-45.9	-46.3	-45.5	-45.8	-44.0	-44.9
2.0	-37.0	-34.0	-38.5	-40.0	-40.8	-41.8	-43.2	-47.8
3.0	-33.2	-30.1	-34.4	-34.3	-35.2	-36.7	-39.7	-43.2
4.0	-32.0	-27.9	-30.9	-30.9	-31.6	-33.0	-34.5	-42.6
5.0	-30.5	-25.9	-28.4	-29.4	-29.8	-32.3	-32.5	-34.8
6.0	-29.5	-24.3	-26.1	-26.6	-27.7	-29.9	-30.5	-32.4

Table 3(8) - Measurement of intelligible cross-talk, class C mode. Amplifier optimized for two-equal-carrier input with total P_{in} = +24 dBm. (41652-95)

V_{CC} = 28 V. Baseband level-meter bandwidth = 600 Hz.

Modulation frequency f_b (MHz)	Baseband power level P_{B1} due to modulation transferred to channel f_1. (dBm)					
2-carrier power level →	+19 dBm	+20 dBm	+21 dBm	+22 dBm	+23 dBm	+24 dBm
1.0	-54.2	-61.8	-69.4	-72.8	-70.7	-69.5
2.0	-48.0	-55.2	-60.5	-64.2	-65.2	-65.8
3.0	-44.9	-51.1	-55.7	-57.5	-59.8	-61.2
4.0	-40.8	-47.3	-51.8	-54.6	-56.7	-57.7
5.0	-38.5	-45.5	-49.1	-51.3	-53.4	-55.3
6.0	-37.5	-44.4	-48.2	-50.2	-51.2	-53.2

Modulation frequency f_b (MHz)	Baseband power level P_{B2} due to modulation on channel f_2. (dBm)					
1-carrier power level →	+16 dBm	+17 dBm	+18 dBm	+19 dBm	+20 dBm	+21 dBm
1.0	-24.9	-24.8	-24.7	-24.7	-24.7	-24.7
2.0	-25.3	-24.9	-24.8	-24.8	-24.8	-24.8
3.0	-25.7	-25.3	-25.3	-25.2	-25.2	-25.2
4.0	-26.2	-26.0	-26.0	-26.0	-25.9	-25.8
5.0	-26.3	-26.2	-26.4	-26.4	-26.3	-26.2
6.0	-26.5	-26.5	-26.8	-26.8	-26.7	-26.7

Modulation frequency f_b (MHz)	Hence cross-talk power level $P_C = P_{B1} - P_{B2}$ due to class C transistor amplifier (dBm)					
Level referred to max. (+ 24 dBm) →	-5 dB	-4 dB	-3 dB	-2 dB	-1 dB	0 dB
1.0	-29.3	-37.0	-44.7	-48.1	-46.0	-44.8
2.0	-22.7	-30.3	-35.7	-39.4	-40.4	-41.0
3.0	-19.2	-25.8	-30.4	-32.3	-34.6	-36.0
4.0	-14.6	-21.3	-25.8	-28.6	-30.8	-31.9
5.0	-12.2	-19.3	-22.7	-24.9	-27.1	-29.1
6.0	-11.0	-17.9	-21.4	-23.4	-24.5	-26.5

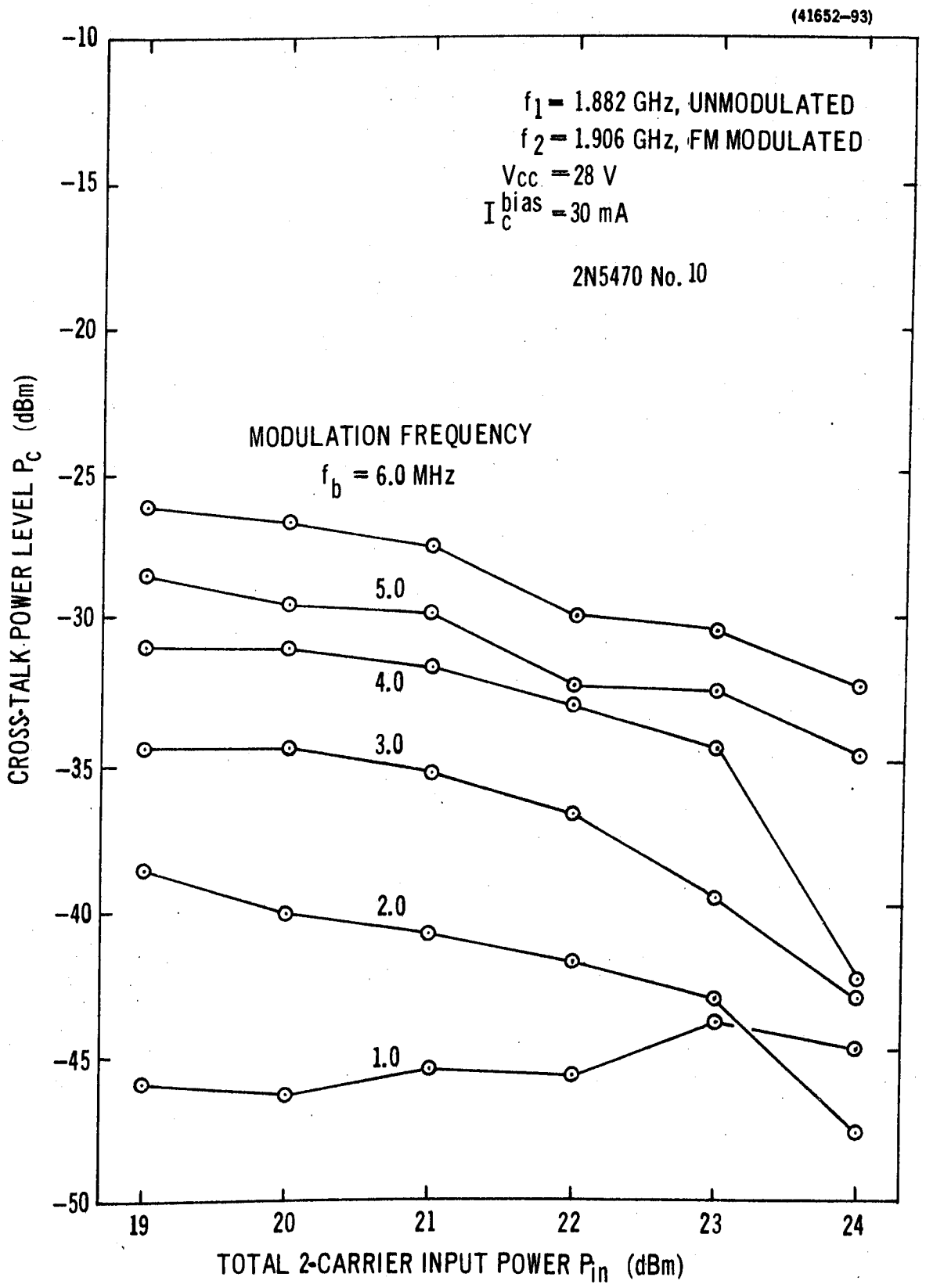

Figure 3-21 Class A two-carrier intelligible cross-talk level P_c as a function of total input power P_{in} and modulating frequency f_b. Amplifier optimized for P_{out} at $\hat{P}_{in}$ = +24 dBm.

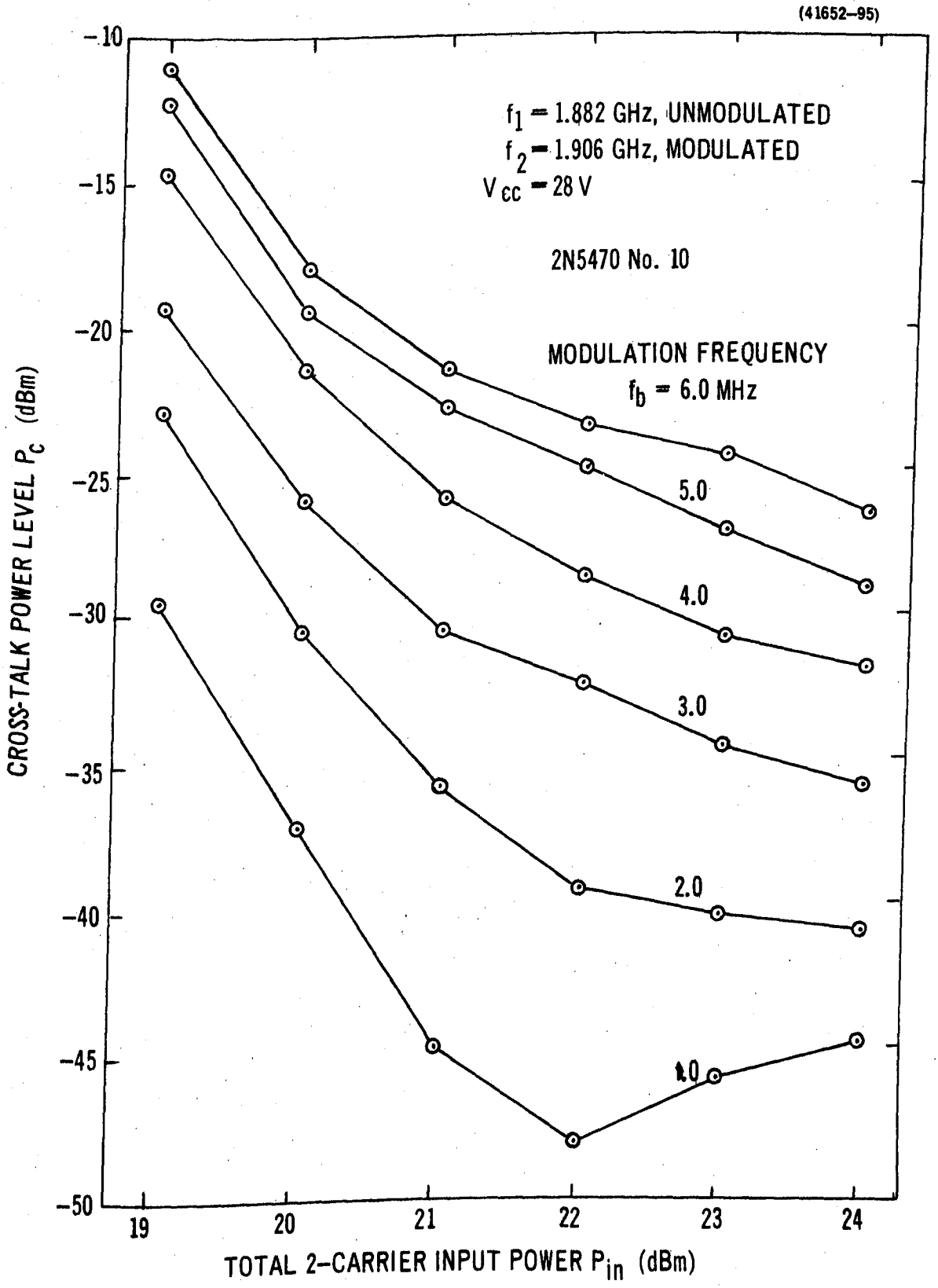

Figure 3-22 Class C two-carrier intelligible cross-talk level P_c as a function of total input power P_{in} and modulating frequency f_b. Amplifier optimized for P_{out} at $\hat{P}_{in}$ = + 24 dBm.

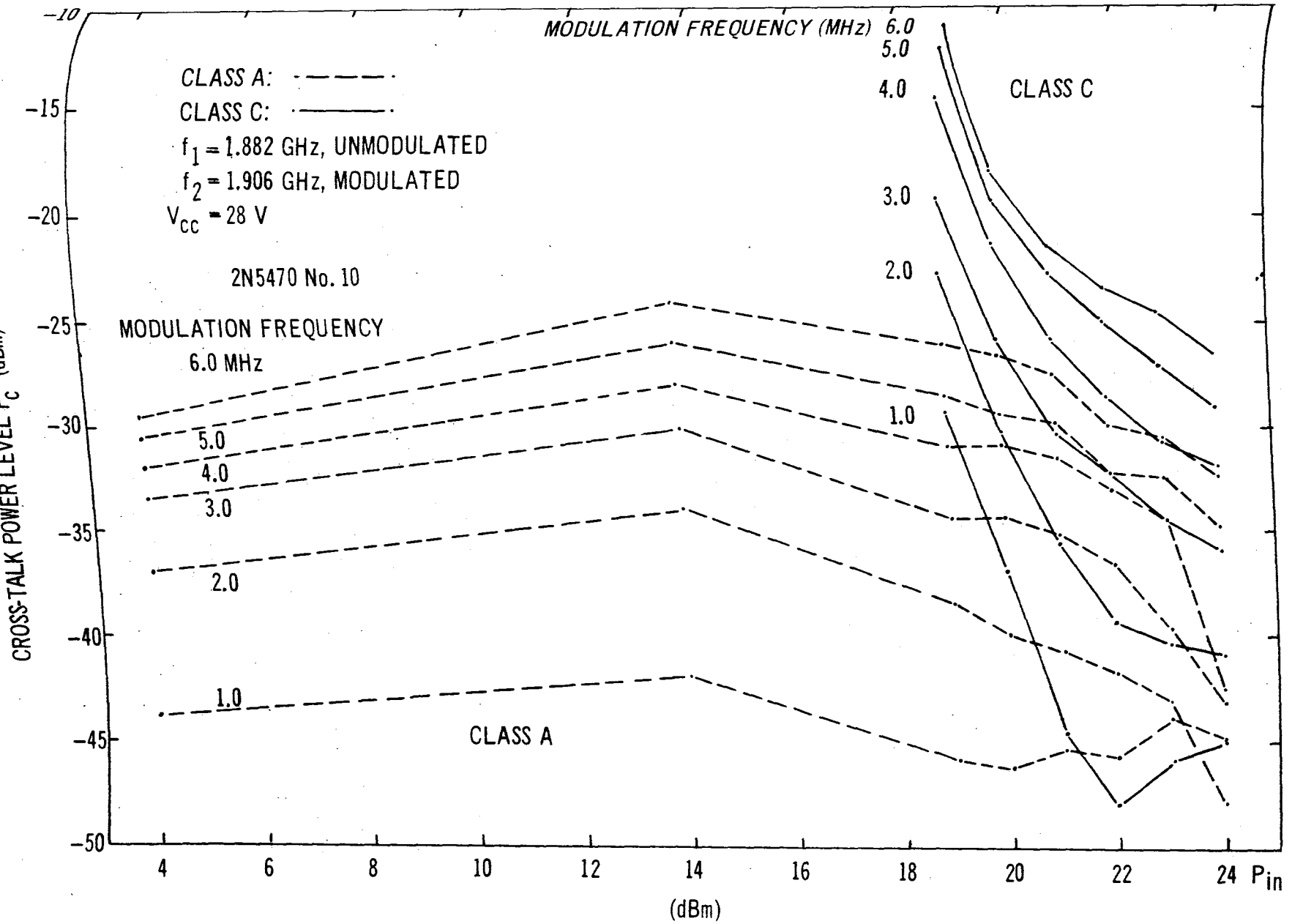

Figure 3–23 Cross-talk data for the Class A and Class C modes compared. Conditions as for previous two figures.

for the two modes are compared over a wider range of values of P_{in}. (Class C values could not be measured for P_{in} < 19 dBm because of the drastic fall in P_{out} at such levels, see for example Figure 3-14).

3.3.2 Dependence of the two-carrier class C cross-talk output spectrum on the input power level

The two sequences of class C amplifier output spectra reproduced in this subsection correspond to Spectrum 2 of Figures 3-19 and 3-20(b). The two different cases considered are:

(1) The amplifier is optimized for the condition of two equal - amplitude carriers at the input, the total input power being +24 dBm, (i.e. +21 dBm for each carrier). Then, without altering the amplifier adjustments, spectra are recorded as P_{in} is reduced in 1 dB steps from +24 to +19 dBm. They are reproduced in Figures 3-24(a) through 3-24(f).

(2) For the second sequence, the amplifier is optimized for the condition of two unequal - amplitude carriers at the input. Because of equipment limitations, the maximum total input power for this sequence is +21 dBm: the unmodulated carrier f_1 is at a level of +10.5 dBm, with the modulated carrier f_2 at a level of +20.5 dBm. These spectra are shown in Figures 3-25(a) to 3-25(f).

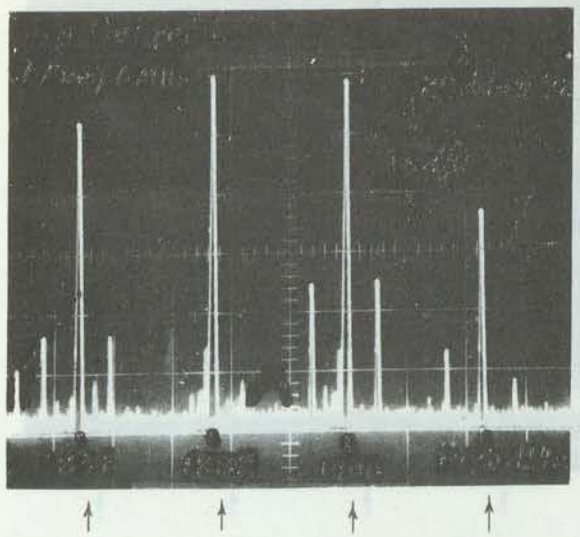

10 dB

3–24(a) Optimized condition.
Total input power P_{in} = +24 dBm,
i.e. +21 dBm each carrier.

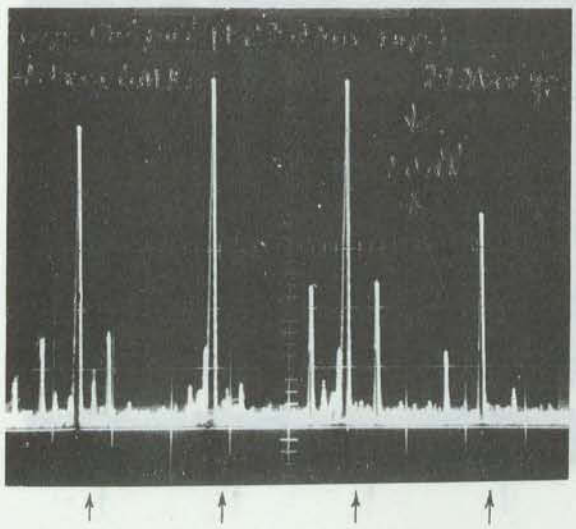

3–24(b) Total input power reduced to
P_{in} = +23 dBm

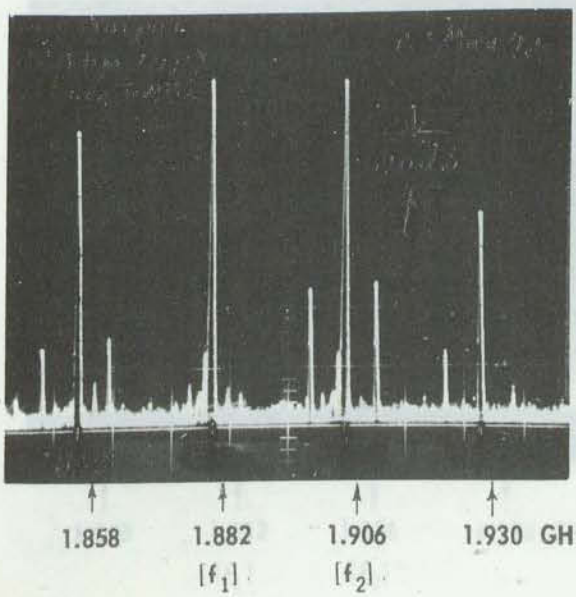

3–24(c) Total input power reduced to
P_{in} = +22 dBm

Figure 3–24 Output spectra of Class C amplifier for two equal carriers at input.

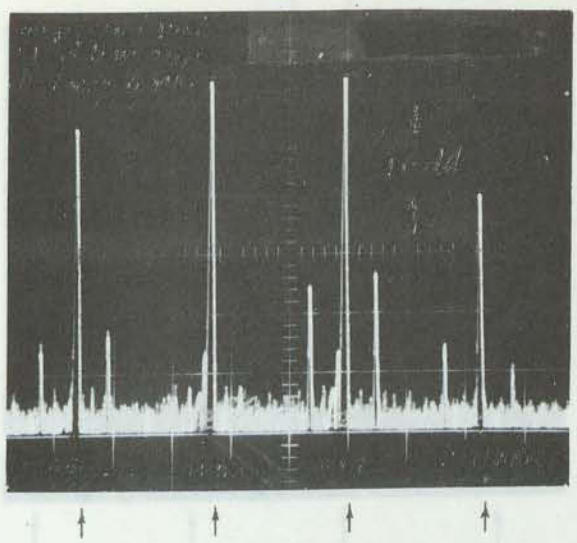

10 dB

3–24(d) Total input power reduced to P_{in} = +21 dBm

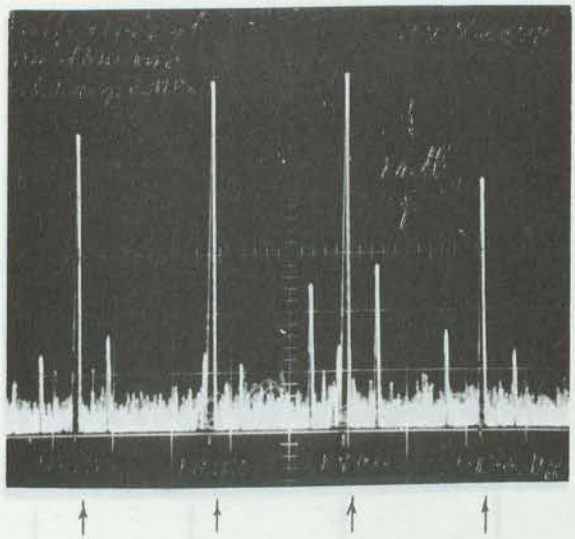

3–24(e) Total input power reduced to P_{in} = 20 dBm

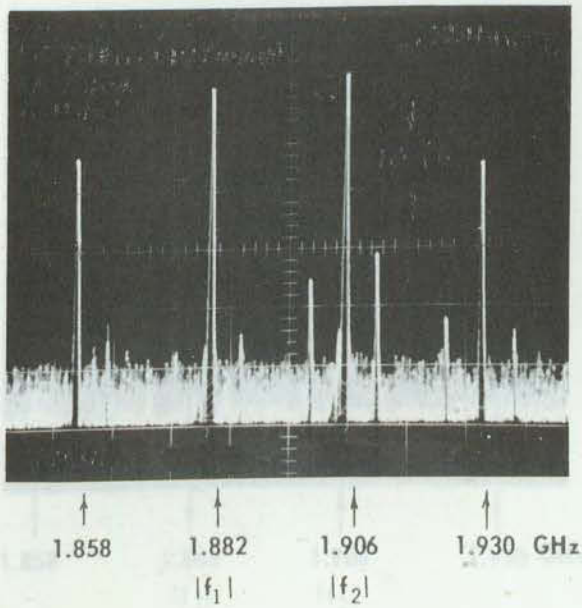

3–24(f) Total input power reduced to P_{in} = 19 dBm

Figure 3–24 (continued) Output spectra of Class C amplifier for two equal carriers at input.

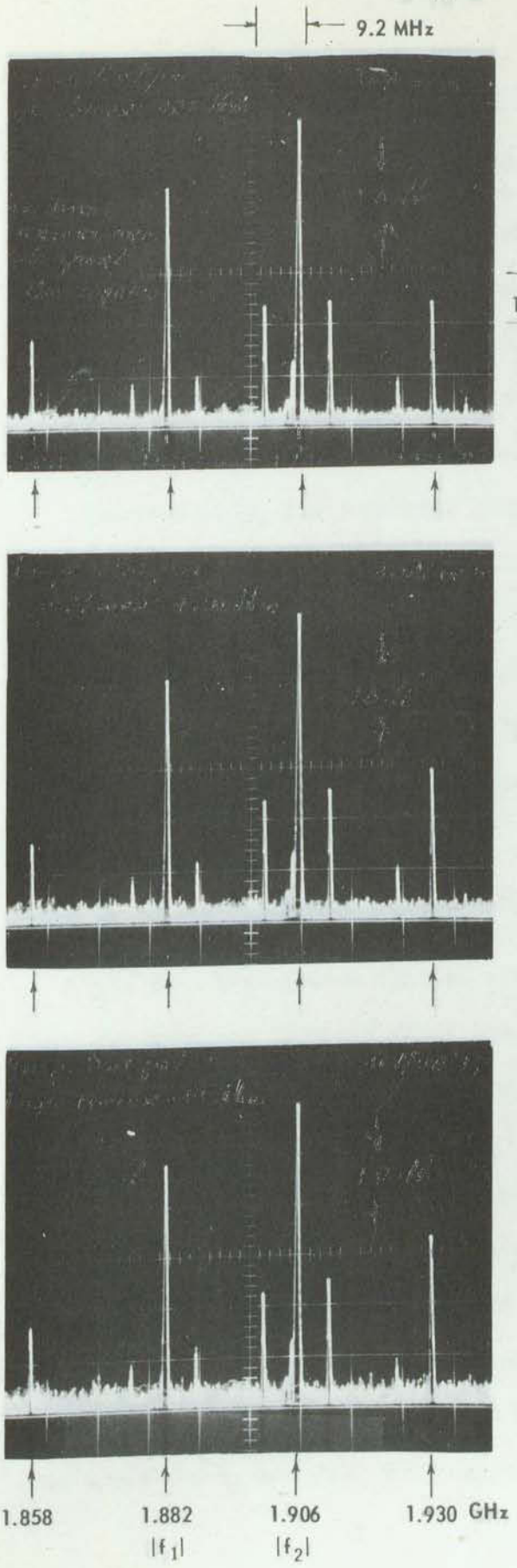

3–25(a) Optimized condition.
Total input power
P_{in} = + 21 dBm

3–25(b) Total input power reduced to
P_{in} + 20 dBm

3–25(c) Total input power reduced to
P_{in} = + 19 dBm

Figure 3–25 Output spectra of Class C amplifier. Initially optimized for two unequal carriers at input; total P_{in} 21 dBm; carrier f_1 at + 10.5 dBm, carrier f_2 at + 20.5 dBm.

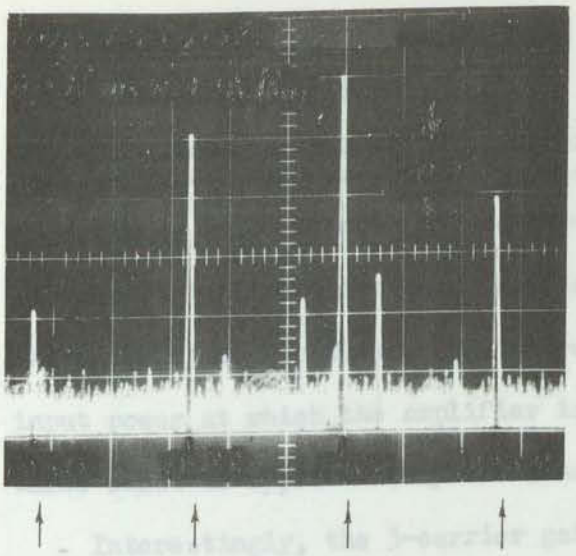

3–25(d) Total input power reduced to P_{in} + 18 dBm

10 dB

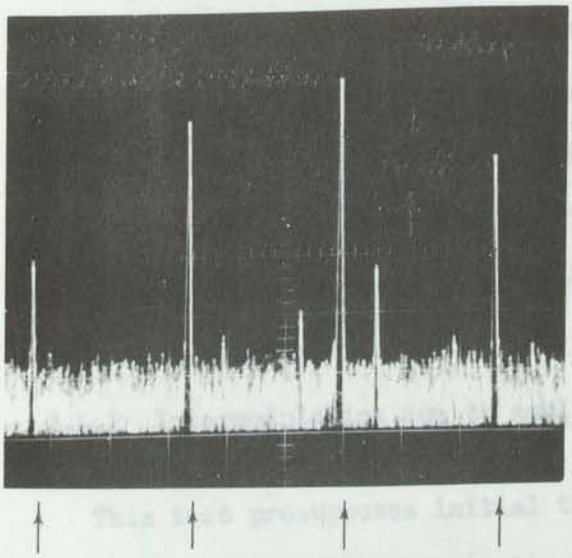

3–25(e) Total input power reduced to P_{in} + 17 dBm

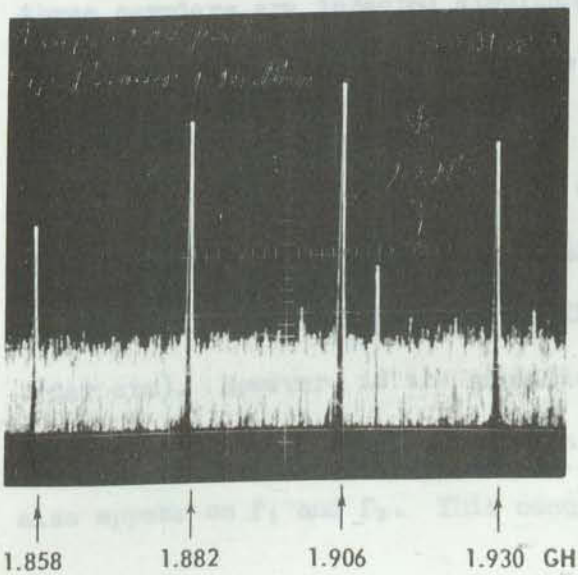

3–25(f) Total input power reduced to P_{in} = + 16 dBm

1.858 1.882 ($|f_1|$) 1.906 ($|f_2|$) 1.930 GHz

Figure 3–25 (continued) Output spectra of Class C amplifier for two unequal carriers at input.

3.4 Three-Carrier Tests

3.4.1 Three-carrier $P_{in,out}$ - characteristic

Figure 3-26 compares the measured dynamic class C P_{in}-P_{out} characteristic for three input carriers with the corresponding characteristics for the one - and two-carrier cases. The total input power at which the amplifier is gain-optimized in each of the three cases is approximately the same.

Interestingly, the 3-carrier gain is greater than the 2-carrier gain in the vicinity of the optimization level. This is interpreted as being due to the fact that as the number of carriers is increased, the total input power being maintained constant, the power in each carrier becomes less so that a more linear part of the nonlinear amplitude - characteristic is traversed leading to an increase in the overall gain.

3.4.2 Intermodulation due to amplitude and phase nonlinearity at IF

This test presupposes initial tuning for maximum P_{out}, when three carriers are injected simultaneously. Two of these carriers, f_1 and f_2, are derived from CW sources, the third, f_3, is derived from an FM modulated source.

If the amplifier exhibits only amplitude nonlinearity, then the spectrum of the output will be similar to the input spectrum, except that there will be gain and IM products (of second and third order etc). However, if the amplifier has both amplitude and phase nonlinearity, then the FM modulation originally present on f_3 will also appear on f_1 and f_2. This occurrence indicates the presence

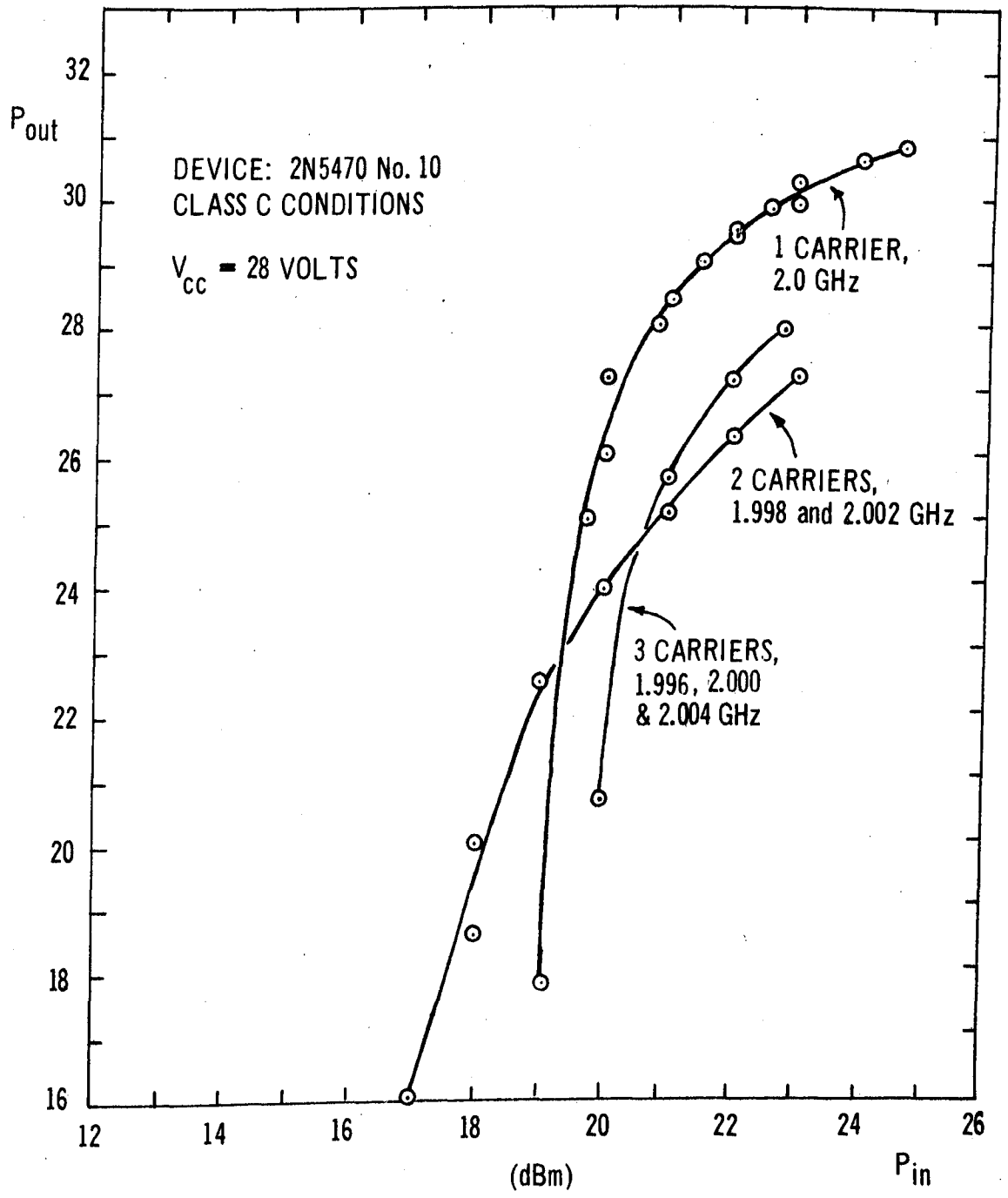

Figure 3–26 P_{in}, P_{out} – characteristics for Class C conditions (zero dc emitter bias). In the 1– and 2– carrier cases the amplifier is optimized at P_{in} = 23 dBm. In the 3– carrier case, it is optimized at P_{in} = 22.8 dBm, the largest total 3–equal–carrier power attainable with the available equipment.

of AM to PM conversion and constitutes intelligible cross-talk as well as intermodulation distortion due to the phase-nonlinearity.

In general, there will be three types of distortion:

(1) Intermodulation distortion products at frequencies $2f_1-f_2$, $f_1+f_2-f_3$, etc. due to a nonlinear relationship between output amplitude and input level.

(2) Intermodulation distortion products at the same frequencies as above due to a nonlinear relationship between output phase-angle and input level (AM-to-PM conversion).

(3) The transference of frequency-modulation to a previously unmodulated carrier due to the simultaneous presence of AM-to-PM conversion and a frequency-dependent gain (gain slope).

The intelligible cross-talk in (3) may not be significant in a narrow-band system in which the gain slope is negligible.

3.4.2.1 Three-carrier cross-talk measurement

The experimental set-up for the three-carrier cross-talk measurements is basically the same as shown in Figure 3-19. However, because three input carriers are now required, the circuitry between the up-converter and the input to the transistor amplifier is now as shown in the upper part of Figure 3-27. The FM modulation is accomplished as before, but the resulting signal is now combined with two unmodulated carriers instead of one. To this end, the first stage of combining is done in a -10 dB directional coupler, with 10 dB of gain to compensate for the coupler loss. The second stage of combining is done as before using a coaxial 3-dB hybrid.

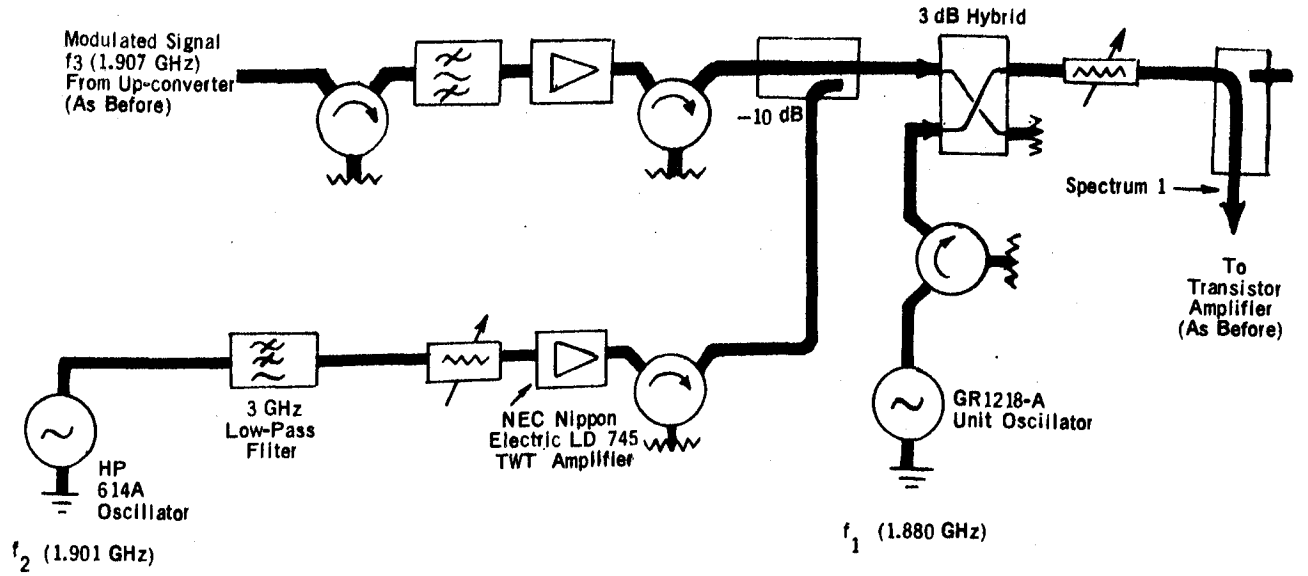

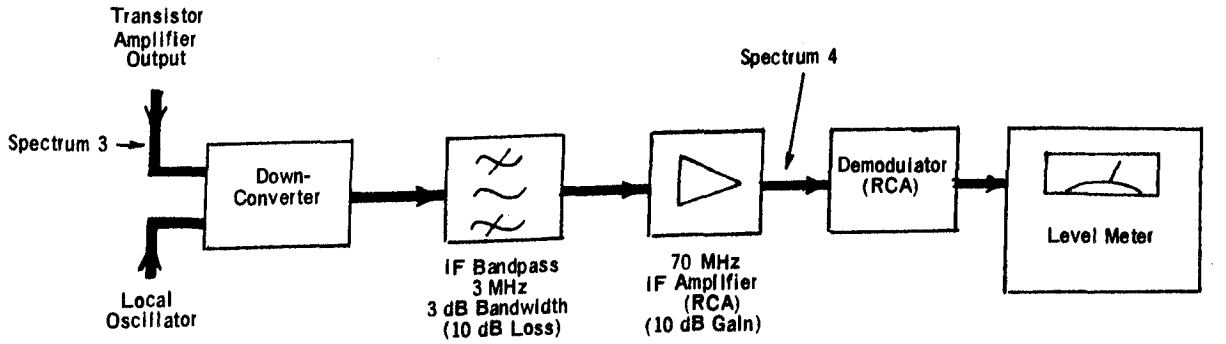

Figure 3-27 **Modification to Figure 3-19 required for 3-carrier cross-talk measurements**

The output circuitry between the down-converter and the demodulator is also changed, as shown in the lower part of Figure 3-27. The IF bandpass filter is now changed for another with a -3 dB bandwidth of 3 MHz and with a very steep-sided frequency response. The 10 dB insertion loss of this filter is compensated by including in the set-up a 70 MHz IF amplifier.

System spectra for a typical class A three-carrier cross-talk measurement are shown in Figures 3-28(a) to 3-28(d). Figure 3-28(a) illustrates spectrum 1 (see Figure 3-27) at the input to the transistor amplifier with the two unmodulated carriers f_1 and f_2 at 1.880 and 1.901 GHz respectively, as well as the FM-modulated carrier f_3 at 1.907 GHz. Each carrier is at the level of +19.2 dBm for a total P_{in} of +24 dBm. Figure 3-28(b) shows spectrum 2 at the class A amplifier output, (refer to Figure 3-27). The same three carriers are visible, still with nearly equal amplitudes, but now the previously unmodulated f_1 and f_2 carriers show transferred cross-talk. Spectrum 3, reproduced in Figure 3-28(c), shows the effect on the output spectrum of the ± 6 MHz bandwidth bandpass filter centred at 1.882 GHz. Finally, Figure 3-28(d) depicts the spectrum at the input to the demodulator. The dominant signal here is the 70 MHz carrier with its transferred cross-talk.

Cross-talk measurements

Three-carrier intelligible cross-talk measurements are performed for both the class A and class C modes. In general, the procedure is the same as previously described for the two-carrier cross-talk measurements. The results for modulation at

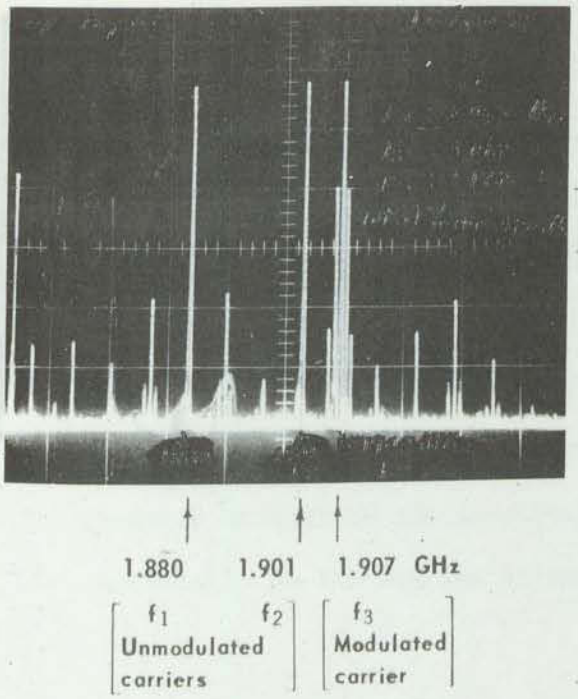

Figure 3–28 (a)
Spectrum of Class A amplifier input signal for crosstalk test using three equal amplitude carriers. Each carrier is at a level of +19.2 dBm for a total P_{in} of +24 dBm.
[Spectrum 1, Figure 3–27]

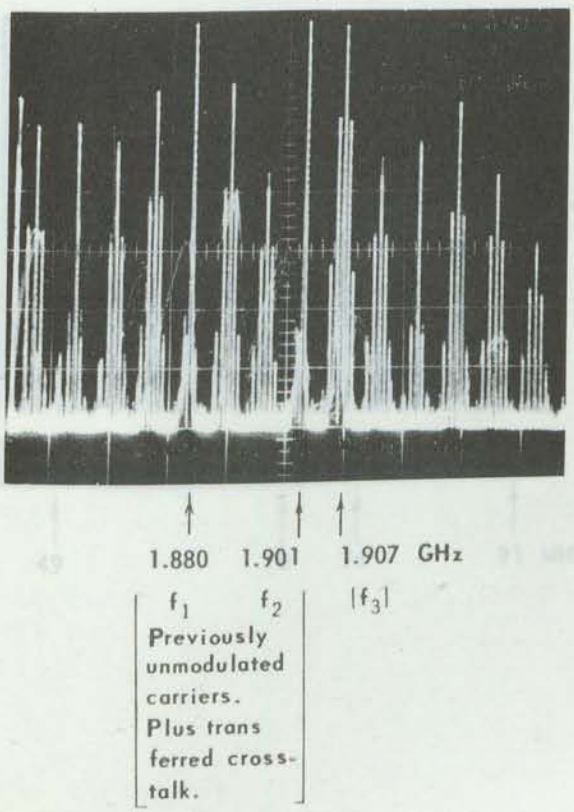

Figure 3–28 (b)
Spectrum of Class A amplifier output for 3–carrier crosstalk test.
[Spectrum 2, Figure 3–27]

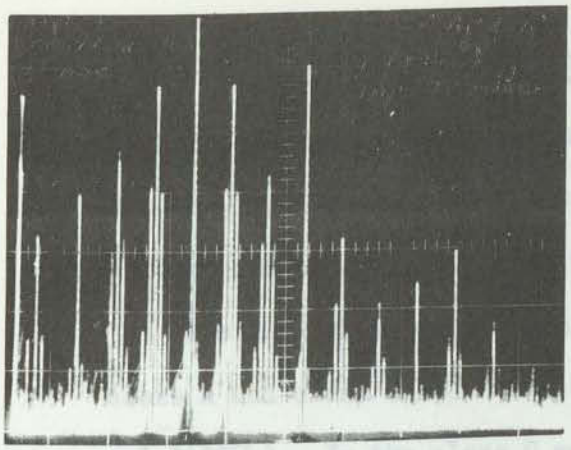

Figure 3–28 (c)
Spectrum at input to downconverter (after 1.880 GHz bandpass filter). Three-carrier crosstalk test using Class A amplifier.
[Spectrum 3, Figure 3–27]

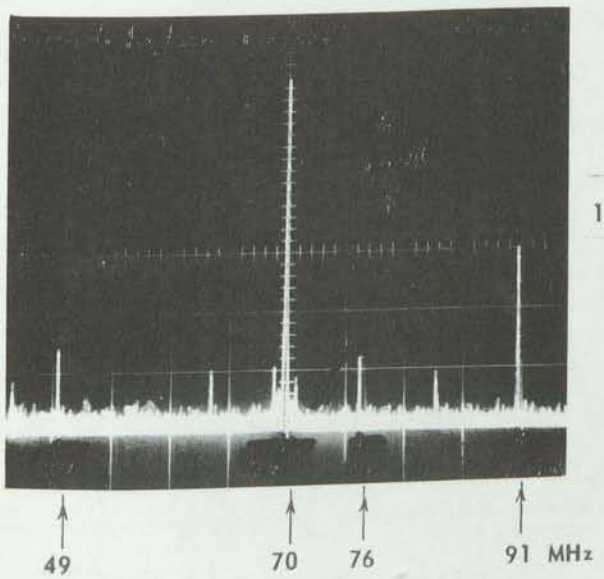

Figure 3–28 (d)
Spectrum at input to demodulator. Three-carrier test using Class A amplifier.
[Spectrum 4, Figure 3–27]

1.0 MHz are given in Tables 3(9) and 3(10) and are plotted in Figure 3-29. In each case, the amplifiers are gain-optimized at a total input power of P_{in} = +24 dBm. Considerable differences between the class A and class C behaviour are again apparent.

The amplifier output spectra (spectrum 2) observed for the class A and class C modes are directly compared in Figures 3-30(a) and 3-30(b). In the class C mode the noise level tends to be greater throughout the spectrum. The effect is particularly noticeable on the originally unmodulated carrier f_1 (1.880 GHz).

Table 3(9) - Measurement of three-carrier intelligible cross-talk, class A mode. Amplifier optimized for +24 dBm input consisting of three equal-amplitude carriers:

f_1 = 1.880 GHz } unmodulated

f_2 = 1.901 GHz }

f_3 = 1.907 GHz, modulated at 1.0 MHz.

	Baseband power level P_{B1} due to modulation transferred to channels f_1 and f_2.						
3-carrier Power level (dBm)	+ 14	+ 19	+ 20	+ 21	+ 22	+ 23	+ 24
P_{B1} (dBm)	- 77	-82.3	-80.5	-77.8	-76.5	-74.9	-73.8

	Baseband power level P_{B2} due to modulation on channel f_3 alone						
1-carrier Power level (dBm)	+9.2	+14.2	+15.2	+16.2	+17.2	+18.2	+19.2
P_c (dBm)	-25.9	-25.9	-25.9	-25.9	-25.9	-25.9	-25.9

	Hence intelligible three-carrier cross-talk level $P_C = P_{B1} - P_{B2}$ due to class A transistor amplifier.						
Level referred to max. (+24 dBm)	-10 dB	-5 dB	-4dB	-3dB	-2dB	-1 dB	0 dB
P_c (dBm)	-51.1	-56.4	-54.6	-51.9	-50.6	-49	-47.9

Table 3(10) - Measurement of three-carrier intelligible cross-talk, class C mode. Amplifier optimized for +24 dBm input consisting of three equal-amplitude carriers:

f_1 = 1.880 GHz
f_2 = 1.901 GHz
} unmodulated

f_3 = 1.907 GHz, modulated at 1 MHz.

	Baseband power level P_{B1} due to modulation transferred to channels f_1 and f_2.					
3-Carrier Power Level (dBm)	+19	+20	+21	+22	+23	+24
P_{B1} (dBm)	-65.9	-66	-68	-70.2	-74.7	-76.2

	Baseband power level P_{B2} due to modulation on channel f_3 alone.					
1-Carrier Power Level (dBm)	+14.2	+15.2	+16.2	+17.2	+18.2	+19.2
P_{B2} (dBm)	-26	-26.1	-26.2	-25.8	-25.6	-25.7

	Hence intelligible three-carrier cross-talk level $P_c = P_{B1} - P_{B2}$ due to class C transistor amplifier.					
Level referred to max. (+24 dBm)	-5 dB	-4 dB	-3 dB	-2 dB	-1 dB	0 dB
P_c (dBm)	-39.9	-39.9	-41.8	-44.4	-49.1	-50.5

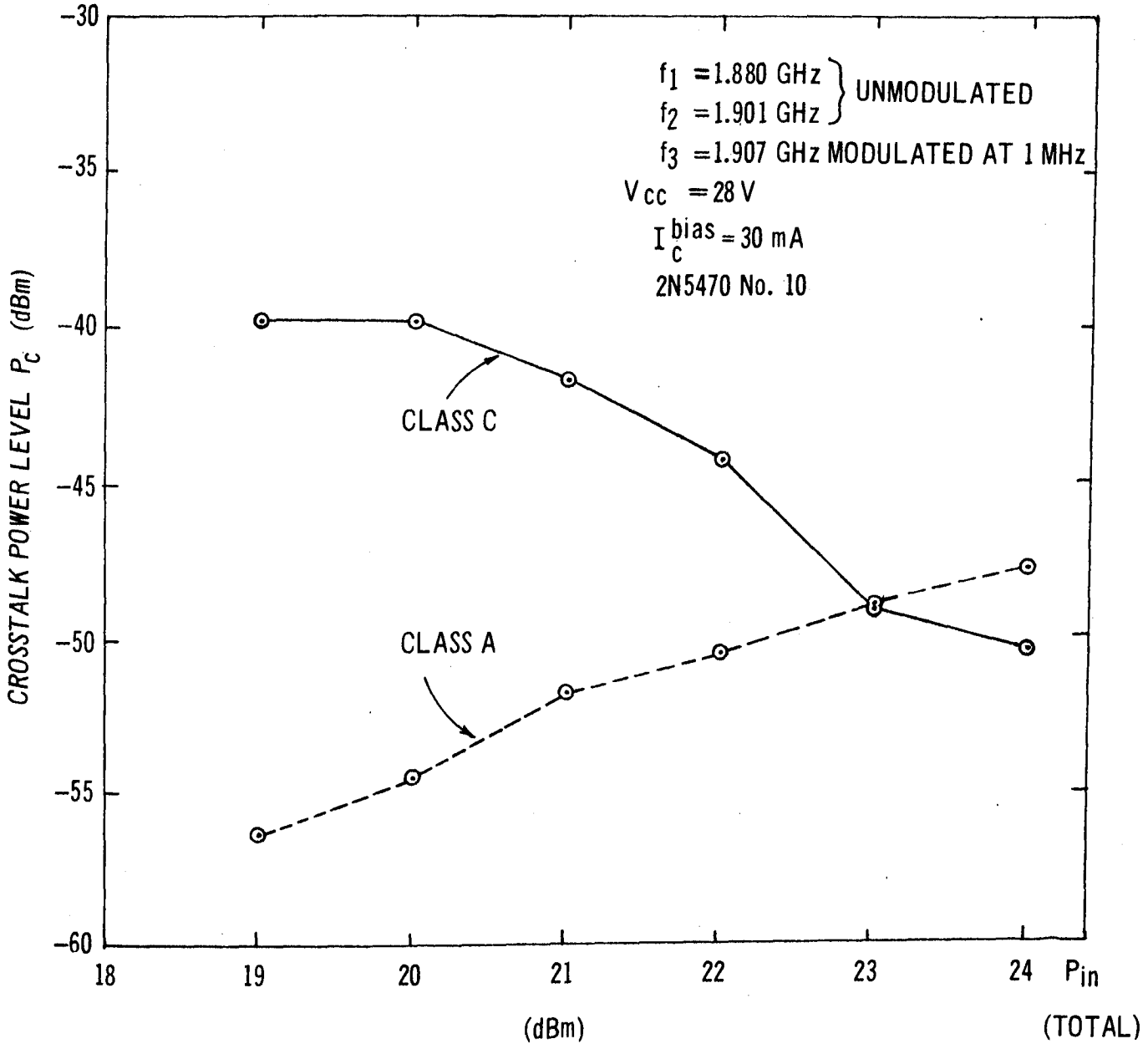

Figure 3-29 Results of three-carrier cross-talk measurements: Class A and Class C modes compared.

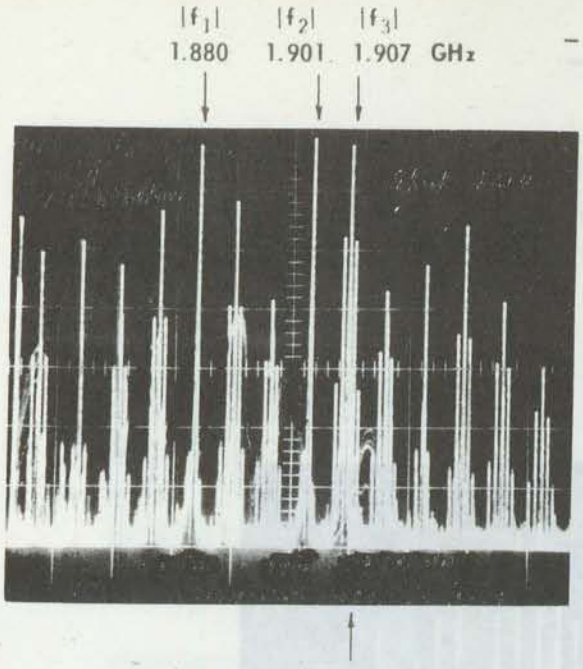

(a) Class A spectrum

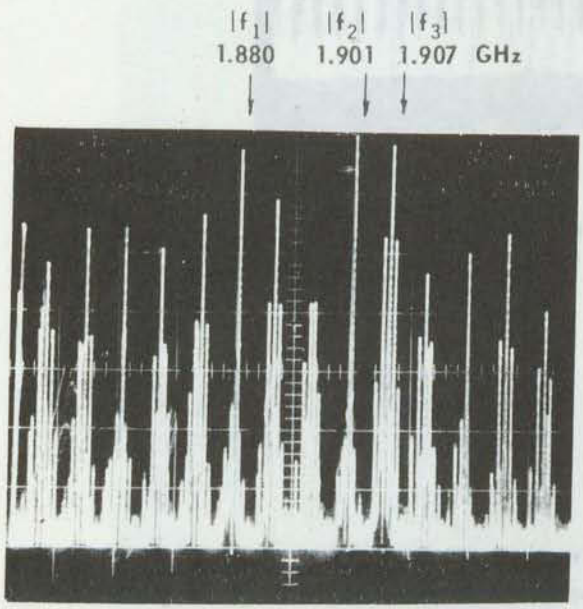

(b) Class C spectrum

Figure 3–30 Crosstalk measurement with 3 equal-amplitude carriers: transistor amplifier output spectra for (a) Class A and (b) Class C. The input consists of three equal-amplitude carriers, each +19.2 dBm, so that the total input power is +24 dBm.

3.4.3 Dependence of the three-carrier class C output spectrum upon the input power level in the absence of modulation.

This sub-section contains a sequence of class C amplifier output spectra when three input carriers are present. As in the first sequence of 3.3.2 (which dealt with two input carriers), the amplifier is optimized for the condition that the total imput power is initially +24 dBm (19.2 dBm for each carrier). As before, the spectra are then recorded as P_{in} is reduced in 1 dB steps from +24 to +19 dBm.

Figure 3-31 is an over-view of the output spectrum at the maximum level, displayed over a wide bandwidth. The sequential spectra shown in Figures 3-32(a) to 3-32(f) show only the frequencies in the immediate vicinity of the three carriers f_1, f_2 and f_3.

Figures 3-33(a) to 3-33(d) consist of a group of class C amplifier output spectra for four different combinations of input carrier power levels, in each case totalling +24 dBm. In the first photograph, all carriers are at the same level. In subsequent photographs, carrier f_1 is reduced successively to 3, 10 and 20 dB below the other carrier levels, the total power being kept constant.

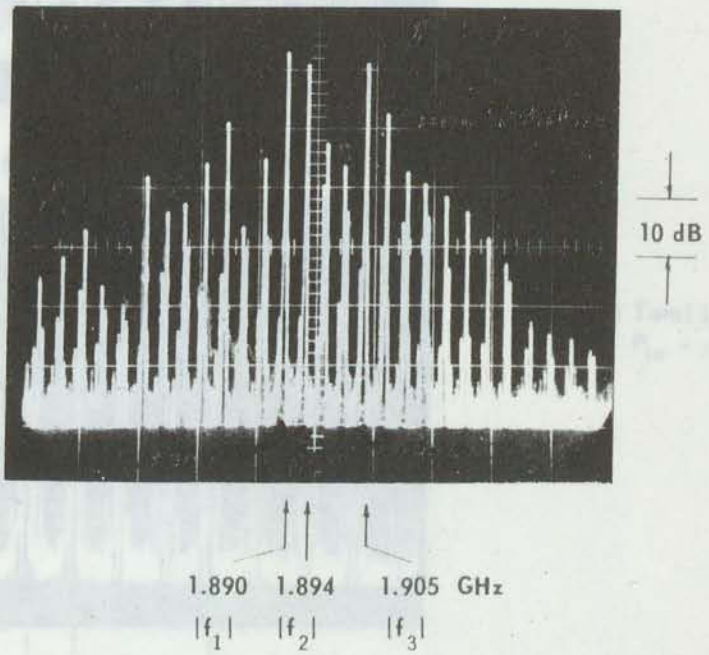

Figure 3–31 Overview of the output spectrum when the input consists of THREE equal-amplitude carriers at the frequencies f_1, f_2 and f_3.
Total P_{in} = +24 dBm, no carrier modulated.

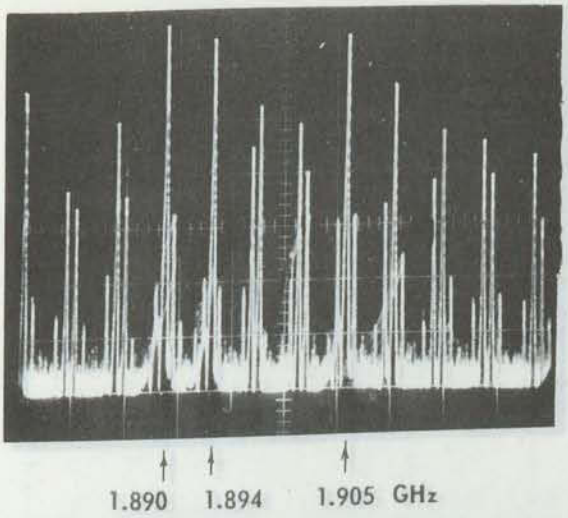

(a) Optimized condition.
Total input power P_{in} = +24 dBm,
i.e. +19.2 dBm each carrier.

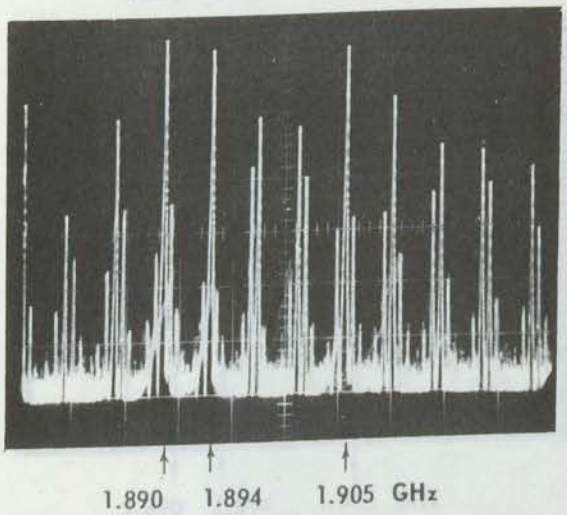

(b) Total input power reduced to
P_{in} = +23 dBm

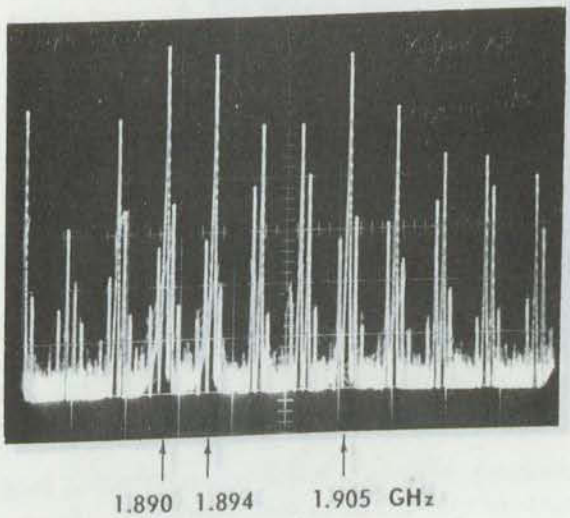

(c) Total input power reduced to
P_{in} +22 dBm

Figure 3–32 Output spectra of Class C amplifier for three equal-amplitude carriers at the input; effect of varying the input power level.

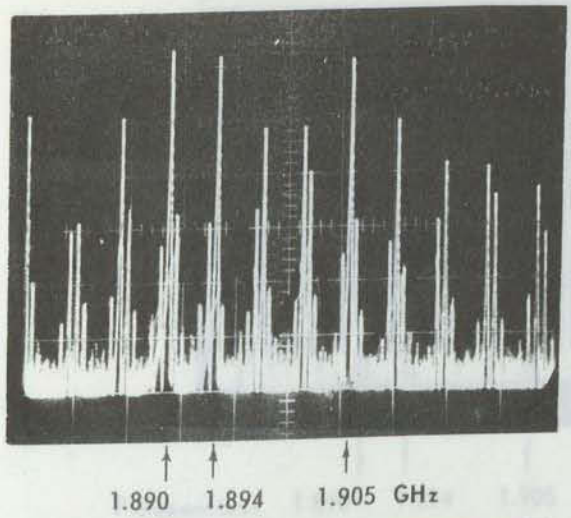

(d) Total input power reduced to P_{in} 21 dBm

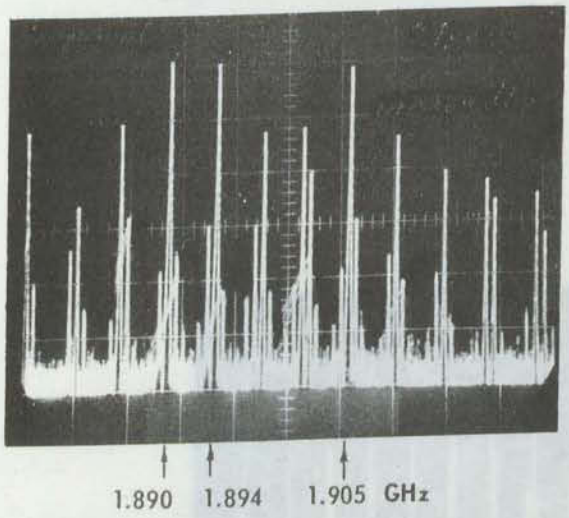

(e) Total input power reduced to P_{in} 20 dBm

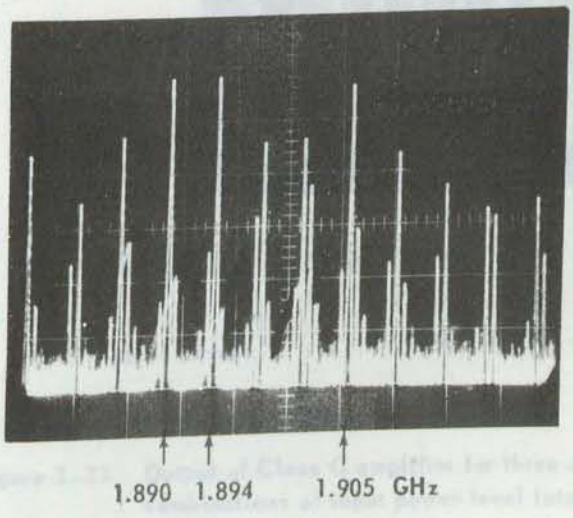

(f) Total input power reduced to P_{in} 19 dBm

Figure 3–32 (continued) Output spectra of Class C amplifier for three equal carriers at the input; effect of varying the level.

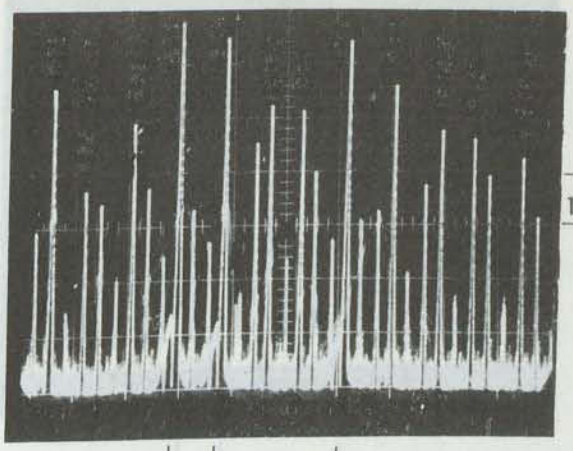

(a) Three equal input carriers

10 dB

Frequencies: 1.890 ($|f_1|$) 1.894 ($|f_2|$) 1.905 ($|f_3|$) GHz

Input Levels: +19.2 +19.2 +19.2 dBm, total P_{in} = +24 dBm

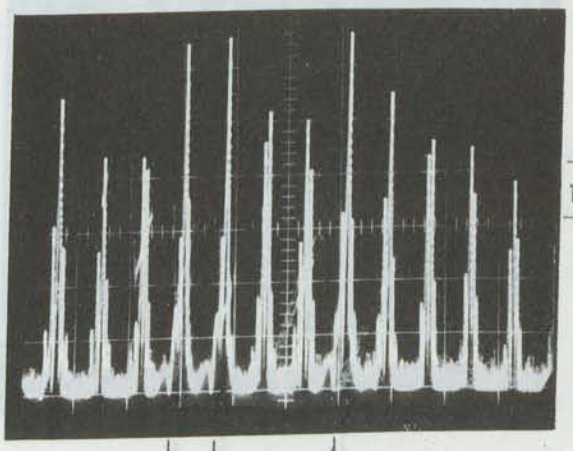

(b) Carrier f_1 is 3 dB below carriers f_2 and f_3

10 dB

Frequencies: 1.890 ($|f_1|$) 1.894 ($|f_2|$) 1.905 ($|f_3|$) GHz

Input Levels +17 +20 +20 dBm, total P_{in} +24 dBm

Figure 3–33 Output of Class C amplifier for three carriers at the input, for various combinations of input power level totalling +24 dBm.

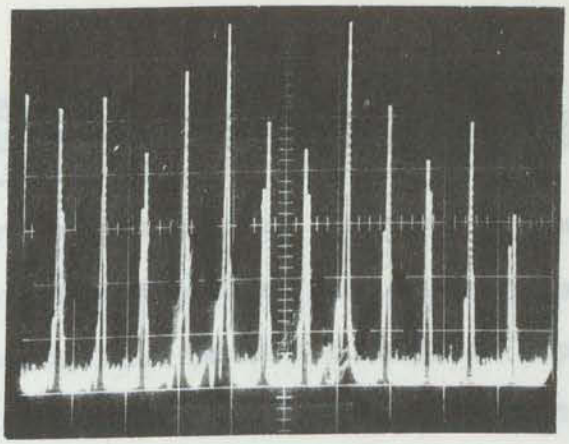

(c) Carrier f_1 is 10 dB below the other two.

Frequencies: 1.890 ($|f_1|$) 1.894 ($|f_2|$) 1.905 ($|f_3|$) GHz

Input Levels: +10.8 +20.8 +20.8 dBm, total P_{in} +24 dBm

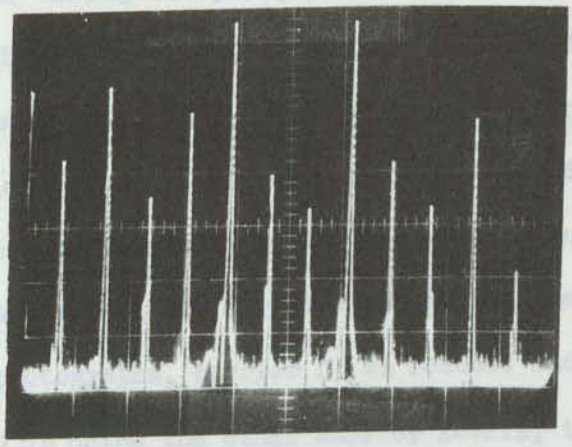

(d) Carrier f_1 is 20 dB below the other two.

Frequencies: 1.890 ($|f_1|$) 1.894 ($|f_2|$) 1.905 ($|f_3|$) GHz

Input Levels: +1 +20.9 +20.9 dBm, total P_{in} +24 dBm

Figure 3–33 (continued) Output spectra of Class C amplifier for three carriers at the input, for various combinations of input power level totalling +24 dBm.

4. METHODS OF NONLINEAR CIRCUIT ANALYSIS AND THEIR RELEVANCE TO STUDIES OF INTERMODULATION DISTORTION.

4.1 Introduction

The conventional approach to finding the response of an electrical system to a given input signal is to construct a mathematical model of the system (here the microwave power transistor embedded in its associated circuitry) as accurately as possible and then to determine its response to an appropriate periodic forcing function. If the system happens to be linear, many general-purpose computer programs exist which can be used to get the answers. Most of them can perform linear dc, ac (frequency domain) and transient (time domain) analysis. Examples include ECAP [15], NATFREQS[16], LISA[17] and CAD-1[18], all of which employ nodal analysis.

If the system is nonlinear, the situation is quite different. The number of possible methods is sharply reduced and many complications arise.

4.2 Time-Domain

The most direct approach to nonlinear analysis is numerical integration in the time-domain of the set of differential equations which describe the system. Numerical integration, however, permits only the transient solution to be found. When the input (forcing function) is periodic, numerical integration can be economically reasonable provided certain conditions are met. Among these conditions are:

(1) The network must not have excessive mathematical stiffness.

(2) The periodic forcing function (carrier) must consist of a single frequency.

Condition (1) means that the system should not be characterized by a wide range of time-constants. If this condition is not met, computation time can become very long: the integration step-size has to be sufficiently small to resolve the waveform "fine structure" due to the shortest time constant, while the total number of integration steps needed to achieve a periodic solution depends on the longest time constant. That is, the computation must continue until the evanescent modes excited by the initial conditions have died away.

If condition (2) is not met, the time-domain approach becomes much less feasible. This is particularly true when the forcing functions (carriers) are closely-spaced in frequency, as they often are in practical communications systems. Since superposition does not apply, sum and difference frequencies (intermodulation products) of all orders will appear in the output in addition to harmonics (and possibly subharmonics). The output spectrum can now occupy an extremely large bandwidth, the lowest frequency being the minimum carrier separation*, the highest harmonic being determined, as before, by the shortest system time-constant.

Virtually all of the general-purpose nonlinear network analysis programs such as NET-1[19], SCEPTRE[20], TRAC[21] and

* or less, under some conditions

CIRCUS[22] are based on numerical integration and most of them contain built-in nonlinear transistor and diode models.

NET-1 has been used successfully at RCA Limited to simulate the single-carrier nonlinear (class C) operation of the 2N5470 microwave power transistor at a frequency of 2.0 GHz and a power level of 1 Watt[1]. However, this application of NET-1 turned out to be at the limit of feasibility since computer times of as much as 20 minutes were required for a single convergence run*. These long runs and the relative inflexibility of the NET-1 program motivated the development of a new program, CWFIND[23], specifically designed to find the CW steady state response of a nonlinear microwave device, imbedded in a realistic network environment, to a single-frequency carrier. Like the large-scale programs mentioned above, CWFIND employs numerical integration but unlike them, it contains provisions for automatically seeking the steady-state solution as well as certain features, such as exponential extrapolation, which save considerable amounts of computer time under appropriate conditions.

It is based on finding the transient response of the network to a periodic forcing function and monitoring the resulting oscillatory transient response until such time as cycle-to-cycle periodicity (within predetermined error limits) has been established. At that point, numerical integration is halted and the (stored) data for the most-recent complete cycle of network waveform data is processed to yield information of interest. This information can include the

* On an IBM 7094 computer.

following:

(a) Any function of one or more circuit or device waveforms, including multiplication, division, differentiation, integration, etc.

(b) Instantaneous power flows at any point.

(c) Detection of voltage or current excursions leading to potential unreliability, even at physically inaccessible locations.

(d) Fourier analysis of any waveforms, including dc components.

(e) Calculation of average power dissipations in both device and external circuit.

(f) Derivation of effective impedances and VSWR's on the basis of power flows.

(g) Calculation of impedances at the fundamental and harmonic frequencies.

(h) Gain and efficiency.

The program also contains means for the computation of Rieke diagrams (also known as load-pull diagrams or power-load contours) for a large-signal microwave transistor model.

All of the above results can be computed on the basis of a single accurate characterization of the device and its associated circuitry. Obtaining the corresponding results experimentally is either very time-consuming or, as in the case of internal device waveforms, impossible. CWFIND is written in the CSMP[24]

simulation language for the IBM 360/75 computer. Typical multi-solution runs (e.g. 10 different CW steady-state solutions) require about 6.8 seconds per solution including compilation time.

As indicated above, see conditions (1) and (2), CWFIND can reasonably be used for applications such as computing the fundamental-frequency behaviour under class C conditions, or determining the harmonic distortion terms caused by device nonlinearities. Such terms would be given by the Fourier analysis of the CW output waveform obtained when the input is a single sinusoid.

The problems encountered when one tries to use CWFIND for intermodulation studies may be illustrated by a simple example. As noted above, a simulation of a single-carrier class C 2N5470 amplifier at 2.0 GHz requires approximately 6.8 seconds per solution. In a typical two-carrier case one might have input carriers:

$f_1 = 2.000$ GHz

$f_2 = 2.004$ GHz

i.e. the fundamental frequency becomes 4 MHz instead of 2 GHz; a lowering by a factor of 500. This would necessitate a corresponding increase of computer by a factor of 500, i.e. from 6.8 sec to 56 min. 40 sec per solution!

4.3 Frequency-Domain

Compared with the situation in nonlinear transient-analysis (time-domain) programs, little development of nonlinear frequency-domain methods seems to have taken place, even though the earliest (pencil-and-paper) nonlinear analysis techniques, such as those of Poincaré[25] and Krylov-Bogoliubov-Mitropolsky[26, p. 329] were frequency-domain methods in the sense that periodic solutions were sought from the outset.

The problem considered by Poincaré was to ascertain the conditions under which systems described by differential equations of the form[26, p. 234]:

$$\ddot{x} + x + \mu F(t, x, \dot{x}) = f(t) \quad \ldots\ldots \quad (4.1)$$

have periodic solutions. Here μ is a small parameter, $F(t,x,\dot{x})$ is a nonlinear analytic function of its arguments and $f(t)$ is a periodic function of time. Solution is possible only if μ is sufficiently small to guarantee convergence of a series solution of the form

$$x(t) = x_0(t) + \mu x_1(t) + \mu^2 x_2(t) + \quad \ldots\ldots \quad (4.2)$$

$$\dot{x}(t) = y(t) = y_0(t) + \mu y_1(t) + \mu^2 y_2(t) + \quad \ldots\ldots \quad (4.3)$$

where the $x_i(t)$ are all strictly periodic functions of time. The term $x_0(t)$ is the linear simple-harmonic solution obtained by putting $\mu = 0$. Then for the first approximation

$$x(t) = x_o(t) + \mu\, x_1(t) \quad \ldots\ldots\ldots\ldots \quad (4.4)$$

$$\dot{x}(t) = y(t) = y_o(t) + \mu\, y_1(t) \quad \ldots\ldots\ldots\ldots \quad (4.5)$$

the objective is to determine $x_1(t)$ such that $x(t)$ remains periodic. This turns out to be possible only for certain fixed values of the zero-th approximation denoted x_o^* and y_o^*. The corresponding zero-order solution is called the <u>generating solution</u> and the first-order solution becomes:

$$x(t) = x_o^*(t) + \mu\, x_1(t) \ldots\ldots\ldots\ldots \quad (4.6)$$

$$y(t) = y_o^*(t) + \mu\, y_1(t) \ldots\ldots\ldots\ldots \quad (4.7)$$

A specific example is given by Stoker [27, pp. 99-103] for the case of a Duffing equation

$$\ddot{x} + (\alpha x + \beta x^3) = F \cos\omega t \quad \ldots\ldots\ldots \quad (4.8)$$

A later development was the so-called asymptotic method of Krylov-Bogoliubov-Mitropolsky(KBM). [26, p. 356] The equations considered have the general form

$$\ddot{x} + \omega^2 x = \mu \sum_{n=-N}^{N} \left[e^{jn\nu t}\, \mathcal{Y}_n(x,\dot{x}) \right] \quad \ldots\ldots\ldots \quad (4.9)$$

where μ is again a small parameter, the n are integers, ω and ν are constant frequencies and the nonlinear functions $\mathcal{Y}_n(x,\dot{x})$ are all polynominals in x and $\dot{x}$.

One starts with a linearized (harmonic) solution of the form

$$x = a \cos \psi$$

where the amplitude a and phase ψ are given by the equations

$$\dot{a} = 0$$

$$\dot{\psi} = \text{constant}.$$

The KBM method for the nonautonomous (i.e. driven) case determines solutions of (4.9) in the form

$$x = a \cos \psi + \sum_{n=0}^{\infty} \mu^n f_n(a, \psi, \nu t) \quad \ldots\ldots\ldots \quad (4.10)$$

where $f_n(a,\psi,\nu t)$ is a periodic function of ψ and νt and the amplitude and phase are given by the first-order differential equations

$$\dot{a} = \sum_{n=1}^{\infty} \mu^n A_n (a) \quad \ldots\ldots\ldots \quad (4.11)$$

$$\dot{\psi} = \omega + \sum_{n=1}^{\infty} \mu^n B_n (a) \quad \ldots\ldots\ldots \quad (4.12)$$

in whioh the RHS's depend only the amplitude. The functions $A_n(a)$, $B_n(a)$ and $f_n(a,\psi)$ are calculated iteratively. Thus they are first found for n = 1; these results are used to oalculate the functions for n = 2 and so on. When A_n, B_n and f_n have been determined with sufficient accuracy, (4.11) and (4.12) are integrated to give a(t) and ψ(t) which are then substituted in (4.10) to yield the desired

solution. A thorough discussion is given by Minorsky[26, pp.358-380]. Recently Rink and Streifer[28] have developed computer programs in the FØRMAC algebraic-manipulation language which use the KBM method to solve analytically differential equations of type (4.9). These programs remove some of the difficulties attending the manipulation of the very large number of algebraic terms which must be included to obtain the final results.

However, even these sophisticated techniques have not yet been extended to cover the present type of problem. It has been found that in the case of a microwave power transistor amplifier, a reasonably accurate simulation[23] requires a nonlinear differential equation of at least eighth order (or a corresponding system of eight first-order differential equations). Not only this, but intermodulation distortion studies require in addition the presence of two or more periodic forcing functions simultaneously. The prospect of treating such a problem algebraically is formidable indeed.

A new direction of research in nonlinear frequency-domain analysis has been established by Neill[8,12] and is currently being further developed by Heywood and Moore[29] and by Heywood[30].

Neill's method is, in a sense, a generalization of the Laplace transform method commonly used for linear network analysis. In the original description[8] the network nonlinearities are restricted to those which can be represented as voltage-dependent current generators. Thus the generator in branch j is assumed to produce the output

$$i_j = f_j\left(\underline{A}\{v_k\}\right) \quad \ldots\ldots\ldots\ldots \quad (4.13)$$

where: f_j is a nonlinear function,

$\underline{A}$ is the branch-node incidence matrix[32] with the "ground" column deleted,

$\{v_k\}$ is the vector of node voltages and k is the node number.

The complete vector of currents due to the nonlinear generator is

$$\{i_j\} = \underline{A}^T \left\{ f_j\left(\underline{A}\{v_k\}\right) \right\} \quad \ldots\ldots \quad (4.14)$$

Including the vector of external nodal current sources, $I_k(t)$, this becomes

$$\{i_k(t)\} = \{I_k(t)\} + \underline{A}^T \left\{ f_i\left(\underline{A}\{v_k(t)\}\right) \right\} \ldots \quad (4.15)$$

The Laplace transform of $\{i_k(t)\}$ is *

$$\mathcal{L}\{i_k(t)\} = \underline{Y}(s) \cdot \mathcal{L}\{v_k(t)\} \quad \ldots\ldots \quad (4.16)$$

so that we may write

$$\underline{Y}(s)\mathcal{L}\{v_k(t)\} = \mathcal{L}\{I_k(t)\} + \mathcal{L}\left[\underline{A}^T \left\{ f_j\left(\underline{A}\{v_k(t)\}\right) \right\} \right] . \quad (4.17)$$

or solving for $\mathcal{L}\{v_k(t)\}$:

---

* where $\underline{Y}(s)$ is the nodal admittance matrix of the linear part of the network

$$\mathcal{L}\{v_k(t)\} = \underline{Y}^{-1}(s).\mathcal{L}\{I_k(t)\} + \underline{Y}^{-1}(s)\mathcal{L}\left[\underline{A}^T\left\{f_j.(\underline{A}\, v_k(t))\right\}\right] \quad . . (4.18)$$

The term $\underline{Y}^{-1}(s).\mathcal{L}\{I_k(t)\}$ is the response of the linear part of the network. Noting that $\underline{Y}^{-1}(s)$ is simply the Laplace transform of the impulse response $\underline{h}(t)$ of the linear part of the network we may write for the time-response

$$\{v_k(t)\} = \{v(t)\}^{(o)} + \underline{h}(t)* \underline{A}^T\left\{f_j(\underline{A}\{v_k(t)\})\right\} \quad . . (4.19)$$

where $\{v(t)\}^{(o)}$ is the periodic time-response of the linear part of the network to the vector of nodal current sources, the * denotes convolution and use has been made of the fact that[32,p.262]

$$\mathcal{L}[x(t)].\,\mathcal{L}[y(t)] = \mathcal{L}[x(t)* y(t)] \quad . . . . . (4.20)$$

Formally, (4.19) represents the time-domain response of the network. The practical snag is that $\{v_k(t)\}$ appears on both sides of the equation. Neill's solution to this problem is to set up the following Picard iteration.

$$\{v_k(t)\}^{(n)} = \{v_k(t)\}^{(o)} + \underline{h}(t)*\underline{A}^T\left\{f_j(\underline{A}\{v_k(t)\}^{(n-1)})\right\}$$

. . . (4.21)

and to circumvent the difficulties of doing the convolution by using the Fourier transform to go directly to the frequency domain. The convolution now degenerates into a product:

$$\left\{V_k(\omega)\right\}^{(n)} = \left\{V_k(\omega)\right\}^{(o)} + \underline{H}(\omega).F\left[\underline{A}^T\left\{f_j(\underline{A}\, V_k(t)\right\}^{(n-1)})\right] \quad \ldots . \quad (4.22)$$

Here $V_k(\omega)$ and $\underline{H}(\omega)$ are the Fourier transforms $F[v_k(t)]$ and $F[\underline{h}(t)]$ respectively and we have used

$$F[x(t)].\ F[y(t)] = F[x(t)^*\ y(t)] \quad \ldots . \quad (4.23)$$

Note that the terms $\left\{V_k(\omega)\right\}^{(o)}$ and $\underline{H}(\omega)$, which appear in each step of the iteration, need only be calculated once. Each step involves going from the time-domain to the frequency-domain and back. In practice this is expedited by using the fast Fourier transform (FFT)[33]. If the sequence (4.17) converges then the frequency-domain solution $\left\{V_k(\omega)\right\}$ will be approached directly without going through <u>any</u> transient-response calculations.

Neill has used this method to calculate the harmonic and inter-modulation distortion products of a quasilinear common-emitter transistor amplifier. The transistor is represented by a nonlinear equivalent circuit given by Narayanan[34] in which the following sources of nonlinearity are approximated by Taylor-series expansions about the operating point and truncated at the third term:

(1) The experimental relation between emitter current and emitter voltage:

$$i_e(t) = I_o \exp\left[(q/kT)v_e(t) - 1\right] \quad \ldots \quad (4.24)$$

(2) Avalanche multiplication, [6, eqn.(14)].

(3) The variation of h_{FE} with collector current, [6, eqn. (13)].

Using carriers f_1 and f_2 at 10.0 and 11.0 MHz, the program based on the above procedure computed all the spectral lines (at 1 MHz intervals) from 1.0 to 160.0 MHz, i.e. from the difference frequency (f_2-f_1) to the sixteenth harmonic of 10 MHz ($16\ f_1$). The time taken was 13 minutes on an Elliot 503 computer. Comparison with experimental results was not given.

Some preliminary work on applying this method was done during the course of the present project. This included the use of the FFT to calculate the spectrum corresponding to $F\left[\underline{A}^T\left\{f_j(\underline{A}\ V_k(t))\right\}\right]$ for the particularly simple case of an ideal ZMNL exponential diode model. Since the present project is particularly concerned with large-signal operation, a truncated Taylor-series approximation was not used. Instead, the representation (4.24) was used intact. As described in the Appendix for carriers f_1 and f_2 at 2.000 and 2.004 GHz, 4096 ($=2^{12}$) spectral lines (at 4 MHz intervals), covering the range 4.00 MHz to 16.384 GHz, were calculated in 4.2 sec. using a CDC 6400 computer. This work was intended as a preliminary step towards performing a full-scale intermodulation analysis on the detailed nonlinear model for the 2N5470 microwave power transistor which is described in References [1] and [2]. This model consists of a modification of the classical Ebers-Moll representation and includes for each junction non-approximated relationships for

the exponential current-voltage characteristic, the current-dependent diffusion capacitances and the voltage-dependent depletion capacitances. Avalanche multiplication and h_{FE} current-dependency are not included. The model is completed by a network of lumped-element inductors and capacitors which simulate the parasitics of the coaxial transistor package.

However, before writing a comprehensive analysis program incorporating Neill's method, it was reflected that the method depends on iterating from a linear approximate frequency-domain solution. This means that it could only be used in quasi-linear situations, such as the intermodulation-distortion of a class A amplifier in which the behaviour is qualitatively unchanged from very low levels ("linear") up to saturation. It could not be used in the case of a class C amplifier in which qualitatively discontinuous changes in behaviour are seen (see for example Fig. 3-9) as one increases the input power from very low to saturation levels. This is a consequence of the fact that the very existence of the class C mode depends on device nonlinearities and means that the linearized frequency-domain solution-vector $\{V_k(\omega)\}^{(o)}$ in (4.22) may fail to be even a coarse approximation to $\{V_k(\omega)\}$, the nonlinear solution.

Correspondence with Neill[35] revealed that special methods may be required to produce a convergent iteration and this possibility was confirmed by Heywood and Moore [29] who derived a rigorously sufficient condition for convergence. They also reported instability of the sequence (4.22) in cases involving frequency-dependent Y

and capacitive nonlinearities. Subsequent correspondence with Heywood[30] further revealed that he is continuing the development of Neill's method but is restricting it to examples involving polynomial approximations to device nonlinearities. His network analysis program will determine the frequency-domain response of a forced nonlinear network which may contain any or all of the following lumped elements:

(1) Linear: R, L, C voltage controlled current source, independent current source.

(2) Nonlinear: Conductance, incremental capacitance, and voltage controlled current sources expressed as polynomials of the form*

$$i_k = G(v_k) = G_1 v + G_2 v^2 + \ldots\ldots + G_n v^n$$

$$i_k = \frac{dQ}{dt} = \frac{dQ}{dv_k}\frac{dv_k}{dt} = C(v_k)\frac{dv_k}{dt} = C_1\frac{dv_k}{dt} + C_2 v_k \frac{dv_k}{dt} + \ldots$$

$$i_j = GM(v_k) = GM_1\, v_k + GM_2\,(v_k)^2 + \ldots + GM_n (v_k)^n$$

branch $j \neq$ branch k.

The program can accomodate 20 nodes, 10 nonlinear elements, 100 discrete frequencies and 5 independent signal sources. Output data includes the spectrum for each voltage controlling a nonlinear element, the spectrum of any other branch voltage specified and the estimated accuracy of the solution.

Two examples of the use of this program include

* The program accepts nonlinear functions of one variable only.

(a) The optimization of a 7-mode parametric frequency multiplier, using a 3-term series approximation for the varactor characteristic.

(b) A harmonic distortion analysis of a two-stage transistor amplifier with 9 nodes and a single input carrier. The series approximations for the conductance and transconductance nonlinearities extend to 6 terms; the capacitances are linearized.

Because Heywood has promised us a copy of his final Ph.D thesis together with his program listings, and in view of the limited time available for this project, it was decided not to attempt to duplicate his efforts. This line of attack was therefore temporarily discontinued in favour of another approach. This, in essence, is a descendant of the "empirical" approach of Berman and Podruczky[5], and incorporates ideas due to many workers including Seddon[36], Sinclair[37], Shimbo[10] and Moody[38]. Originally intended for calculations of intermodulation distortion in travelling-wave tubes under multi-carrier conditions, the later development of the approach has predicted intermodulation-distortion products for a gain-optimized power transistor with remarkable accuracy. This work is described in Section 6. It has also given good agreement with experimental results obtained for a particular combination of tuning and dc-bias conditions which gave rise to a low-intermodulation-distortion mode of operation[39] which is characterized by useful values of gain, dynamic range and efficiency.

4.4 Summary

This section has surveyed some of the possible methods which

could be applied to the analysis of intermodulation noise in a multicarrier microwave transistor power amplifier. The methods considered have been confined to those belonging to the "device modelling tradition" and it is by no means clear that presently-existing methods are fitted for the task. Areas of particular concern appear to be:

(1) The preparation of nonlinear device models sufficiently accurate to afford reliable prediction of distortion levels as much as 40 to 50 dB below output carrier level. It is particularly difficult to do this when the device works under a saturated-gain condition; precisely the condition of greatest interest for satellite applications.

(2) The provision of efficient frequency-domain methods of numerical analysis which are capable of handling device models incorporating highly nonlinear characteristics, without resorting to truncated power-series approximations.

The next section surveys those methods for attacking the IMD-analysis problem which belong to the "empirical tradition". Hitherto these methods have been primarily the preserve of TWT analysists, but as mentioned above, we have found that they can be applied very successfully to microwave power transistors also.

5. ANALYSIS OF INTERMODULATION DISTORTION BY EMPIRICAL METHODS

Many of the methods discussed in this section have already been introduced in Section 2. In contrast to the methods discussed in Section 4, in which an attempt is made to generate an explicit physical-mathematical model of the nonlinear (active) device, this section is concerned with approaches which predict the multicarrier performance of the device on the basis of its measured single-carrier performance. Hitherto, such approaches have been confined to the study of travelling-wave tubes; the present interest is in their potential for application to transistors. The motivation for the development of these empirical approaches appears to have been not only the sheer difficulty of generating sufficiently accurate device models, but also the severe problem of how to analyze their behaviour in a multicarrier environment.

Some of the methods to be discussed here use perhaps the most straight-forward single-carrier representation of a communications amplifier. This is simply a measurement of its output power P_{out} as a function of its input power (P_{in}). Such a measurement is done at a fixed frequency and without adjusting the tuning or bias conditions. Thus, the measurement is not a "universal" one, as a conventional device-model attempts to be. Instead, it is specific to the particular conditions of frequency, tuning and bias under which it was made. However, this limitation seems a small price to pay for the consequent possibilities for predicting the multicarrier performance.

Since the instantaneous power in a composite multicarrier signal can fluctuate from zero to levels perhaps 12 dB above the saturation level [5, p. 73], accuracy requirements dictate that the $P_{out}(P_{in})$-characteristic be measured over as wide a dynamic range as possible.

At frequencies where nonlinear reactances become important, the simple $P_{out}(P_{in})$ representation is insufficient and one requires in addition the $\phi_{out}(P_{in})$-characteristic which relates the relative output phase-angle to the input power.

5.1 Amplitude Nonlinearity Only

The earlier empirical work considered amplitude nonlinearities only, so that the device could be represented as zero-memory nonlinear (ZMNL) with input $x(t)$ and output $y(t)$:

$$x(t) \rightarrow \boxed{\text{ZMNL}} \rightarrow y(t) = \mathcal{F}\{x(t)\} \tag{5.1}$$

A variety of different representations for the nonlinear function $\mathcal{F}\{x\}$ have been employed. Examples are given below:

5.1.1 Hard limiter

In the case of the classical "hard limiter" the characteristic is similar to Figure 2-1:

$$y(t) = \mathcal{F}\{x(t)\} = \begin{cases} cx, & -a \leq x \leq a \\ ca, & |x| > a \end{cases} \tag{5.2}$$

and in general cannot be identified with any physical amplitude characteristic of the device. Examples of the use of this representation occur in Cahn[3] and Sunde[4] and are discussed in Sections 2.1 and 2.2 respectively. The only way to fix the values of the parameters a

and c is to adjust them until the predicted (e.g. single-carrier) performance agrees sufficiently well with the measured performance. In general, good agreement cannot be expected with only two adjustable parameters.

5.1.2 Power-series representation

Better agreement can be obtained by using the measured amplitude data to fit the coefficients of a power series of the form

$$y(t) = \mathcal{F}\{x(t)\} = \sum_{m=1}^{\infty} c_m x^m(t) \quad . \tag{5.3}$$

In practice, of course, the summation is truncated at a fairly small number of terms. Examples of the use of this representation in the prediction of IMD product levels occur in Hilling and Salmon[7] and Meyer, Shensa and Eschenbach[13,II] and are discussed in Sections 2.5 and 2.10 respectively.

5.1.3 Fourier-series representation

For a given number of terms, a Fourier series representation can give a better approximation to a ZMNL amplitude characteristic than does the simple power series of 5.1.2. The form of the Fourier series is

$$y(t) = \mathcal{F}\{x(t)\} = \sum_{m=1}^{\infty} c_m \sin[m\alpha\, x(t)] \tag{5.4}$$

where α is a scaling factor (equal to $\pi/4$), and the c_i are adjustable coefficients. Examples of use may be found in Berman and Podraczky[5] and in Seddon[36]. In both cases four-term series are used with m = 1,2,3 and 5. A discussion of the work of Berman and Podraczky

is given in Section 2.3.

5.2 Simultaneous Amplitude and Phase Nonlinearities

A more complete empirical representation involves characterization of both amplitude and phase nonlinearities. In this case, the device is treated as nonlinear-with-memory (NLWM):

$$x(t) \rightarrow \boxed{\text{NLWM}} \rightarrow y(t) = \mathcal{F}\left\{x(t), \int x\,dt\right\} \tag{5.5}$$

Again, a number of different representations of the nonlinear function f $x, \int x\,dt$ have been employed. Examples follow.

5.2.1 Volterra series representation

For a NLWM system, the power series, which was sufficient to characterize a ZMNL system, may be replaced by the Volterra series, which can be regarded as a generalization of the power series. In this case

$$\begin{aligned} y(t) &= \mathcal{F}\left\{x, \int x\,dt\right\} \\ &= \int_0^t c_1(t-\tau)x(\tau)\,d\tau + \\ &+ \int_0^t\int_0^t c_2(t-\tau_1,\ t-\tau_2)x(\tau_1)x(\tau_2)\,d\tau_1\,d\tau_2 \\ &+ \int_0^t\int_0^t\int_0^t c_3(t-\tau_1,\ t-\tau_2,\ t-\tau_3)x(\tau_1)x(\tau_2)x(\tau_3)\,d\tau_1\,d\tau_2\,d\tau_3 \\ &+ \cdots \end{aligned} \tag{5.6}$$

wherein the first term is the response of the linear part of the representation as given by the convolution of the input $x(t)$ with the impulse-response $c_1(t)$ of the linear part of the system. Narayanan[6] has used

this approach to investigate the IMD behaviour of a small-signal (quasilinear) feedback transistor amplifier as described in Section 2.4. Another example of the use of this approach was given by Meyer, Shensa and Eschenbach[13], see Section 2.10.

In general, it is considered that approaches based on the Volterra series are unsuitable for the type of problem with which this report is concerned because of the restriction to small-distortion conditions. Gross nonlinearities cause the series to converge very slowly so that the cumbersome higher-degree terms of (5.6) cannot be neglected.

5.2.2 Power-series with complex coefficients

In a NLWM system, suppose that the input signal, which may be single or multicarrier, can be written

$$x(t) = \rho(t)\cos\left\{\omega_o t + \mu(t)\right\} \tag{5.7}$$

where $\rho(t)$ is the instantaneous amplitude

$\mu(t)$ is the instantaneous phase

ω_o is a reference frequency.

If the output can be represented as

$$y(t) = g(\rho)\cos\left\{\omega_o t + \mu(t) + f(\rho)\right\} \tag{5.8}$$

where $g(\rho)$ is due to the amplitude nonlinearity

$f(\rho)$ is caused by AM-to-PM conversion

then it has been shown by Shimbo[10] that the magnitude of the IMD product whose angular frequency is

$$\omega_o + k_1\omega_1 + \ldots + k_n\omega_n \tag{5.9}$$

(where k_i are $\pm$ integers or zero and $\sum_{i=1}^{n} k_i = 1$) is given by the modulus

of the complex quantity

$$M(k_1, k_2, \ldots, k_n) = \int_0^\infty r \prod_{m=1}^{n} J_{k_m}(V_m r) \left[\int_0^\infty \rho g(\rho) e^{jf(\rho)} J_1(r\rho) \right] dr \qquad (5.10)$$

where V_i is the amplitude of the i^{th} input carrier (see also 2.22).

In order to calculate M numerically, a particular form has to be specified for the function occurring in (5.10):

$$g(\rho) e^{jf(\rho)} \qquad (5.11)$$

which represents both the nonlinear gain and the AM-to-PM conversion.

A simple form for (5.11) is a power series[10, p. 233] with complex coefficients a_m:

$$g(\rho) e^{jf(\rho)} = \sum_{m=0}^{\infty} a_m \rho^{2m+1} \qquad (5.12)$$

In this case it can be shown that

$$M(k_1, k_2, \ldots, k_n) = \sum_{m=0}^{\infty} (-1)^m m!(m+1)! 2^{2m+1} a_m b_{m+1} \qquad (5.13)$$

where the terms b_i are coefficients of the expansion

$$r \prod_{m=1}^{n} J_{k_m}(V_m r) = \sum_{n=1}^{\infty} b_n r^{2n} \qquad (5.14)$$

which has to be computed separately for each IM product. In practice one measures the single-carrier $P_{out}(P_{in})$ and $\phi_{out}(P_{in})$ characteristics and from them derives $g(\rho)$ and $f(\rho)$ respectively. Then the complex coefficients a_i of the power series in (5.12) must be fitted to the measured function (5.11), using a suitable curve-fitting procedure.

In practice, the power series must, of course, be truncated at a finite number of terms.

5.2.3 Fourier series with complex coefficients

An alternative form for (5.11) in the previous section is a Fourier-series expansion[10, p. 233] with complex coefficients a_m:

$$g(\rho)e^{jf(\rho)} = \sum_{m=1}^{\infty} a_m \sin(m\alpha\rho) \tag{5.15}$$

In this case,

$$M(k_1, k_2, \ldots, k_n) = \sum_{m=1}^{\infty} a_m \sum_{k=0}^{\infty} \frac{k!(k+1)!}{(2k+1)!} 2^{k+1} b_{k+1} (m\alpha)^{2k+1} \tag{5.16}$$

where the b_i are again given by (5.14). The Fourier series in (5.15) must, of course, be truncated at a finite number of terms for a practical curve-fitting of experimental data.

5.2.4 Bessel series with complex coefficients

A particularly advantageous form for (5.11) is a Bessel series with complex coefficients a_m:

$$g(\rho)e^{jf(\rho)} = \sum_{m=1}^{\infty} a_m J_1(m\alpha\rho) \tag{5.17}$$

In this particular case, Eq. (5.10) takes a simple form in which the coefficients b_i do not appear:

$$M(k_1, \ldots, k_n) = \sum_{m=1}^{\infty} a_m \prod_{m=1}^{n} J_{k_m}(m\alpha V_m) \tag{5.18}$$

This leads to considerably improved computational efficiency and has been used to derive the results described in Section 6 of this report.

6. PREDICTION OF INTERMODULATION DISTORTION LEVELS CAUSED BY A MICROWAVE POWER TRANSISTOR

As indicated earlier in this report, this section refers to work done after the expiration of the contract period and will therefore be described only briefly. A more complete discussion, including the practically important question of the prediction of the multicarrier* IMD levels under the "low-IMD" condition, may be found in Reference [39].

6.1 Experimental

The set-up used is similar to the one shown in Figure 3-1, modified for two input carriers as indicated in Figure 3-12. Both input and output ports are provided with double-dielectric-slug tuners and adjustable dc bias supplies. The device is protected from excessive dc collector currents by means of a crowbar circuit in series with the collector bias supply V_{cc}. The total output power is monitored by a wideband power meter, the average dc current in the output circuit by a clip-on type milliammeter and the levels of the IMD products by a spectrum analyzer.

Having set the two oscillators to the desired frequencies f_1 and f_2, the gain of the TWTA is adjusted so that the level of each carrier in the combined input signal to the amplifier under test is the same. Then the absolute level of the combined signal can be controlled by the adjustable attenuator. The power incident on the

---

* Up to 12 equal-amplitude carriers.

amplifier input is initially determined by replacing the amplifier by the 50 ohm thermistor head of a power meter.

When the amplifier has been tuned and biased for the required operating condition, one of the input carriers is removed and the output power and the relative output phase-angle are measured as functions of the input power using a Hewlett-Packard network analyzer in a set-up similar to the one shown in Figure 3-10. This characterization is done over as wide a range of power-levels as possible. The resulting $P_{out}(P_{in})$ and $\phi_{out}(P_{in})$ transfer characteristics constitute a mathematical representation of the rf behaviour of the active device together with its package and parasitics and its immediate network environment (tuning elements, etc.). This representation can be used to make predictions of the IMD products and effective gain under multi-carrier conditions. It cannot, however, be used to predict efficiency. In that case, a more conventional physical model of the active device would be required. The other shortcoming of the gain and phase characterization is that it is specific to a particular tuning and bias condition (but not to a particular power level.) Its overwhelming advantage is that it is at present the only mathematically satisfactory representation for calculations of the multi-carrier behaviour.

6.2 Computational Procedure

From equations (5.7) and (5.8) it is evident that ρ is proportional to $\sqrt{P_{in}}$ and $g(\rho)$ is proportional to $\sqrt{P_{out}}$. The function $f(\rho)$ in

(5.8) is just the output phase-angle (in radians). Since the present interest is in the relative rather than the absolute levels of the IMD products, it is convenient to normalize ρ, $g(\rho)$ and $f(\rho)$ such that $g(\rho) = 1$ at the saturation level and $f(\rho) = 0$ at the zero input-power level.

The double curve-fitting of the measured $P_{out}(P_{in})$ and $\phi_{out}(P_{in})$ characteristics to the Bessel series in (5.17) is accomplished by means of a modified version of the nonlinear-regression program NLRGRES[44]. First the in-phase (real) part of (5.11) is fitted, namely

$$g(\rho)\cos f(\rho) \ ,$$

then the quadrature (imaginary) part is fitted:

$$g(\rho)\sin f(\rho) \ .$$

It is found in practice that the in-phase part usually fits much better than the quadrature part. In general, the scaling factors α in (5.17) will be different in the two cases. To minimize the number of times the Bessel functions have to be computed, it is advantageous for both in-phase and quadrature components to have the same α. Thus, when a satisfactory quadrature fit has been achieved, the resulting value of α is prescribed as a fixed parameter for the in-phase curve-fitting operation.

In the present case both in-phase and quadrature components are fitted by a Bessel series truncated at the ninth term.

When the double curve fitting has been accomplished, the in-house computer program MING is used to compute the IMD levels for the

desired number of carriers. The original version of this program[36], which was written by Seddon of RCA Limited, was based on the work of Berman and Podraczky[5] and was designed to run on an IBM 360/65 computer. A description of the theoretical background for this version has been given by Sinclair[37]. The original form of MING utilized the four-term Fourier-series nonlinear gain characteristic described in Section 5.1.3 and did not consider the variation of output phase with input power. MING has subsequently been modified by Moody of RCA Limited in two major respects:

(i) The amplitude-only Fourier-series representation was augmented by the Bessel-series representation (given in Section 5.2.4) for both amplitude and phase nonlinearities.

(ii) The program was translated for a CDC 6400 computer.

The present version of MING accomodates carriers of arbitrary amplitude and spacing; the results reported here, however, are for equal amplitudes and constant spacing. Although the program contains numerous special features, the IMD products are effectively computed according to (5.18) where the a_m are the fitted complex coefficients of the Bessel series in (5.17).

Using a CDC 6400, the NLRGRES double curve-fitting operation consumed 109.7 seconds of CPU time, while the MING computation of the third, fifth and seventh order IMD products (and other data including gain) required 46.2 seconds. Both of these times include compile time.

6.3 Result

The result described here is the one which first indicated the validity of the complex Bessel series for a microwave power transistor.

The device was biased for class A operation and tuned for maximum single-carrier gain at the saturation level. The single-carrier operating conditions are summarized in Table 6(1) and the measured nonlinear $P_{out}(P_{in})$ and $\phi_{out}(P_{in})$ characteristics are shown in Figure 6-1.

Next, two carriers were applied simultaneously to the amplifier at a total power level somewhat less than the saturation level, and the resulting amplifier performance measured. These results, together with the predictions of the MING program, are compared in Table 6(2). The rather satisfactory agreement between the computed and measured levels of the third- and fifth-order IMD products (relative to the carrier levels) prompted a similar investigation for the special case in which the transistor amplifier is optimized for the low-IMD condition. This work is reported in detail in Reference [39].

Table 6(1) - Single-carrier data for a gain-optimized class A amplifier at the saturation level.

Transistor:	2N5470
Mode:	Class A, common base
Frequency:	2.00 GHz, single carrier
Collector Bias:	30 mA, no RF applied
V_{cc}:	28 volts
At the gain optimum:	P_{in} = +26.6 dBm P_{out} = +31.5 dBm G = 4.9 dB η_c = 30%

(41652-79)

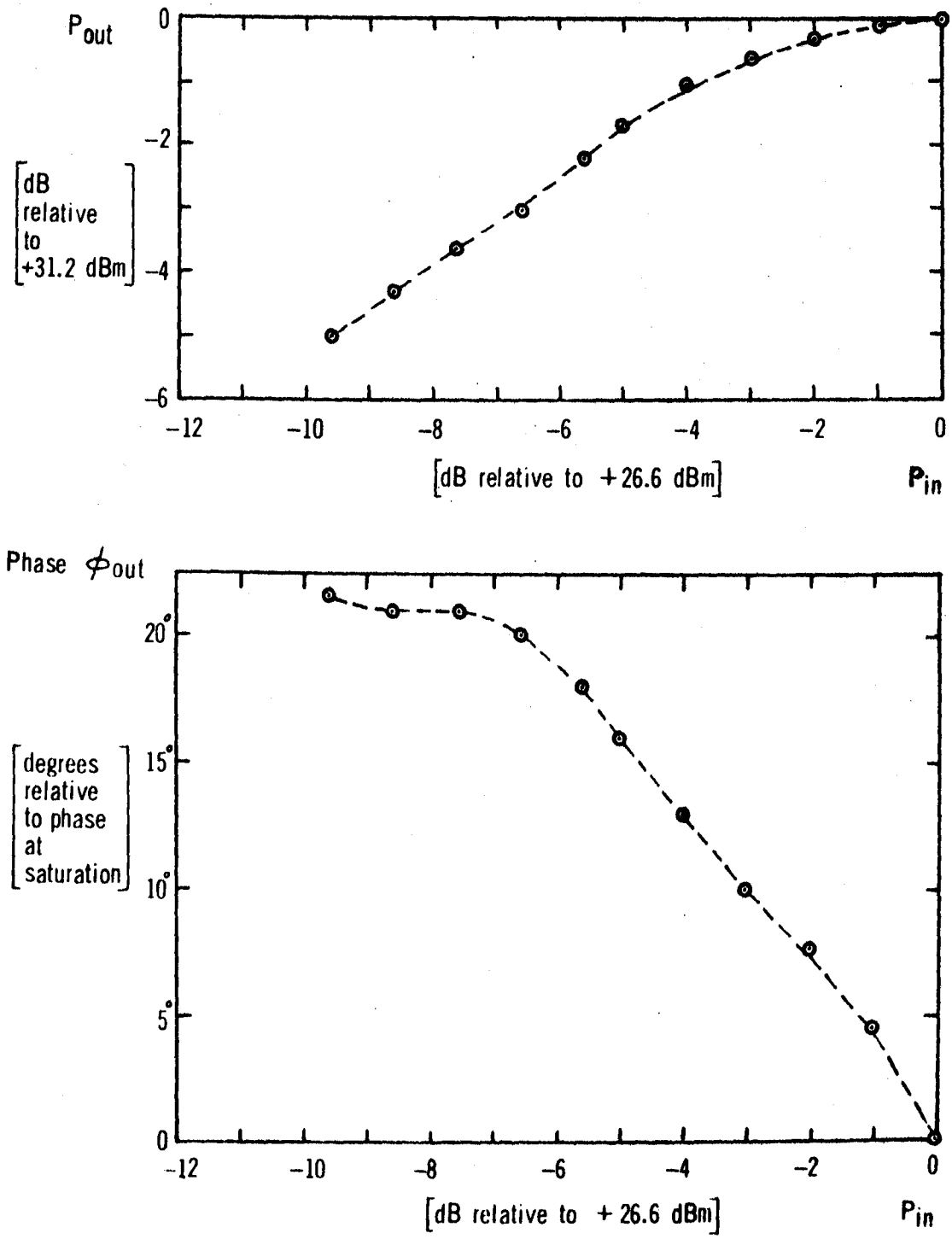

Figure 6-1 Nonlinear $P_{out}(P_{in})$ characteristic (top) and nonlinear $\phi_{out}(P_{in})$ characteristic (below) for the gain-optimized amplifier. In both cases saturation is the zero reference.

Table 6(2) - Measured 2-carrier behaviour of the gain-optimized class A amplifier compared with the predictions of the MING program.

Quantity		Measured	Computed
Carrier Frequencies	f_1	1.998 GHz	-
	f_2	2.002 GHz	-
Collector bias, no RF		30 mA	-
V_{cc}		28 V	-
P_{in}(total)		+ 23.00 dBm	+ 22.72 dBm
P_{out}(total)		+ 29.5 dBm (wideband)	+ 29.5 dBm (carriers only)
Efficiency η_c		28.9%	-
Gain G		6.5 dB	6.7 dB
Relative levels of spectral components	$3f_1 - 2f_2$	-23 dB	-24.7 dB
	$2f_1 - f_2$	-15 dB	-15.6 dB
	f_1	0 dB	0 dB
	f_2	-2 dB	0 dB
	$2f_2 - f_1$	-15 dB	-15.6 dB
	$3f_2 - 2f_1$	-25 dB	-24.7 dB

(41652-70)

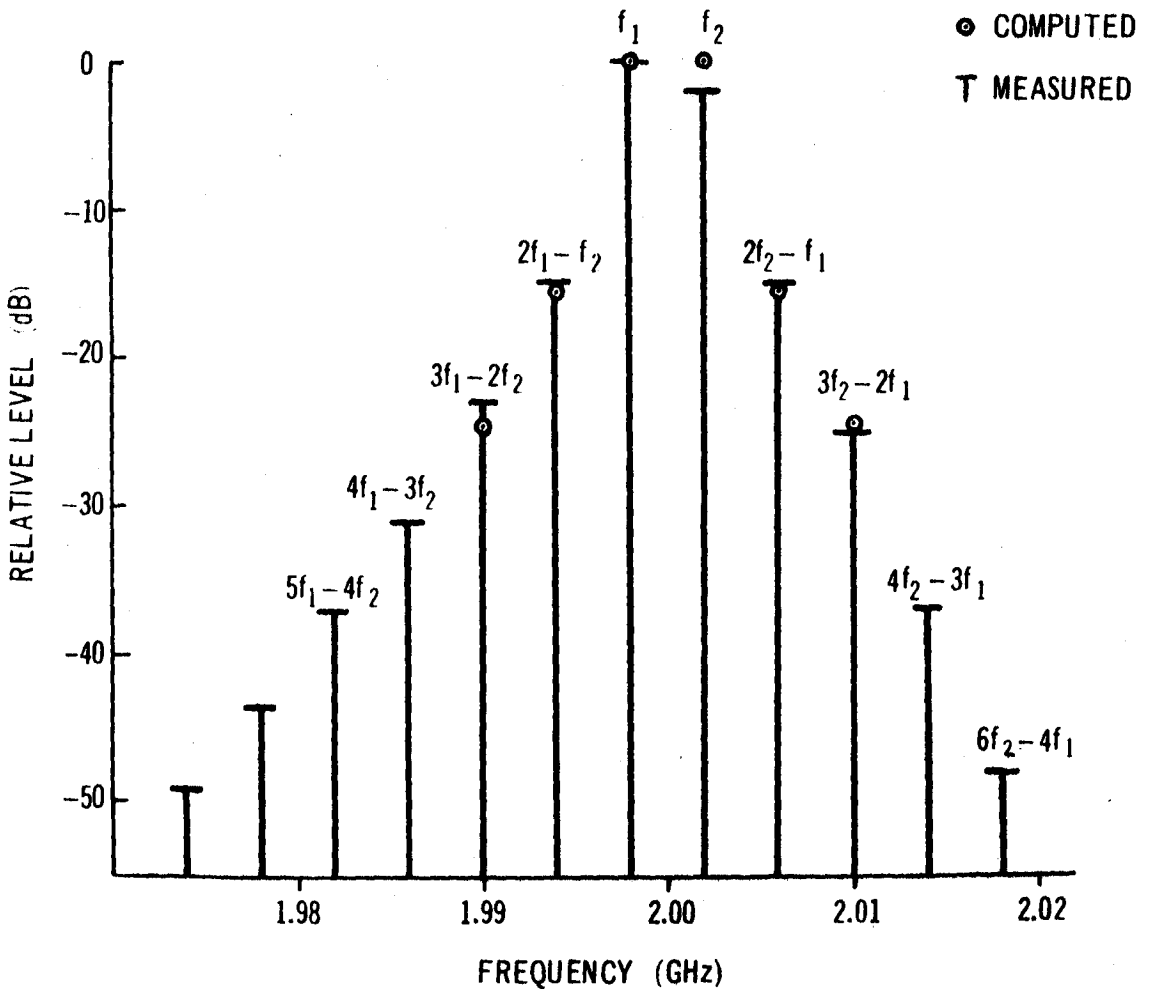

Figure 6-2 Measured 2-carrier IMD spectrum compared with values computed by the MING program; gain-optimized case.

7. CONCLUSIONS

This report has covered a wide range of topics relating to the use of a microwave power transistor in a multicarrier FM communications environment. Even so, it cannot be regarded as more than a starting-point in this field of study, primarily because of the difficulty experienced when one tries to relate practically useful measurements with what can be handled theoretically.

A survey of previous work on distortion in frequency multiplexed communications systems revealed a remarkable variety of different approaches, the "best" approach being by no means apparent. Since most of this work was related to low-frequency data or somewhat limited microwave data, a comprehensive series of measurements was made to determine the basic communications performance of a microwave power transistor. This showed that the device is, in general, unlike a TWT, particularly under class C conditions. Contrary to the situation in class A, the IMD levels in class C can actually increase when the input levels are "backed-off" from saturation. Work arising out of the present study has, however, revealed the presence of a low-IMD condition which requires special tuning and bias settings: this condition should receive detailed further study.

An investigation of the potential of many different methods of nonlinear circuit analysis for the prediction of IMD levels showed that the traditional kind of nonlinear device model, which attempts to represent the device behaviour by a limited number of equations

(the simpler the better) corresponding to the physical structure of the device, is not at present feasible for the present application. This is due to the following reasons:

(1) The accuracy required of the model must be very high if high-order IMD products are to be predicted correctly.

(2) This kind of model is unsuitable for any known computer analysis method when:

(a) Gross nonlinearities are present.
(b) Multicarrier operation is desired.

Under certain conditions 2-carrier analysis would just be feasible but would be unjustifiably extravagant of computer time.

It is shown that a modification of an in-house computer program based on an empirical approach originally used to predict the IM distortion in travelling-wave tubes can also be used to predict IMD in a class A microwave power transistor with good accuracy. A useful extension would be to apply this method to the prediction of IMD under class C conditions and even to other types of microwave device, such as transferred electron amplifiers. Work done outside the contract period has also shown that the method is valid when the microwave transistor is tuned and biased to achieve a condition of unusually low IMD levels.

APPENDIX: ANALYSIS OF INTERMODULATION DISTORTION DUE TO EXPONENTIAL DIODE USING FAST FOURIER TRANSFORM

The following analysis was done to determine the potential of the fast Fourier transform (FFT) technique[45] as part of a frequency-domain nonlinear analysis program.

To get the FFT to work properly the proper number of input time-function samples has to be specified. This number must be of the form 2^K (K = integer) and has to be equal to the number of lines required in the output spectrum (or a multiple thereof). For realism we choose an experimental situation with two microwave carriers spaced 4 MHz apart:

$$\begin{aligned} f_1 &= 2.000 \text{ GHz} \\ f_2 &= 2.004 \text{ GHz} \end{aligned} \tag{A.1}$$

For simplicity, the nonlinear device chosen should be a zero-memory nonlinear (ZMNL) element. Again, for realism, it should have a nonlinear characteristic which is not approximated by a polynomial. These requirements are satisfied by the ideal diode equation:

$$i(t) = I_o \left\{ \exp[(q/kT)v(t)] - 1 \right\} \tag{A.2}$$

The number of points required is given by

$$N = \frac{2Mf_2}{f_2 - f_1} \tag{A.3}$$

where M is the order of the highest harmonic of interest, and the factor 2 appears because we require at least 2 points per period of the highest

harmonic. With the frequencies given in (A.1) and specifying the fourth harmonic (M=4), Eq. (A.3) gives N=4008 points. The nearest power of 2 is 2^{12} = 4096 points, which will give a spectrum extending from 4 MHz to 16.384 GHz.

Normalizing Eq. (A.2)

$$y(t) = \exp[x(t)] - 1 \tag{A.4}$$

where

$$y(t) = i(t)/I_o$$

$$x(t) = \frac{qv(t)}{kT}$$

We apply two simultaneous cosine voltages having the same amplitudes but different frequencies:

$$x(t) = A(\cos \omega_1 t + \cos \omega_2 t), \quad \omega_2 > \omega_1 \tag{A.5}$$

so that the period of the fundamental is

$$T = 2\pi/(\omega_2 - \omega_1)$$

and for $N = 2^K$ time-samples, the time increment is

$$\Delta T = \frac{1}{N(f_2 - f_1)} \tag{A.7}$$

The composite input voltage given by (A.5) is applied across the ideal diode described by (A.4) and a FFT subroutine is used to transform the 2^{12} = 4096 time-samples of y(t) into 2^{12} frequency-points. To limit the quantity of computer output, the program specifies that only spectral lines 1 to 10 and 490 to 510 are to be printed out, although all 4096 are in fact computed. The specified lines include the "DC" end of the spectrum from 0 - 36 MHz as well as the

carriers and their adjacent intermodulation products in the range 1.960 - 2.040 GHz.

Using a CDC 6400, the main program plus FFT subroutine compiled in 4.6 seconds and all 4096 spectral lines were computed for an execution time of 4.2 seconds. The resulting IMD power spectrum for the case $A = 1$ (in Eq. (A.5)) is shown in Figure A1. The levels of the IMD products are referred to the individual carrier levels.

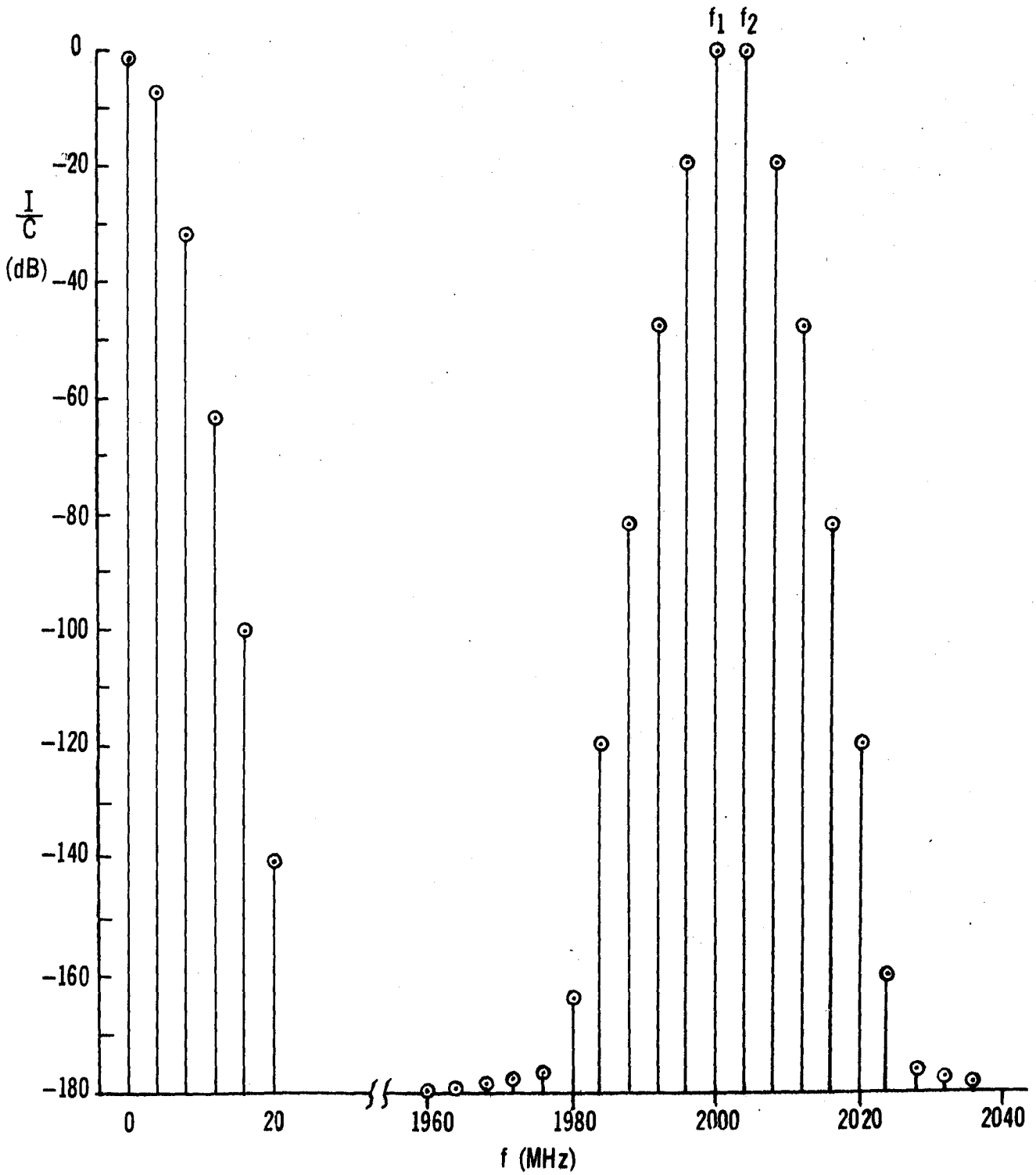

Figure A1 – Part of a 4096-line IMD spectrum due to an ideal exponential diode as calculated using the Fast Fourier transform.

REFERENCES

1. R.G. Harrison, "Modelling a microwave power transistor", RCA Limited Research Labs Report 96122.26, July, 1970 (52 pp.).

2. R.G. Harrison, "Computer simulation of a microwave power transistor", IEEE Journal of Solid-State Circuits, Vol. Sc-6, No. 4, August 1971, pp. 226-235.

3. C.R. Cahn, "Crosstalk due to finite limiting of frequency-multiplexed signals", Proc. IRE, Vol. 48, No. 1, January 1960, pp. 53-59.

4. E.D. Sunde, "Intermodulation distortion in multicarrier FM systems", IEEE International Convention Record, Vol. 13, Part 2 - Communications II: Radio Communication, Broadcasting and Audio, 1965, pp. 130-146.

5. A.L. Berman and E.I. Podraczky, "Experimental determination of intermodulation distortion produced in a wideband communications repeater", IEEE International Convention Record, Vol. 15, Part II, 1967, pp. 69-88.

6. S. Narayanan, "Transistor distortion analysis using Volterra series representation", Bell System Technical Journal, Vol. 46, No. 5, May/June 1967, pp. 991-1024.

7. A.E. Hilling and S.K. Salmon, "Intermodulation in common-emitter transistor amplifiers", Electronic Engineering, July 1968, pp. 360-364.

8. T.B.M. Neill, "Improved method of analysing nonlinear electrical networks", Electronics Letters, Vol. 5, No. 1, 9th January 1969, pp. 13-15.

9. C.R. Cahn, "Calculation of intermodulation due to amplitude limiting of multiple carriers", IEEE Transactions on Communication Technology, Vol. COM-17, No. 6, December 1969, pp. 743-745.

10. O. Shimbo, "Effects of intermodulation, AM-PM conversion, and additive noise in multicarrier TWT systems", Proc. IEEE, Vol. 59, No. 2, February 1971, pp. 230-238.

11. J.C. Boag and E. Newby, "Intermodulation distortion measurements on a microwave class C transistor", RCA Limited Research Memorandum No. 300, August 1971.

12. T.B.M. Neill, "Spectral analysis of quasi-linear systems", Private Communication received 3 September 1971, 8 pp.

13. R.G. Meyer, M.J. Shensa and R. Eschenbach, "Cross modulation and intermodulation in amplifiersat at high frequencies", IEEE Journal of Solid-State Circuits, Vol. SC-7, No. 1, February 1972, pp. 16-23.

14. O.P. Jain, "Software Package for analysis of noise and intermodulation performance of communications transponders", RCA Limited Engineering Report No. 301, March 24, 1972, 17 pp.

15. "1620 electronic circuit analysis program [ECAP][1620-EE-02X] user's manual", IBM Application Program, File H20-0170-1, 1965.

(See also: G.R. Hogsett, "ECAP/360-E electronic circuit analysis program for the IBM System/360", S/360 General Program Library, File 360D-16.4.001, August 1966).

16. P.E. Gray and C.L. Searle, "NATFREQS (FORTRAN)", in Electronic Principles, Physics, Models and Circuits, New York: Wiley (Appendix C), 1969.

17. K.L. Deckert and E.T. Johnson, "User's guide for LISA", IBM Corporation, San Jose, California, U.S.A. File 7094-IBM0001, August, 1967.

18. H.G. Bown, "CAD-1: a DRTE computer program for ac and dc network analysis", Defence Research Telecommunications Establishment Technical Memorandum No. 489, Defence Research Board, Ottawa, Canada, September 1967.

19. A.F. Malmberg, F.L. Cornwell and F.N. Hofer, "NET-1 Network analysis program, 7090/94 version", Report No. LA -3119, Los Alamos Scientific Laboratory of the University of California, Los Alamos, New Mexico, U.S.A., September 1964.

20. H.W. Mathers, S.R. Sedore and J.R. Sents, "Automated digital computer program for determining responses of electronic circuits to transient nuclear radiation (SCEPTRE)", IBM Electronics Systems Centre, Owego, New York, Report issued by Air Force Weapons Laboratory, Kirtland AFB, New Mexico, Technical Report No. AFWL-TR-66-126, February, 1967.

21. E.D. Johnson, C.T. Kleiner, L.R. McMurray, E.L. Steele and F.A. Vassallo, "Transient radiation analysis by computer program (TRAC)", Autonetics Division, North American Rockwell Corp. Anaheim, California, report issued by Harry Diamond Labs., Washington, D.C., June 1968.

22. L.D. Milliman, W.A. Massena and R.H. Dickhaut, "CIRCUS - digital computer program for transient analysis of a electronic circuits - user's guide", Boeing Corporation, Seattle, Washington, Harry Diamond Labs, Report AD-346-1, January 1967.

23. R.G. Harrison, "CWFIND - a computer program for the nonlinear analysis of simple microwave transistor circuits", RCA Limited Research Laboratories Report (in preparation).

24. "System/360 continuous system modelling program user's manual (4th edition)", IBM Corp. White Plains, N.Y., 1969.

25. H. Poincaré, "Les méthodes nouvelles de la mécanique céleste" Vol. 1, Paris: Gauthier-Villars, 1892.

26. N. Minorsky, "Nonlinear Oscillations", Princeton, N.J: D. van Nostrand Company Inc, 1962.

27. J.J. Stoker, "Nonlinear Vibrations", New York: Interscience Publishers Inc., 1950.

28. R.A. Rink and W. Streifer, "Application of digital computers to solve analytically a class of second-order nonlinear ordinary differential equations", IEEE Transactions on Computers, Vol. C-20, No. 8, August 7971, pp. 901-910.

29. D.R. Heywood, A.D. Moore, "Comment on an improved method of analysing nonlinear electrical networks", Electronics Letters, Vol. 5, No. 12, 12th June 1969, pp. 269-271.

30. D.R. Heywood, Printouts from nonlinear frequency-domain analysis programs forming basis of Ph.D Thesis, TRIUMF Meson Facility, University of British Columbia, Vancouver 8, B.C., private communication received 5th April 1972.

31. F. Branin, "Computer-aided design: part 4. Analyzing circuits by the numbers", Electronics, Vol. 40, No. 1, January 9th, 1967, pp. 88-103.

32. H. Margenau, "The mathematics of physics and chemistry", Princeton, N.J.: D. van Nostrand CO. Inc., Second Edition, 1956.

33. J.W. Cooley, P.A.W. Lewis, P.H. Welch, "Application of the fast Fourier transform to computation of Fourier integrals, Fourier series, and convolution integrals", IEEE Transactions on Audio and Electroacoustics, Vol. AU-15, No. 2, June, 1967, pp. 79-84.

34. G.D. Bergland, "A guided tour of the fast Fourier transform", IEEE Spectrum , July 1969, pp. 41-51.

35. T.B.M. Neill, private correspondance received 1 September 1971.

36. J. Seddon, "Computer program for calculating multicarrier intermodulation noise due to gain nonlinearity in a TWT (MING)", circa 1969.

37. J. Sinclair, "Computer program to obtain the intermodulation noise spectrum due to the transfer characteristic nonlinearity of a TWT with multicarrier operation", (Documentation for original version of the MING program), unpublished, undated. Private communication received from H. Moody, June 1972.

38. H. Moody, "Modified version of MING program including Bessel series representation of gain and phase nonlinearities", private communication received May 1972.

39. R.G. Harrison, H.J. Moody, "Preliminary investigation of conditions for low intermodulation distortion in a microwave power transistor", RCA Limited Research Labs., Technical Report MNLD-72-004, August 1972, pp. 34.

40. Y.H. Ku and A.A. Wolfe, "Volterra-Wiener functionals for the analysis of nonlinear systems", Journal of the Franklin Institute, Vol. 281, no. 1, January 1966, pp. 9-26.

41. L.C. Thomas, "Broadband linearization of transistor amplifiers", International Solid-State Circuits Conference, February 17, 1967, Digest of Technical Papers, Vol. X, pp. 88-89.

42. O. Shimbo, private communication to H. Moody, RCA Limited, 17 February 1972.

43. "UHF Communications Satellite System", Final Report, Vol. 11, Final Report under DDS Contract OPL1-0005 "Consulting services for cost studies of UHF Satellite Communications Studies", RCA Limited, December 9, 1971 (see pp. 57 to 59).

44. D.W. Marquardt, "Least squares estimation of nonlinear parameters", a computer program in the Fortran IV language (NLRGRES); IBM SHARE library, Distribution no. 3094, March 1964. (Successor to Distribution no. 1428).

45. B.P. Bogert (editor) et al., Special Issue on Fast Fourier Transform and its Application to Digital Filtering and Spectral Analysis, IEEE Transactions on Audio and Electroacoustics, Vol. AU-15, No. 2, June 1967.

DISTRIBUTION LIST

Director General, Communications Research Centre, Shirley Bay
Ottawa, Ontario K1N 8T5 (3)

RCA Limited:

M.P. Bachynski
R.J. McIntyre
W.A. Chisholm
H.J. Moody
G. Kadar
M. Gauvin
R.G. Harrison (3)
File

as

RCA